REPORT DOCUMENTATION PAGE

AFRL-SR-AR-TR-03-

0206

1. REPORT DATE (DD-MM-YYYY)	2. REPORT TYPE	3. DATES COVERED (FROM - TO)
03-03-2003	FINAL PERFORMANCE	01-01-2000 TO 31-01-2003

4. TITLE AND SUBTITLE

VISUAL AND AUDITORY SENSITIVITIES AND DISCRIMINATIONS

5a. CONTRACT NUMBER
F49620-00-1-0053

5b. GRANT NUMBER

5c. PROGRAM ELEMENT NUMBER

6. AUTHOR(S)

REGAN, DAVID, M

5d. PROJECT NUMBER
2313/BX

5e. TASK NUMBER

5f. WORK UNIT NUMBER

7. PERFORMING ORGANIZATION NAME(S) AND ADDRESS(ES)

MRS. NOLI SWATMAN, OFFICE OF
RESEARCH ADMIN., S414 ROSS,
4700 KEELE ST., TORONTO,
ONTARIO, CANADA, M3J 1P3

8. PERFORMING ORGANIZATION REPORT NUMBER

9. SPONSORING / MONITORING AGENCY NAME(S) AND ADDRESS(ES)

Sponsoring:
AFOSR/NL
801 N. Randolph St. Rm 732
Arlington, VA 22203-1977

Monitoring:
AFOSR/NL - Rm. 713
4015 Wilson Blvd
Arlington, VA 22203-1954

10. SPONSOR/MONITOR'S ACRONYM(S)
AFOSR/NL

11. SPONSOR/MONITOR'S REPORT NUMBER(S)

12. DISTRIBUTION / AVAILABILITY STATEMENT

UNRESTRICTED

20030618 122

13. SUPPLEMENTARY NOTES

14. ABSTRACT

Self-motion causes large errors in estimates of time to collision (TTC) based on monocular information (i.e. tau), errors that improve the margin of safety. When moving in a straight line (e.g. NOE flight) closing speed adaptation can produce potentially dangerous errors in estimating TTC. A new equation gives TTC from binocular information without involving distance. The human visual system contains a mechanism that rapidly compares contours at two distant sites so as to encode the location, size and shape of an object. Contours may be defined by luminance or motion in depth contrast. Spatial frequency discrimination for cyclopean gratings is little inferior to that for luminance gratings, and seems to be supported by opponent processing. Evoked potential recording showed an inverse oblique effect for cyclopean gratings. Amplitude- and frequency-modulated auditory tones differ only in phase spectra, but the ear's hair cells introduce a difference in power spectra. This finding may be important for theories of speech processing.

15. SUBJECT TERMS

Time to collision; collision avoidance; self motion; spatial vision; long-distance interactions, cyclopean vision; evoked potentials; auditory models.

16. SECURITY CLASSIFICATION OF:			17. LIMITATION OF ABSTRACT	18. NUMBER OF PAGES	19a. NAME OF RESPONSIBLE PERSON
a. REPORT	b. ABSTRACT	c. THIS PAGE			LARKIN, WILLARD
U	U	U	UU	104	19b. TELEPHONE NUMBER (include area code) 703-696-7793

VISUAL AND AUDITORY SENSITIVITIES AND DISCRIMINATIONS

AFOSR F49620-00-1-0053

Final Performance Report 16 Dec. 1999— 31 Jan. 2003

P.I. D. Regan

York University, 4700 Keele St., North York, Ontario, Canada, M3J 1P3

CONTENTS

1. AIMS AND RELEVANCE

1.1 Long Term Aims

1.1.1 We will further develop the channeling hypothesis by: (a) identifying new visual channels; (b) elucidating rules for cue combination in rich visual environments; (c) advancing understanding of eye-limb coordination in skilled visual performance and the role of inter-individual variations of visual sensitivities in limiting skilled visual performance.

1.1.2 We will apply the channeling hypothesis as follows: (a) to inform the design of visual displays in flight simulators so as to improves transfer of training; (b) to provide design criteria for better interfacing night vision aids to the human user's visual system; (c) to inform the design of stereo visual displays used by operators of remotely-controlled vehicles such as unmanned air vehicles or operators of maneuverable land or sea vehicles used to inspect or repair equipment in environments hostile to life; (d) to inform the design of spatially-complex static or dynamic displays such as displays of infra-red, radar or visual imagery; (e) to design tests to screen personnel for their visual competence in specific tasks such as, for example, NOE helicopter flight, low-level aviation over snow-covered terrain, highway driving in high-glare conditions (low sun, approaching headlamps at night).

1.1.3 We will advance our understanding of the auditory processing of complex sounds.

1.1.4 We will use evoked potential recording techniques to achieve the following aims: (a) identify the brain sites of different kinds of visual processing and auditory processing, and relate these sites to the organization of visual and auditory areas in macaque monkey cortex; (b) relate objective data on visual and auditory processing in human brain to psychophysical models of human vision and hearing.

1.2 Specific aims:

Ground-Based Flight Simulator Studies

1.2.1 We will establish the relative contributions of monocular and binocular information to the ability of a pilot who is flying through a simulated three-

dimensional environment to judge (a) whether he or she is on a collision course with a simulated object on which he or she is closing, and (b) to estimate the time to collision with the object. We will use a variety of simulated three-dimensional arrangements of external objects, and compare results obtained with a symbolic external environment (small squares) and with a closely-realistic external environment.

1.2.2 We will establish the effect of viewing distance on the performance data obtained in 1.2.1.

1.2.3 We will find how the collision-avoidance data collected in 1.2.1 and 1.2.2 are affected when the observer is closing onto a rotating nonspherical object rather than a spherical object.

1.2.4 We will find whether visual adaptation caused by looking straight ahead in NOE flight through a cluttered environment produces errors in the visual judgements required for collision avoidance.

1.2.5 We will establish the relative importance for training collision avoidance skills of the spatial and dynamic fidelity of the simulation of (a) an approaching object's boundaries versus (b) the object's surface texture.

1.2.6 We will find whether the performance data obtained in 1.2.1 and 1.2.2 also hold when closing on a semi-camouflaged object whose residual visibility is created entirely by motion parallax or entirely by texture contrast.

Helicopter-Borne Flight Simulator Studies

1.2.7 We will establish the extent to which a mismatch of the dynamics of object size and texture element size in a simulator display could affect transfer of training.

1.2.8 We will establish whether the use of collimated display optics in parallel-axes goggles affects the accuracy of judging (a) whether one is on a collision course with an object and (b) the time to collision with that object in a head-mounted stereo simulator.

Visual Psychophysics

1.2.9 Following up on our finding that the human visual system contains orientation-selective spatial filters for texture-defined form, we will investigate the spatial-frequency selectivity of these filters.

1.2.10 We will find whether the human visual system contains filters for motion-defined form that are selective for orientation and spatial frequency.

1.2.11 We will establish the degree to which spatial filters for textured-defined, motion-defined and luminance-defined form are independent.

1.2.12 We will follow up our early work on *coincidence detectors* in the human visual system to establish the importance of a specific visual sensitivity to relationships between parts of luminance-defined object's edges in judging the location, size, shape, and orientation of the object.

1.2.13 We will carry out experiments analogous to experiment 1.4.1 on texture-defined form and binocular disparity-defined form.

Development of Visual Screening Tests

1.2.14 We will develop a test for determining a pilot's accuracy of judging whether an approaching object is on a collision course

1.2.15 We will develop a test for determining a pilot's ability to judge the time to collision with an object on a collision course.

Auditory Studies

1.2.16 We will extend our theoretical work on the response of auditory hair cells to complex sounds so as to make the work more relevant to speech perception. In particular, we will develop a theoretical treatment of the distortion produced by hair cells on inputs that consist of sums of tones that are modulated in both amplitude and frequency. We will allow for noise and also for adaptive changes in the hair cell transducer characteristic.

Brain Recording Studies

1.2.17 *Brain Neurons Sensitive to Cyclopean Form: Tuning Bandwidths for Orientation, Spatial Frequency and Temporal Frequency*

We will measure the orientation tuning bandwidths, spatial frequency tuning bandwidths and temporal frequency tuning bandwidths of cyclopean neurons in human visual cortex by recording responses from the human brain to two superimposed cyclopean grating and by using our nonlinear systems analysis technique.

1.2.18 *Brain Neurons Sensitive to Motion-Defined Form: Tuning Bandwidths for Orientation, Spatial Frequency and Temporal Frequency*

We will repeat experiment 1.2.17 using two superimposed motion-defined gratings.

1.2.19 *Brain Neurons Sensitive to Texture-Defined Form: Tuning Bandwidths for Orientation, Spatial Frequency and Temporal Frequency*

We will repeat experiment 1.2.17 using two superimposed texture-defined gratings.

1.2.20 *Brain Neurons Sensitive to Colour-Defined Form: Tuning Bandwidths for Orientation, Spatial Frequency and Temporal Frequency*

We will repeat experiment 1.2.17 using two superimposed equiluminant chromatic gratings.

1.2.21 *Brain Neurons Sensitive to More than One Kind of Contrast*

We will repeat experiment 1.2.17 using a cyclopean grating superimposed on a luminance grating, a texture grating superimposed on a luminance grating, and so on.

2. ACCOMPLISHMENTS /NEW FINDINGS

2.1 Ground–Based Simulator Studies

Relevance: The relevance of this line of research is as follows: collision avoidance in both fixed-wing and rotary-wing aviation; the design of binocular and monocular flight simulators and, in particular, the effectiveness of training in collision avoidance.

2.1(a) Estimating time to collision with an approaching object in the situation of simulated self–motion using a research flight simulator

Long–Term Aims 4.1.1, 4.1.2; Specific Aims 4.2.1, 4.2.4 Part of this project has been completed and a paper has been published. Gray, R. & Regan, D. (2000). Simulated self–motion alters perceived time to collision. Current Biology, 10, 587–590.

Methods

By using the optics of a flight simulator we were able to create a flow pattern that subtended 39° horizontally x 27° while appearing to be located at a

great distance (Figure 1a,b). For forward flow, texture elements flowed radially outward from the focus, simulating forward self-motion; for backward flow, texture elements flowed radially inward toward the focus. For the expanding flow pattern, the texture elements increased speed and grew larger as they moved radially outwards. The contracting (backward) flow pattern was the reverse. Results obtained with these two flow patterns were compared with those obtained using a static condition, in which the squares remained stationary. We used the optical arrangement shown in Figure 1a,b to simulate a sphere moving at a constant speed along a straight line towards a point between the eyes. A sensation of approaching motion in depth was created by changing the size of the simulated object appropriately. The simulated approaching sphere was presented at the center of the radial flow pattern. Figure 1c gives a rough impression of what the observer saw. No texture elements were presented in a central square area with a side length of 9°.

Procedure

Our method has been described previously (Gray & Regan, 1988). In brief, each trial consisted of one presentation of the simulated approaching sphere with a mean duration of 700 msec. The flow pattern was only visible during this presentation interval. At the designated time of collision, some time after the sphere and flow pattern had been switched off, a brief auditory click was generated. The observer's task was to indicate whether the auditory click occurred before or after the simulated approaching sphere would have arrived at their eyes. The initial TTC of the simulated approaching object $[\theta/(d\theta/dt)$ was varied from trial to trial according to a transformed staircase method (Levitt, 1971). The staircase converged onto a TTC that gave a 50% probability that the observer would judge that the simulated approaching object would arrive before the auditory click. Nine staircases corresponding to all possible combinations of three values of designated TTC (1.8 sec, 2.3 sec and 2.8 sec) and three values of initial angle that the sphere subtends (1.1°, 1.7° and 2.3°) were randomly interleaved. The use of multiple staircases had the following two consequences: it was not possible for observers to anticipate trial-to-trial variations in TTC, and

Fig.1

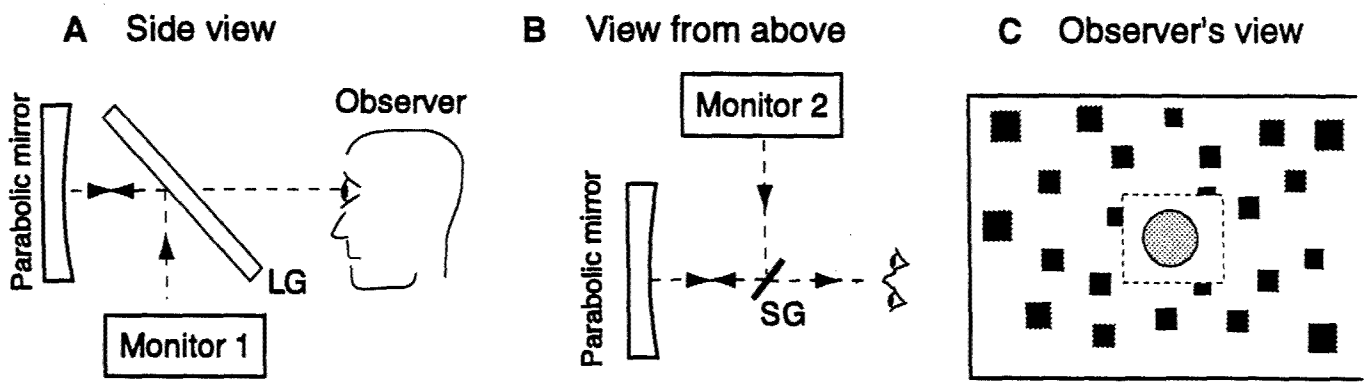

The radially expanding or contracting flow field consisted of a randomly scattered pattern of squares whose size and instantaneous speed increased radially to simulate self-motion. (a) The squares were displayed on a large (80cm horizontal x 56cm) electrostatically driven display (monitor 1, Hewlett-Packard model 1321A) that was viewed through the optics of an F-18 flight simulator. A large glass sheet (LG) reflected the display onto a large (75 cm horizontal x 90cm) high-quality prabolic mirror (PM) so that the display seemed to be at a great distance, though it subtended 39^{o} horizintal x 27^{o}. (b) An approaching spherical object of luminance $16cd/m^2$ was simulated on a second monitor (monitor 2, Tektronix model 608 with green P31 phosphor) that ran at 50 frames/sec. A thin sheet of glass (SG) reflected this second display into the parabolic mirror so that it also seemed to be at a great distance. Note that, for clarity, the glass sheet LG is omitted from (b). (c) The observer's view of the approaching object (gray circle) and flow field (black squares). The dashed squares (not presented in the actual display) indicates the central area in which no flow elements were presented.

Fig.2

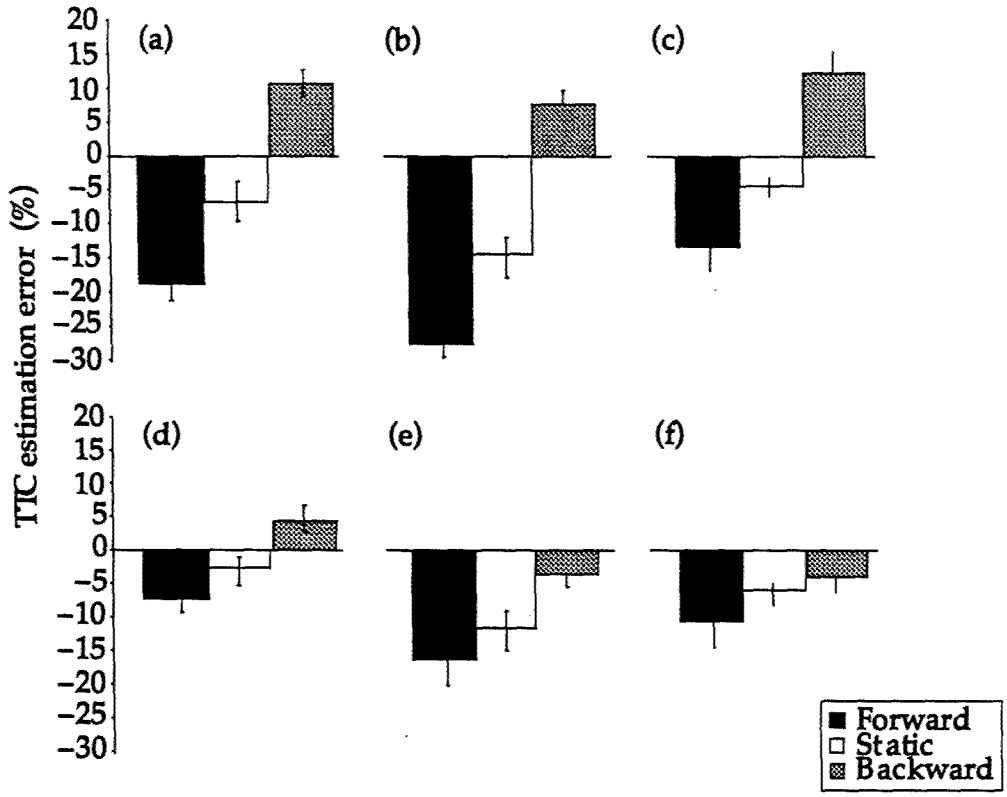

Mean percentage TTC estimation error for the different flow conditions. Black bars are for forward flow, gray bars are for backward flow and white bars are for the static condition. (a–c) Squares grew larger as they moved radially outwards and vice versa. (d–f) Square size was constant. Error bars are standard errors. (a,d) Observer 1; (b,e) observer 2; (c,f) observer 3. Stepwise multiple regression analysis revealed that the task–relevent variable, $\theta(d\theta/dt)$, accounted for a high proportion of total variance for all three flow condition. For the three observers, the task–relevent variable accounted for 74-90% of the variance in the forward condition, 81-93% in the static condition and 79-86% in the backward condition. Task–irrelevent variables (θ_o, $d\theta/dt$, and $\Delta\theta$) accounted for only a small amount of additional variance (ranging from 3% to 8%).

Fig.3

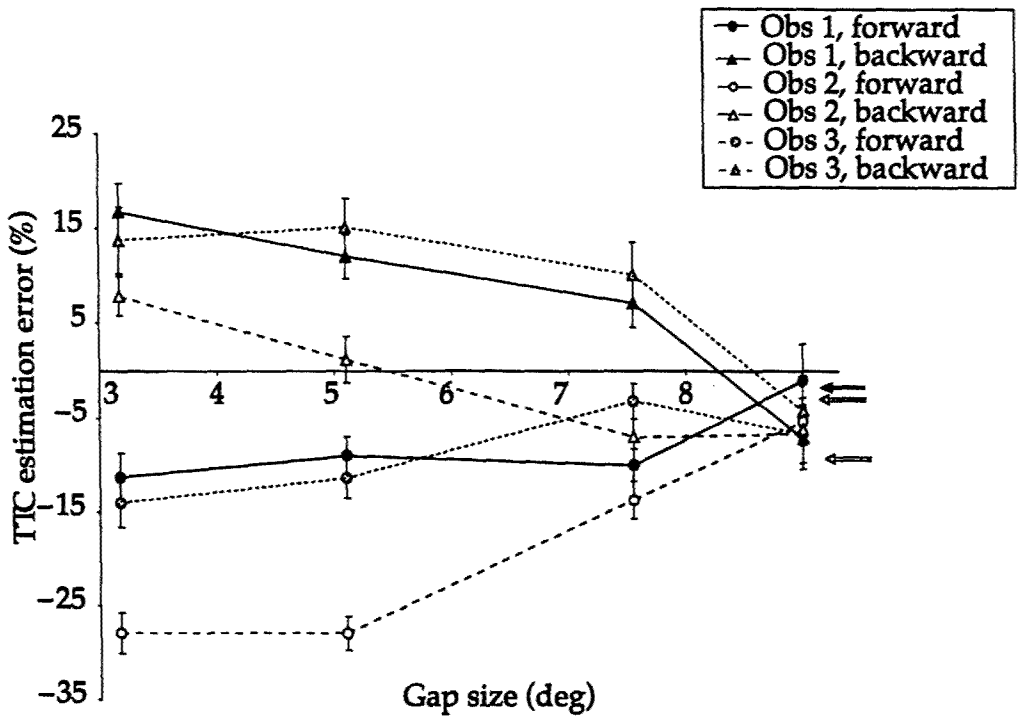

TTC estimation error as a function of the gap between the outer edge of the object and the inner edge of the flow pattern. Solid, dashed and dotted lines plot TTC estimation errrors for observer (obs) 1,2 and 3, respectively. Circles show TTC estimates for forward flow and triangles show estimates for backward flow. Small arrows indicate the mean estimation error in the static condition for each observer. Error bars are standard errors.

Fig.4

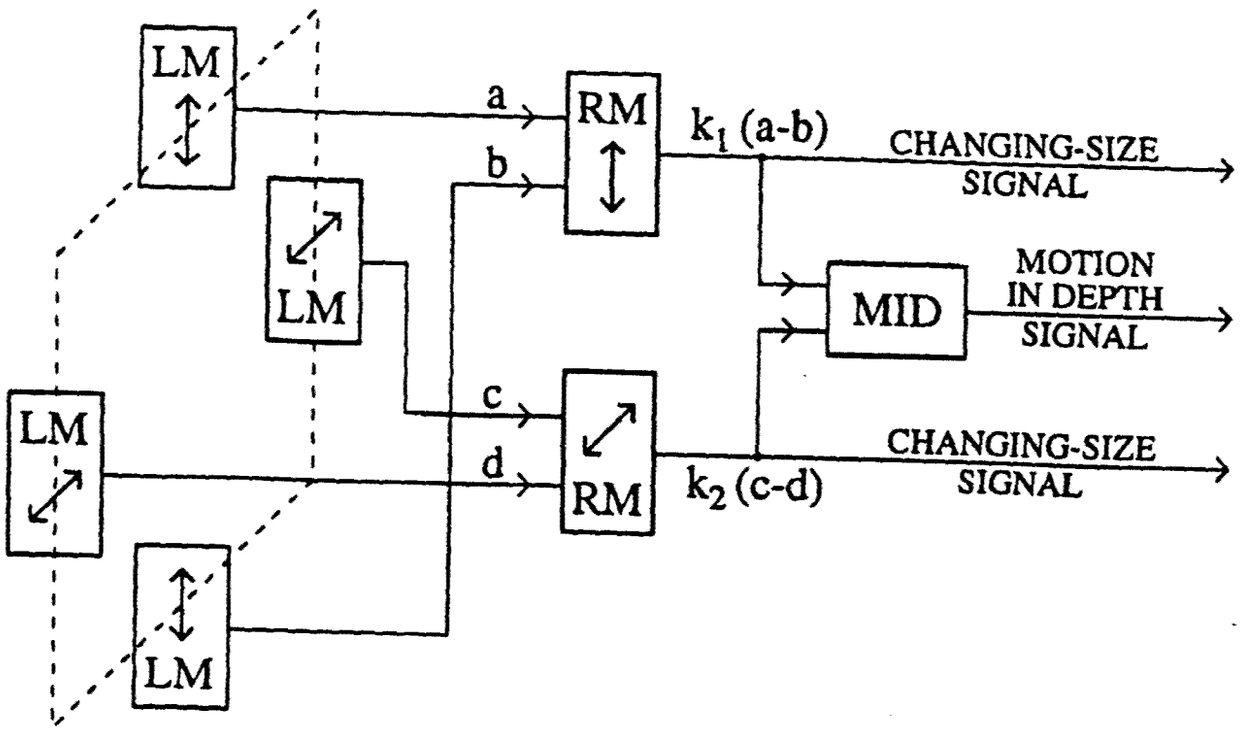

Model of the processing of changing size and of the encoding of time to collision for an untextured object. The retinal image boundary is shown dotted. LM are filters sensitive to local motion along the directions arrowed. Their outputs (*a, b, c* and *d*) assume a magnitude that encodes local speed, and a sign that represents the direction of motion. RM are one-dimensional relative motion filters whose outputs signal the speed and sign (expansion versus contraction) of relative motion along some given retinal meridian. MID is a two-dimensional relative motion filter for which the most efficient stimulus is isotropic expansion of the retinal image, i.e. the situation that $k_1(a-b) = k_2(c-d)$. We assume here that the amplitude of the output of the MID filter is equal to that of any one of its inputs from RM filters. If so, this output is inversely proportional to time to collision. From Regan, D., & Hamstra, S.J. (1993). Dissociation of discrimination thresholds for time to collision and for rate of angular expansion. Vision Research, 33, 447-462. Reprinted with permission.

after collecting the response data we could perform a stepwise regression analysis to determine which optical variables were used in making estimates of TTC. This method also has the advantages that it removes any effect of motor delay on the TTC estimate as well as any cognitive strategy for controlling collisions.

Results and discussion

Figure 1 shows the experimental set-up used. The observer saw a sphere that appeared to be moving towards them. Forward self-motion was simulated by squares moving away from the center of the visual display and increasing in size and backward self-motion by squares moving towards the center and contracting. Figure 2a –c shows the mean percentage error in estimating TTC (that is the percentage difference between the estimated and calculated TTC)for three observers. It is clear from Figure 2 that the pattern of simulated self-motion had a large effect on estimates of TTC. Consistent with previous findings with a background of static texture elements, all three observers made small (3 –14%)underestimates of TTC in simulated static conditions. When forward self-motion was simulated, all three observers made larger (by 11%,13%and 9%)underestimates of TTC than in the static condition. Conversely, when backward self-motion was simulated, all three observers overestimated TTC. The differences in TTC estimates between backward and static flow were 17%,23% and 19%for the three observers. A repeated measures analysis of variance (ANOVA)revealed a significant main effect of flow type ($F(2,4)=149, p<0.001$). When the size of the moving squares in the flow pattern was held constant, the effect of the flow pattern on TTC estimates was dramatically reduced. Estimation errors for this condition are shown in Figure 2d –f. In this condition, the forward –static difference was only 3%,6%and 5%for the three observers and the backward –static difference was only 7%,9%and 2%for observers 1 –3,respectively. In Figure 2a –c, the flow pattern was visible only during a presentation. But TTC judgements were not significantly different when the observer adapted to the flow pattern for 10 minutes prior to beginning the run and the pattern remained on throughout the run. For observer 1,%errors in

this condition were –16%,–6%and 12%for the forward, static and backward flow conditions, respectively. This finding suggests that the effect was not chiefly caused by adaptation to the flow pattern. To examine the lateral spread of the flow effect, we next varied the size of the square hole at the focus of the flow pattern (see Figure 1c). We used four hole sizes (9. 7°, 13. 6°,18. 5° and 21. 4°). Figure 3 shows TTC estimation errors for these four hole sizes expressed as the gap between the outer edge of the object and the inner edge of the flow pattern (3. 2°,5.1°,7. 5° and 9°, respectively). It is clear that the effect of simulated self-motion on perceived TTC decreased at an accelerating rate as the separation between the flow pattern and the simulated approaching sphere was increased. A two-factor repeated- measures ANOVA revealed a significant effect of flow condition ($F(1,2)=452.2, p<0.01$)and a significant inter- action between flow condition and gap size ($F(3,6)=25.2, p<0.01$). At a gap size of 9°, TTC estimates for the forward and backward flow conditions were not significantly different (observer 1:$t(26)=0.7, p>0.5$;observer 2: $t(26)=0.4, p>0.5$;observer 3:$t(26)=0.6, p>0.5$).

Psychophysical evidence has been reported for the following model of visual sensitivity to changing size and TTC depicted in Fig. 4 (Regan & Gray, 2000; Beverley & Regan, 1979a, b; Regan & Hamstra, 1993; Regan & Vincent, 1995). At the first stage of processing, the opposite edges of an approaching object 's retinal image stimulate detectors with small receptive fields that are sensitive to unidirectional motion (for example, elaborated Reichardt detectors)(VanSanten & Sperling, 1985). At the second stage of processing, the outputs of pairs of these local-motion detectors are subtracted to create a changing-size mechanism that is sensitive to expansion along one direction, and has a small receptive field (1. 5°–2. 0°). And at the third stage of processing, a motion-in-depth signal is generated whose magnitude is inversely proportional to TTC, provided that the retinal image expansion is isotropic (that is, without change of shape). The local changing-size detector is excited when its small receptive field is precisely at the center of radially expanding flow pattern, but is not excited when the center of the flow pattern is covered by an occluder that

creates a 0. 5° gap between the outer edge of its receptive field and the inner edge of the flow pattern (Regan & Beverley, 1979c; Beverley & Regan, 1982). Thus, this local changing-size mechanism would not have been directly stimulated when we introduced a 5° gap between the outer edge of the simulated approaching object and the inner edge of the flow pattern. Yet, as reported above, the effect of the flow pattern on estimates of TTC were unaffected by the 5 °gap. We conclude that the effects reported here could not have been caused by a direct effect of the flow pattern upon the local second-stage changing-size mechanism. Rather, we propose that the long-range lateral interaction that produced the effects reported here occurred at a processing stage subsequent to the changing-size mechanism. In particular, the motion–in-depth signal that supported estimates of TTC was a weighted sum of the motion-in-depth signal generated by stimulating the local changing-size detector and the motion-in-depth signal generated by the flow pattern.

Our finding that the effect of the flow pattern was almost abolished when the size of texture elements was held constant brings into question the relevance to everyday life of the considerable literature on optic flow in which texture element size was held constant.

There is a possible ecological role for the interactions we report here. When a stationary observer attempts to catch an approaching object, there is a clear advantage that a τ-based estimate of TTC should be an underestimation: the unavoidable variability in the estimate will never create the situation in which there is no time left to acquire the stereo information about TTC that is required to correctly time the finger flexions that take place during the final tens of milliseconds of a successful catch. It has been shown that this stereo information is acquired only when the approaching object is within a few metres of the catcher (Alderson, Sully & Sully, 1974). When the whole body is moving forward (for example, a monkey swinging from branch to branch)the mass that must be controlled when using close-range stereo information to make fine corrective adjustments is very much greater than when remaining stationary. A simple solution would be a lateral neural interaction that allows the expanding flow field produced by self-motion to increase the underestimation of TTC based on

monocular information only (i. e. τ)to be even greater than when stationary. Some neurons in the pigeon 's brain are sensitive to the ratio $\theta/(d\theta/dt)$(where θ is the angle subtended by the approaching object and t is time), that is, τ , while others are sensitive to the rate of expansion $d\theta/dt$ (Sun & Frost, 1998). By itself, this finding leaves the relation between the activities of such τ-sensitive neurons and the animal's behavior a matter of conjecture. However, if behavioral studies showed that the human findings reported here extrapolate to pigeons, a stronger link between physiology and behavior would be established if it were found that τ -sensitive neurons were affected by flow fields whereas neurons sensitive to rate of expansion were not. Electrophysiological studies suggest that birds have separate mechanisms for processing object motion and self-motion (the tectofugal pathway and the accessory optic system, respectively) (Frost, Wylie & Wang, 1990). Our findings raise the possibility that there may be long-range connections between these ecologically distinct systems.

Summary

Many authors have assumed that motor actions required for collision avoidance and for collision achievement (for example, in driving a car or hitting a ball) are guided by monitoring the time to collision (TTC), and that this is done on the basis of moment-to-moment values of the optical variable τ (Hoyle, 1957; Lee, 1976; Regan & Gray, 2000). This assumption has also motivated the search for single neurons that fire when τ is a certain value Sun & Frost, 1998; Rind & Simmons, 1999; Wang & Frost, 1992; Hatsopoulos, Gabbiani & Laurent, 1995; Frost, Wylie, & Wang, 1990). Almost all of the laboratory studies and all the animal experiments were restricted to the case of stationary observer and moving object. On the face of it, this would seem reasonable. Even though humans and other animals routinely perform visually guided actions that require the TTC of an approaching object to be estimated while the observer is moving, τ provides an accurate estimate of TTC regardless of whether the approach is produced by self-motion, object-motion or a combination of both. One might therefore expect that judgements of TTC would be independent of self-motion. We report here, however, that simulated self-motion using a peripheral flow

field substantially altered estimates of TTC for an approaching object, even though the peripheral flow field did not affect the value of τ for the approaching object. This finding points to long range interactions between collision-sensitive visual neurons and neural mechanisms for processing self-motion.

2.1(b). Estimating the instant at which to initiate an overtaking manoevre using a car simulator.

Relevance: Although this study was restricted to a car simulator, the findings presumably apply also to low-level flight in either a helicopter or fixed–wing aircraft. In particular, gazing straight ahead causes time to collision to be considerably overestimated, and may be a cause of collisions or near–collisions.

This project has been completed and published: Gray, R. & Regan, D. (2000). Risky driving behavior: A consequence of motion adaptation for visually guided motor action. Journal of Experimental Psychology: Human Perception and Performance, 26, 1721–1723. The data have also been reported to ECVP at the Trieste meeting, and to the Edinburgh meeting on Event Perception and Action.

Methods

Apparatus

All experiments were performed in a fixed-base driving simulator composed of two main components: the frontal two-thirds of a Nissan 240SX convertible and a wide-field-of-view (60° horizontal x 40° vertical) display of a simulated driving scene. The visual scene was rendered and updated by an Octane workstation (Silicon Graphics Inc.). It was projected onto a wall 3.5 m in front of the driver with a Barco 800G projector and was continually changed at an average rate of 15 frames/s in correspondence with the movement of the car. Unless otherwise stated, a texture pattern resembling black cracks on a gray background was mapped onto the surface of the road. The sky was blue and the surrounding ground was green, so the edges of the road were highly visible. Yellow stripes (1.5 m in length and spaced 10 m center to center) ran down the center of the road. Each lane was 5 m wide and subtended approximately 10° at a

Fig.5

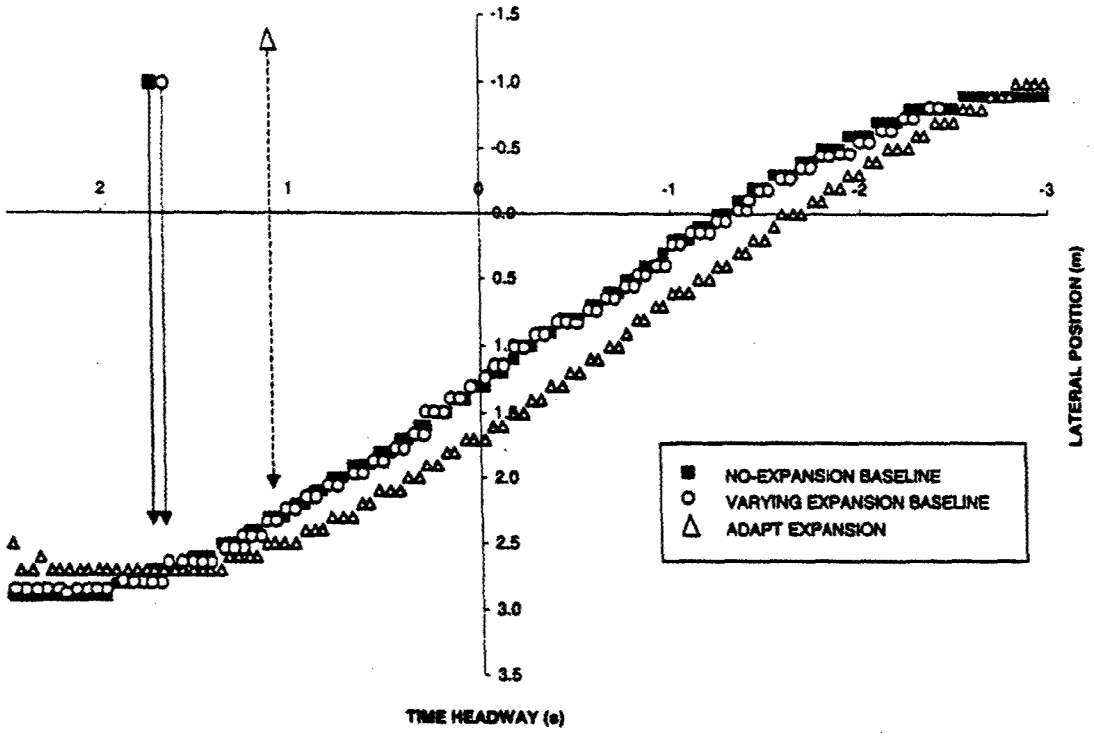

Lateal car position plotted as function of the time headway (TH) with the lead vehicle for Observer 1. Negative lateral positions represent driving in the left lane and positive positions represent driving in the right lane. A negative time headway indicates that the front bumpr of observer's simulated car was further down the road than the slowly moving vehicle's rear bumper. Solid squares are for the no–flow condition, open circles are for the varying–flow–baseline condition, and open triagnels are for the adapt–expansion condition. The speed and intial distnace of the lead car were indentical for all three conditions. The onet of the overtaking maneuvers in the three conditions is shown with black arrows.

Fig.6

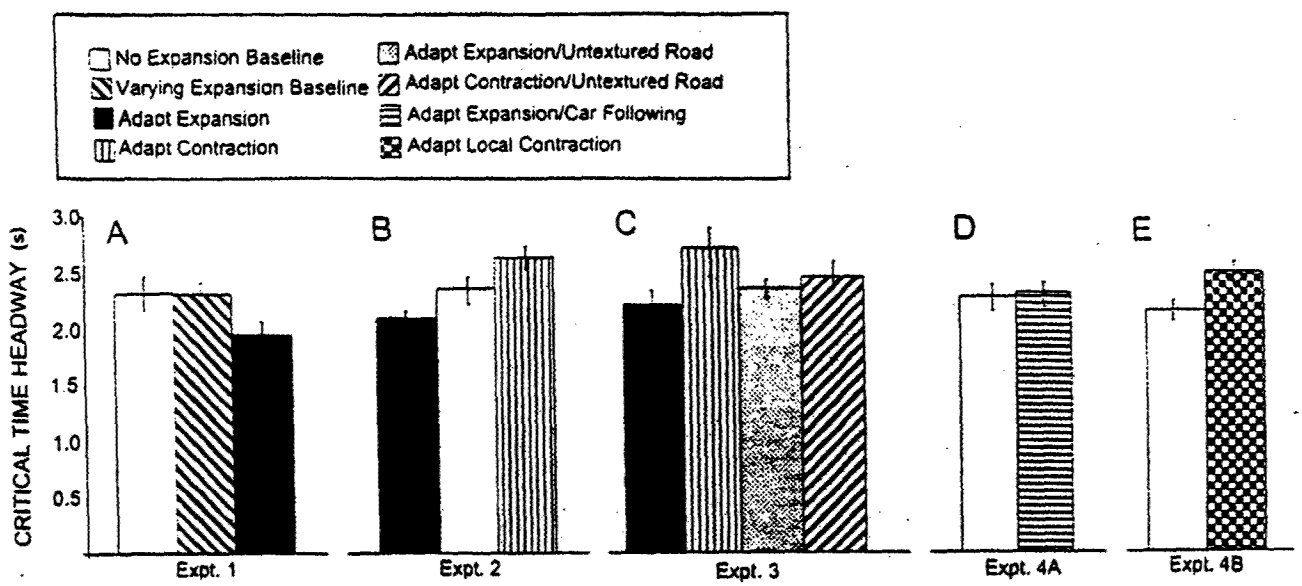

Mean critical time headway values for four experiments. See legend and text for details. Error bars represent ± 1 *SE*. Expt = experiment

Fig.7

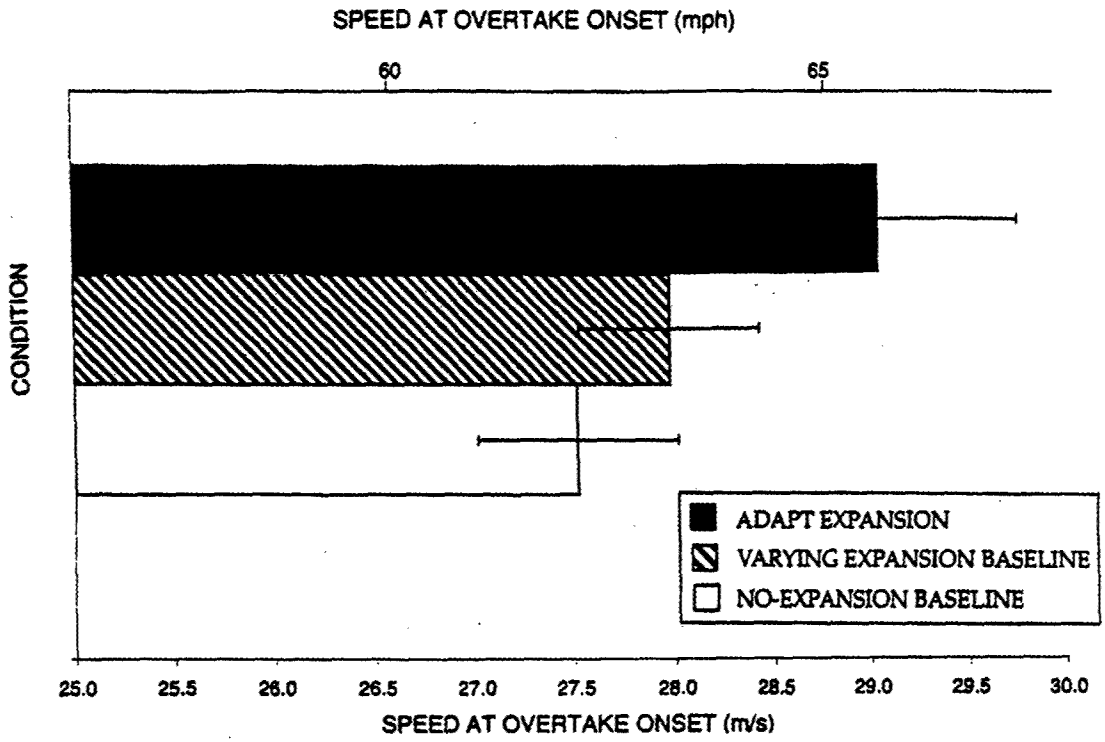

Mean driving speed at the onset of overtaking averaged across the 8 observers who participated in Experiment 1. Solid bars are for the no-flow-baseline condition, open bars are for the varying-flow-baseline condition, and hatched bars are for the adapt-to-expansion condition. Error bars represent ± 1 *SE*.

Fig.8

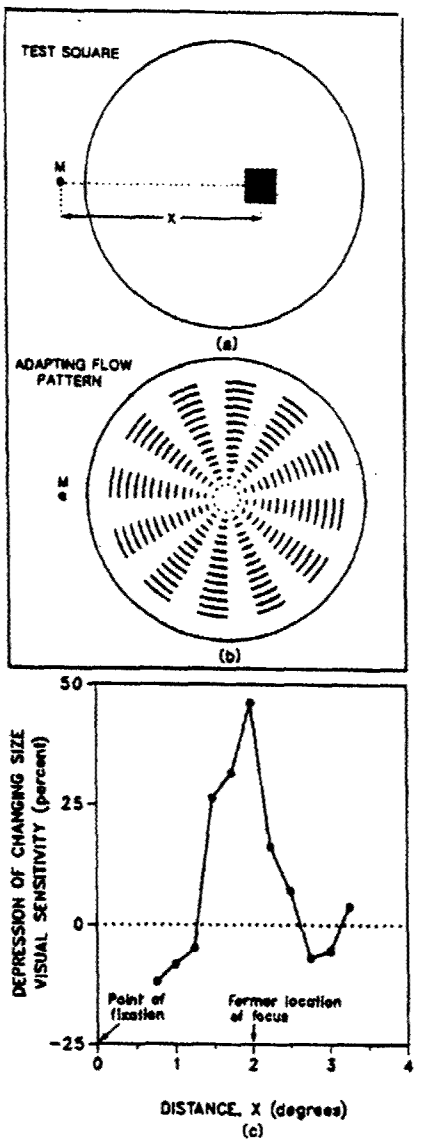

(a) Sensitivity to size oscillations of a 0.5° test square loated a variable distance (X) from the point of fixation (M) were measured before and after adaptation. (b) Observers adapted to a radially expanding flow pattern for 10min. (c) Depression of changing-size sensitivity as a function of distance X. Threshold elevations only occured for points very close to the former location of the flow pattern's focus. From "Visually Guided Locomotion: Psychophysical Evidence for a Neural Mechanism Sensitive to Flow Patterns." by D. Regan and K.I. Beverley. 1979. Science. Copyright 1979 by the American Association for the Advancement of Science. Reprinted with permission.

virtual distance of 20 m from the car. To aid the driver in assessing the 3-D motion of the car, short (0.5 m height) white posts were placed along the edges of the road (10 m apart). Other vehicles in the driving scene had a red body, black tires, and always followed a path down the center of the right lane. The position at which the other vehicles first appeared, and their travelling speed were varied as described below. The driving simulator provided limited kinesthetic feedback through the torque in the steering wheel and audio feedback in the form of engine noise that increased with increased car speed.

Data Analysis

Four measurements were recorded at a rate of 20 samples/s and analyzed: lateral position, distance from the start of the road, speed, and distance from other cars. The smallest change in distance or lateral position that could be detected was 0.1 m. From these records the TTC and time headway (TH) were computed.

The standard deviation of lateral position while driving on the first 200 m of empty straight road (SD_{EMPTY}) was computed for each experimental trial. We defined the initiation of an overtaking maneuver as a change in lateral position toward the center of the road that was greater than SD_{EMPTY}.

Procedure

Each experimental session began with a 10-min practice trial designed to allow observers to become comfortable with driving in the virtual environment. During this session observers drove on a roadway with several curves, and there were no other vehicles on the road. Following this 10-min period, observers performed one practice overtaking trial.

The driving scene during the overtaking portion of the experiment was as follows. Observers drove along 3,000 m of straight road at their own preferred speed. They were instructed to stay in the right lane except when overtaking other vehicles. To control the presentation of other vehicles, the roadway was divided into fifteen 200-m segments. During the first 200-m segment, there were no other vehicles on the road. Within the remaining 14 segments, there were 8

segments (chosen randomly) in which another vehicle appeared. The initial distances of the other vehicles (as measured from the beginning of the particular 200-m road segment they appeared in) ranged from 65—85 m, and their speeds ranged from 14 to 20 m/s (i.e., 32 to 45 mph). All of these vehicles traveled at a constant speed.

During overtaking maneuvers, observers were instructed to overtake the cars in the same way that they would on a real highway. It was emphasized to participants that they should pass early enough to avoid colliding with the lead car but should not to go into the left lane too early because there may be cars coming the other way (this never actually occurred in the present study). No feedback was given as to the success of their overtaking maneuver.

Each test session consisted of three conditions: (1) no-expansion baseline (2) varying expansion baseline, and (3) adaptation to constant expansion. The order of the three conditions was counterbalanced, and there were 10-min breaks between each condition to minimize any carryover of adaptation effects. These conditions were as follows:

No-expansion baseline condition. Observers sat in the car and stared straight ahead at a static view of the driving scene for 5 min. This baseline condition is analogous to the baseline condition we used in a psychophysical experiment examining the effects of adaptation on TTC judgments (Gray & Regan, 1999a). During the 5-min period, pressing down on the accelerator or turning the steering wheel did not alter the visual display. A brief auditory tone signaled the end of the 5-min period after which observers immediately completed one overtaking session. Observers were instructed to begin driving forward immediately after they heard the tone.

Varying-expansion baseline condition. This condition was identical to Condition 1 except for the following. Instead of remaining stationary for the initial 5-min period, observers drove through a road with several curves at any speed they felt comfortable. There were on average 12 curves per 4,000 m of driving so that the driver was essentially continuously negotiating curves for 5 min. In this condition, we predicted that no motion-in-depth (MID) aftereffect would be produced because the focus of expansion of the visual flow field is

continuously changing as the observer steers the car around the curves. Psychophysical studies have shown that MID aftereffects produced by adaptation to a radial flow field only occur for objects very close (within roughly 0.5°) to the prior location of the focus of expansion (Regan & Beverley, 1979).

Adaptation to constant expansion condition. This condition was identical to Conditions 1 and 2 except for the following. During the initial 5 min period observers were instructed to drive straight ahead on a straight empty road at a speed which was comfortable to them. They were further instructed to keep looking at the road in front of the car as if they were taking a long drive on a deserted highway. No fixation point was used. 2 A small lateral drift toward the inside lane was present in all conditions so that drivers were required to actively steer even when driving straight ahead.

Results

Figure 5 plots the lateral position of the car as function of the time headway (TH) with the lead vehicle for Observer 1. These data are for one particular pass during the overtaking session. The speed and initial distance of the lead car were identical for all three conditions. The onset of the overtaking maneuvers in the three conditions is shown with black arrows. The onset of the overtaking maneuver (the critical time headway) occurred at a TH value of 1.74 s for no-flow baseline (solid squares), 1.61 s for the varying-flow baseline (open circles), and 1.13 s for the adapt-expansion condition (open triangles).

Similar results were obtained for 7 other observers. The mean critical TH values averaged across the 8 maneuvers for all 8 observers are shown in Figure 6A . A repeated-measures analysis of variance (ANOVA) comparing the mean critical TH values revealed a significant effect of condition, $F(2, 14) = 41.73$, $p < 0.001$. We made two comparisons of treatment means (Keppel, 1991). The mean critical TH for the two baseline conditions was not significantly different, $F(1, 7) = 0.05$, $p > 0.5$, and the mean critical TH for the adapt-expansion condition was significantly lower than the combined mean for the two baseline conditions, $F(1, 7) = 59.90$, $p < 0.001$. The difference between the combined mean of the two baseline conditions and the mean for the adapt-expansion condition was 345 ms.

We also compared the three conditions using the speed at the onset of the overtaking maneuver as a dependent measure. Mean speeds for the three conditions are shown in Figure 7. A repeated-measures ANOVA revealed a significant effect of condition, F (2, 14) = 3.80, $p < 0.05$, on the speed data. Comparisons between treatment means revealed no significant difference between the mean speeds in the two baseline conditions, F (1, 7) = 0.90, i > 0.5, and that the mean speed in the adapt-to-expansion condition was significantly higher than the combined means for the two baseline conditions, F (1, 70) = 5.60, $p < 0.05$. The finding that observers drive at a higher speed following adaptation to expansion provides further evidence that driving on a straight empty road produces a substantial adaptation effect. The effect of adaptation on driving speed is discussed below.

Finally, we evaluated how well observers followed the instruction to "drive straight ahead down the center of the right lane" during the adapt-expansion condition. If observers did not maintain a roughly straight course during the adaptation condition, the location of the focus of expansion would change during the adaptation period. Our observers maintained their lane position very precisely. The mean lane position ranged from 1.98 m to 2.5 m (measured from the center), and the standard deviation of lateral position ranged from 0.13 m to 0.29 m.

Discussion

Adaptation to retinal image expansion has a dramatic effect on overtaking maneuvers. Following simulated driving on a straight empty road for 5 min, drivers' initiated overtaking 218—510 ms later than comparable maneuvers made following 5 min of remaining stationary or 5 min of curve driving. There are two driving control strategies that could explain these temporal shifts in overtaking: a constant TH strategy and a constant perceived distance strategy. We now consider these two strategies.

If drivers initiate overtaking at a constant TH, the observed changes in overtaking behavior could be explained in terms of an overestimation of the TH with the lead car produced by adaptation to expansion. Regan and Beverley

(1979) have shown that detection thresholds for MID were elevated after adapting to a radially expanding flow pattern for which the divergence of velocity (div **V**) was large in the immediate vicinity of the focus of expansion. Their observers adapted to a radial flow pattern for 10 min. As shown in Figure 8, detection thresholds for oscillations in the size of a small (0.5°) square test target were substantially elevated for objects located at the point in the visual field previously occupied by the focus of expansion of the flow pattern (i.e., at 2°). Threshold elevations fell off sharply for objects located away from this location. No such effect was observed for a test target of constant size that oscillated in location.

The threshold elevation shown in Figure 8 is of similar size to that produced by adapting to changes in the size of a small square (Regan & Beverley, 1978), a kind of adaptation that we have shown also causes observers to overestimate TTC (Gray & Regan, 1999a). On this basis we predicted that adapting to a radially expanding flow pattern would cause observers to overestimate the TTC of objects located at the prior location of the focus of expansion.

In the present experiment, the focus of expansion of the adapting pattern (i.e., the outward flow of the road texture, lane-markers, etc.) was located at approximately the same position in the visual field where the lead vehicle appeared during overtaking maneuvers. If a driver's control strategy was to initiate an overtaking maneuver at a constant TH, the overestimation of TTC would lead to a temporal shift in the pattern of overtaking similar to that shown in Figure 5. In Experiment 1, the mean percentage change in the critical TH was 17% (SE = 3). This value is similar to the mean percentage change in estimated TTC (20%, SE = 2) following adaptation a single expanding object (Gray & Regan, 1999a).

Temporal shifts in overtaking patterns would also be predicted by a constant distance control strategy. In Experiment 1, we found that observers drove significantly faster in the adaptation condition than in either of the baseline conditions (see Figure 7). In a series of studies, Denton (1976 , 1977 , 1980) has shown that prolonged exposure to simulated forward motion produces

underestimations of perceived speed. Following a 250-s adaptation period, observers underestimated their traveling speed by amounts varying from 17—50%. In an interesting field study, Mathews (1978) reported that drivers traveling northbound on a section of road (connected to an expressway with a speed limit of 96 mph) drove 8% faster than drivers traveling southbound on the same stretch of road (connected to an urban road with a speed limit of 64 mph). The increase in driving speed (7.5% on average) following adaptation to expansion we reported in Experiment 1 is consistent with these findings; because drivers feel as though they are going slower following adaptation-to-expansion, they drive at a faster actual speed.

If drivers used a control strategy of initiating overtaking maneuvers at a constant distance from the lead car instead of using a constant TH, this increase in driving speed following adaptation would cause a similar temporal shift in the overtaking pattern. In other words, a driver's critical distance for initiation of overtaking would be associated with a shorter TH when driving speed was increased. In Experiment 2 we attempted to dissociate these two strategies by holding driving speed constant across conditions.

Experiment 2

Purpose and Rationale

To distinguish between a constant TH strategy and a constant distance strategy, we removed the driver's ability to vary the speed of the car in Experiment 2. If the temporal shifts observed in Experiment 1 were solely due to the increase in driving speed following adaptation-to-expansion, we would expect no temporal shifts to occur when driving speed is held constant between the baseline and adaptation conditions.

In Experiment 2 we also tested a new adaptation condition: adaptation-to-contraction produced by an extended period of driving backward.

Method

The procedure was as described for Experiment 1 except for the following. The test session was composed of three conditions: (1) no-expansion baseline, (2)

adaptation to expansion, and (3) adaptation to contraction. We did not use the varying-expansion baseline condition in Experiment 2 because in Experiment 1 it did not produce significantly different results from the no-expansion baseline. For these three conditions and during all the overtaking maneuvers, the car traveled at a constant speed of 24 m/s (50 mph). Thus, unlike Experiment 1, in Experiment 2 the driver only controlled the lateral position of the car. In Condition 3 the simulated car traveled backward (i.e., away from the screen) during the initial 5-min period and switched to travelling forward for the overtaking session. Because speed was held constant, the transition between backward and forward driving was the same for all observers. The order of the 3 conditions was counterbalanced. There were 10-min break periods between each of the conditions to prevent any carryover of adaptation effects.

Results

Figure 6B shows the mean critical TH, averaged across 9 observers, for the three conditions. Similar to Experiment 1, the mean critical TH value for adapt-expansion condition was 252 ms shorter than in the baseline condition. Conversely, the mean critical TH for the adaptation-to-contraction condition was longer (by approximately 270 ms) than in the baseline condition.

A repeated-measures ANOVA revealed a significant effect of condition, $F(2, 16) = 5.40$, $p < 0.025$. A comparison of treatment means revealed a significant difference between the critical TH in the adapt-expansion condition and the critical TH in the adapt-contraction condition, $F(2, 16) = 54.60$, $p < 0.001$.

Discussion

In Experiment 2, significant adaptation effects occurred even though the driving speed was identical in all conditions. This finding indicates that our observers did not use a constant distance strategy for the initiation of overtaking maneuvers in Experiment 2 and that changes in perceived speed following adaptation to expansion are not the only cause of the observed changes in overtaking patterns. With speed held constant, a constant distance strategy should produce no difference in the timing of overtaking maneuvers for the

three conditions used in Experiment 2, assuming that the adaptation conditions do not differentially effect judgments of perceived distance. However, these findings do not rule out the possibility that drivers may use different control strategies depending on the situation (e.g., their driving speed).

Why did drivers initiate overtaking significantly earlier following adaptation-to-contraction? This effect can also be explained by our misestimation of time headway model because adaptation to a continuously contracting visual scene should cause drivers underestimate TH.

Experiment 3

Purpose and Rationale

The relative contribution of central and peripheral visual information to the perception of self-motion has recently garnered a great deal of attention (e.g., Howard & Heckman, 1989 ; Telford, Spratley, & Frost, 1992 ; Warren & Kurtz, 1992). The hypothesis that, in general, peripheral vision dominates the perception and control of self-motion (Brandt, Dichgans, & Koenig, 1973) conflicts with recent findings that perceived self-motion can be driven by central vision under certain conditions, namely, when the central field is perceived as the background of the display (Howard & Heckman, 1989). The purpose of Experiment 3 was to examine the relative contribution of central and peripheral changing-size information to the effects of adaptation on overtaking. We chose to reduce the central changing-size information (i.e., around the location of the focus of expansion) by removing the texture from the surface of the road. All other changing-size information including the expansion of the road stripes, and road-side markers outside the central visual field was still present.

Method

The method was as described for Experiment 2 except for the following. Observers participated in two separate test sessions: Textured road and Untextured road. The textured road was as described above. The untextured road was solid gray. The order of these two sessions was counterbalanced across observers. To keep experimental runs reasonably short, while still preventing

carry-over of adaptation effects across conditions, we only compared the adapt-expansion and adapt-contraction conditions.

Results

The mean critical TH values, averaged across 8 observers, are shown in Figure 6C . Results for the textured-road test (black and vertical-striped bars) were similar to the results of Experiment 2: The critical TH in the adapt-expansion condition was significantly shorter than in adapt-contraction condition, t (10) = 8.29, $p < 0.001$. The difference in critical TTH values was roughly 495 ms. For the untextured-road test (gray and diagonally striped bars), the difference in TH values for the two conditions (113 ms), though significant, t (10) = 2.24, $p < 0.05$, was considerably smaller than for the textured-road test.

A two-factor repeated-measures ANOVA revealed a significant effect of adaptation condition, F (1, 10) = 26.63, $p < 0.001$, and a significant Condition x Road-Type interaction, F (1, 10) = 11.09, $p < 0.01$. Figure 6C shows that the significant interaction occurred because the effect of adapt-condition was larger for the textured-road than for the untextured-road test.

Discussion

The difference between the critical TH for the adaptation-to-expansion and adaptation-to-contraction conditions was considerably larger (by 382 ms) for a textured road than an untextured road. The peripheral changing-size information including the poles on the edge of the road, the road stripes, and the grass texture were identical for these two conditions. We propose that changes in overtaking maneuvers following adaptation are primarily caused by the adaptation of local, central visual field, changing-size detectors that signal motion-in-depth for objects near the focus of expansion. However, although much smaller, the adaptation effect produced with the untextured road was still significant. This suggests that information in the peripheral flow field does contribute to the adaptation effects. In Experiment 4, we further examined the relative contributions of central and peripheral changing-size information.

Beverley and Regan (1982) reported similar effects in an extension of their study examining the effects of adaptation to flow patterns on MID sensitivity. As described above, following adaptation to a radial flow pattern, MID thresholds are elevated for targets located near the point space previously occupied by the focus of expansion (Figure 8). However, occluding the center of the flow pattern dramatically alters this effect. A 2° hole in the adapting flow pattern effectively eliminates the selective elevation of MID thresholds for objects located near the prior location of the focus of expansion. In the present study, the removal of the road texture created a hole at the center of the flow pattern.

Experiment 4

Purpose and Rationale

The results of Experiment 3 suggest that the effects of adaptation on overtaking maneuvers are primarily caused by selective adaptation of mechanisms that signal motion-in-depth near the location of the focus of expansion. If this adaptation effect is due to local adaptation of changing-size detectors, we predict (a) there should be no adaptation effect with a textured road when objects near the focus of expansion remain constant in size, and (b) there should be an adaptation effect on an untextured road when a small adaptation stimulus (e.g., a single changing-size target) is located near the focus of expansion. The purpose of Experiments 4A and 4B was to test these two predictions.

Experiment 4A: Textured Road With Car Following

Method.

In order to reduce the changing size information near the focus of expansion, we introduced a car-following task to the adaptation period. If a driver maintains a constant distance behind a lead car, there will be no stimulation of looming detectors close to the focus of expansion. On the other hand, the radial flow in peripheral vision produced by the road markers, etc., will be identical to the adaptation-to-constant-expansion condition used in Experiments 1—3.

In Experiment 4A we compared this car-following. condition with the no-expansion baseline used in Experiments 1 and 2. During the car-following condition, observers were instructed to speed up until they reached what they felt was a safe distance behind the lead car and then attempt to maintain this separation. The lead car's initial distance was 55 m, and it traveled at a constant speed of 22 m/s (50 mph). At the end of the 5-min period, the lead car pulled off the side of the road and the overtaking session, as described for Experiment 1, began. All observers completed two no-expansion-baseline sessions and two car-following sessions. The order of these sessions was counterbalanced across observers, and there were 10-min breaks between the sessions.

Results.

Figure 6D shows the mean critical TH for 8 observers. Addition of the car-following task during the adaptation phase (horizontally striped bars) effectively eliminated any changes in overtaking maneuvers. The mean critical TH in the baseline condition was not significantly different from the mean critical TH in the car-following condition, t (14) = 0.06, $p > 0.5$.

Experiment 4B: Untextured Road With a Local Adaptation Stimulus

Method.

The procedure and stimuli were identical to Experiment 1 except for the following. Drivers completed two no-expansion baseline and two adapt-local-contraction conditions with the order counterbalanced. In these sessions the observer's car traveled forward at a constant speed of 22 m/s. A constant driving speed was necessary in Experiment 4B to allow for control over the position and rate of contraction of the adaptation stimulus. The local adaptation stimulus was a red square that was centered at the focus of expansion. The initial side length of the adapting square was 4.7°. The square continuously decreased in size at a rate of 2.1°/s. Once the side length reached 1.6°, the square disappeared for 70 ms, reappeared at its original size, contracted in size, and so on. The flyback was never visible to the observer. This ramped contraction can also be thought of as a single object that first appears 30 m down the road from

the observer's car and moves away from the observer at a rate 35 m/s until it is 80 m from the observer's car. When the observer traveled over road segments in which another car was not present, the adaptation stimulus was presented again.

Results.

Figure 6E shows the mean critical TH for 8 observers. Despite the lack of road texture in Experiment 4B, the mean critical TH in the adapt-local-contraction condition (checkered bar) was significantly greater than the mean critical TH in the baseline condition, $t(14) = 2.50$, $p < 0.025$.

Discussion

In Experiment 4A, introducing a car-following task to the adaptation period effectively eliminated overtaking adaptation effects on a textured road. In Experiment 4B, we found a significant adaptation effect on an untextured road when observers adapted to a single contracting target centered on the focus of expansion. These two observations provide further evidence that changes in overtaking maneuvers following adaptation are primarily determined by the output of changing-size filters with receptive fields located near the focus of retinal image expansion.

Summary

We examined the effect of adaptation to expansion on overtaking maneuvers in a driving simulator. Following driving on a straight empty road for 5 min, drivers initiated overtaking substantially later (220—510 ms) than comparable maneuvers made following viewing a static scene or following 5 min of curve driving. Following adaptation to contraction (produced by driving backward), observers initiated overtaking significantly sooner. The removal of the road texture significantly reduced the size of the adaptation effect. We propose that these changes in overtaking behavior are due to misestimation of the time headway produced by local adaptation of looming detectors that signal

motion-in-depth for objects near the focus of expansion. This adaptation effect may increase the risk of rear-end collisions during highway driving.

2.1(c) Accuracy of estimating time to collision in one–eyed observers

This study has been completed and published: Steeves, J.K.E., Gray, R., Steinbach, M.J., & Regan, D. (2000). Accuracy of estimating time to collision using only monocular information in unilaterally enucleated observers and monocularly viewing normal controls. Vision Research, 40, 3783–3789. It was also reported to ARVO at their 2000 meeting.

Methods

Rather than using a real object moving in depth, an approaching object was simulated by creating the retinal images that would be produced by a rigid textured object moving at a constant speed in a straight line toward the viewer. A textured square consisting of a square array of regularly–spaced circular small dots was displayed on a 21 cm (vertical) x 28 cm (horizontal) Super VGA computer monitor that had a resolution of 600 x 480 pixels. The monitor ran at a rate of 30 frames/s and was viewed from a distance of 3 m. At this distance, the monitor subtended 5.3 x 4 deg. The size of the dots in the square array are described below. The luminance profile along any diameter of any given dot was a Gaussian waveform. Dot size, dot separation and the size of the array all increased so as to simulate the constant–speed approach of a real textured object. Further details of this stimulus are described in Gray and Regan (1999a).

Estimates of time to collision were measured using a staircase method developed by Gray and Regan (1996, 1998). The procedure was designed so that the number of trials in a run was sufficient to obtain reliable estimates of TTC but not too many as to cause appreciable adaptation due to repeated exposure to an expanding object (Regan & Beverley, 1978a,b, 1980; Beverley & Regan, 1979a,b; Regan & Hamstra, 1993). Also, the inter–trial interval was sufficiently long (8 s) to minimize adaptation.

Enucleated observers

Seven adult observers, one male and six female, who were unilaterally eye–enucleated for retinoblastoma, a rare childhood cancer of the retina, participated in this study. Age at enucleation ranged from 12 to 43 months (median age = 22 months) and age at testing ranged from 14 to 38 years (mean age = 23; median age = 22 years). For all observers, the remaining eye was ophthalmologically normal with normal visual acuity. Optical correction, if needed, was worn. For five observers, the left eye had been enucleated and for the two others the right eye had been enucleated.

Control Observers

Eighteen normally–sighted observers, ten male and eight female, served as controls. They viewed the stimulus monocularly with the non–preferred eye patched with translucent tape. The translucent tape, which allowed a small amount of light to reach the covered eye, was used in an attempt to minimize the effects of binocular rivalry. Form perception was not possible through the tape. Age at testing ranged from 14 to 46 years with a mean age of 27 and a median age of 26.5 years. All had normal or corrected–to-normal visual acuity in the viewing eye and showed stereopsis of 40 arcsec as measured by the Titmus test (Titmus Optical Co.) Optical correction., if needed, was worn. Four observers viewed with the left eye and 14 with the right.

Results

Consistent with previous findings, the majority of the control observers (13/18) underestimated TTC. One unilaterally enucleated observer was unable to produce reliable TTC estimates. The 95% confidence interval (CI) around the mean of the control group's mean percentage estimation errors (CI=2.04–6.68) was determined in order to compare performance between groups. Three out of the remaining six enucleated observers had larger estimation errors than the 95% CI of the mean of the control group. Two of these three observers showed a large overestimation while the third showed a large underestimation of TTC.

There was no significant correlation between percentage estimation error and age for either group. There was no significant relation between percentage estimation error and age a enucleation for he enucleated observers.

The stepwise regression analysis revealed that the variable that explained the largest amount of response variance for all subjects (both control and enucleated observers) was the time to collision. This indicates that, as instructed, all observers made judgements based on the task–relevent variable TTC [$\theta/(d\theta/dt)$]. Sixty–five to 94% of the variance was accounted for by the TTC variable for controls. These results are similar to the findings of Gray & Regan (1998). Sixty–one to 89% of the variance was accounted for by the TTC variable for enucleated observers. Task–irrelevent variables slightly but significantly influenced the judgements of some of the controls (8/18). Four observers were influenced by the square starting size (θ_0), three by the total change in size ($\Delta\theta$) and one by the rate of expansion of the square ($d\theta/dt$). These task–irrelevent variables accounted for an additional 2.8–9.4% of the variance. The enucleated observers showed a much more consistent pattern of judgement. Five out of six of the enucleated observers were significantly influenced by the task–irrelevent variable square starting size. This task–irrelevent variable accounted for an additional 2.8–10.1% of the variance for these observers.

Summary

Since individuals who have lost and eye early in life rely on monocular information, one asked if they would better estimate the time to collision (TTC) with an approaching object based on the monocular cue [$(\theta/(d\theta/dt)$, i.e. tau] than a control group using only monocular information. Estimates of TTC were measured with a simulated approaching textured object using a staircase procedure. Seven adult observers who were unilaterally enucleated at an early age were compared with 18 normally sighted control observers who viewed the stimuli monocularly. Consistent with previous findings, the majority of the controls (13/18) underestimated TTC. Three enucleated observers had larger estimation errors than the 95% confidence interval of the mean of the control group. One enucleated observer was unable to give reliable results. These results

suggest that unilaterally enucleated observers cannot estimate TTC accurately (and may even be worse) than normal controls when estimates are based on monocular information alone. Further, the majority (83%) of enucleated observers were influenced by perceived distance information derived from the object's initial size when estimating TTC with and approaching object. The use of this other optical variable could account for their reduction in performance. It was suggested that in every day life enucleated individuals make use of as many optical variables as possible to partially compensate for the lack of binocularity.

2.1(d) Collision avoidance in aviation and on the highway

An invited review on collision avoidance was published: Regan, D & Gray, R. (2000). Trends in Cognitive Science. This critical review includes a rationale for field research on visually–guided action using real aircraft.

2.1(e) Does perceived distance play a role in estimates of time to collision based on monocular information?

Long term aims 1.1.1 & 1.1.2

This study is completed and has been published. R. Gray and D. Regan (1999). Do monocular time to collision estimates necessarily involve perceived distance? Perception, 28, 1257–1264.

So far I have assumed that monocular estimates of TTC are based on *tau*, i.e. on the equation $TTC \approx \theta/(d\theta/dt)$, an equation that does not involve distance. I have also assumed that the perceived speed of motion in depth inversely proportional to TTF rather than being determined by the object's actual linear speed (Regan & Hamstra, 1993).

Adopting a quite different approach, some authors have proposed that human observers have access to accurate information about an object's absolute distance and its linear speed of approach, and can estimate TTC by dividing absolute distance by linear speed. A number of authors have attempted to distinguish between the two approaches but, according to Abernethy and Burgess–Limerick (1992), failed to find unequivocal support for one or other approach (reviewed in Gray & Regan, 1999b).

In an attempt to resolve this question we recently measured accuracy in estimating TTC at two viewing distances (1m and 5m) using the "match arrival time to the brief tone" method described earlier. The 5m display was made five times larger than the 1m display so that retinal image information about q/(dq/dt) was identical at the two distances and corresponded to the same TTC. All monocular and binocular cues to the distance of the displays were available.

Differences in estimated absolute TTC for the 5m and 1m viewing distances were very small and nonsignificant (3%, 0.3%, and 2.7% for three observers): the 5:1 variation in distance had essentially no effect on TTC estimation. We concluded that at least in our experimental conditions, observers ignore distance when estimating TTC on the basis of *tau*.

2.2 Visual Psychophysics

2.2(a) Coincidence detectors for luminance–defined form: Long–distance interactions in the early processing of spatial form.

Long–Term Aims 4.1.1, 4.1.2; Specific Aims 4.2.12, 4.2.13. Relevance: In this line of research we investigate the properties of mechanisms that, we suggest, provide "snapshots" of an objects boundaries. Our findings bear on the following: (a) relative importance of imaging an object's boundaries and its interior in flight simulators; (b) camouflage.

Two journal articles have been published: Kohly, R & Regan, D. (2000). Coincidence detectors: visual processing of a pair of lines and implications for shape discrimination. Vision Research, 40, 2291–2306; Kohly, R. & Regan, D (2002). Fast long-range interactions in the early processing of luminance–defined form. Vision Research, 42, 49-63. A book chapter has bee published: Regan, D. & Kohly, R.P. (2001). Selective–feature–based attention directed to a pair of lines: psychophysical evidence and a psychophysical model. In L. Harris & M. Jenkin (Eds.). Vision and Attention, Cambridge University Press, pp. 253-280. Results have been reported to ARVO at their 2000 meeting.

Background

What might be described as the standard model of the early processing of spatial form by the human visual system is framed in terms of the relative activity of an array of first–stage orientation–tuned spatial filters with strictly local receptive fields that are driven from one particular retinal location and respond to the target as a whole (reviewed in Graham, 1989 and Regan, 2000 pp. 140–154). Data reported by Morgan and Ward (1985) cannot be explained by this model. They found that the just–noticeable difference in separation between two test lines was not affected by random trial–to–trial variations in the locations of flanking lines. Because the flanking lines were very close to the test lines their variations of location would have corrupted the signals from any first–stage spatial filters that responded to both test lines. Morgan and Regan (1987) subsequently found that the just–noticeable difference in the separation of two test lines was not affected by random trial–to–trial variations in the contrast of one of the lines. One way of interpreting this finding is to state that, because the contrast variations produced random variations in the Fourier transform of the two lines as–a–whole, the discrimination task could not be based on the Fourier transform of the pair of lines, i.e. that the task was carried out in the spatial domain rather than in the spatial frequency domain. An alternative way of interpreting the finding is that the discrimination could not have been based on the relative activity of spatial filters with strictly local receptive fields that responded to both lines, i.e. the finding could not be explained in terms of the standard model (e.g. Wilson, 1991).

Morgan and Regan accounted for their data by proposing that the human visual system contains a second–stage mechanism that supports comparisons of the properties of localized targets that are situated some distance apart. In particular, they proposed that the human visual system contains *coincidence detectors* (Fig. 9), each of which has the following characteristics: (*i*) it is driven by two first–stage spatial filters, one of which is best driven from a particular retinal location, the other being best driven from a retinal location some distance away from the first; (*ii*) it is insensitive to stimuli that fall between the two receptive fields that feed it; (*iii*) it responds much more strongly to simultaneous than to successive stimulation of the two receptive fields that feed it. Morgan and Regan

(1987) proposed that the line separation discrimination threshold is determined by the pattern of activation within a population of coincidence detectors, each of which preferred a different line separation. This proposal accounted for their findings that the just–noticeable difference in line separation was not affected by random variations in the contrast of one line, and was independent of line contrast for contrasts more than about three times line detection contrast threshold.

Morgan et al. (1990) investigated whether observers could discriminate trial–to–trial variations in the relationship between two test targets while ignoring one or two noise targets located between the test targets, thus testing requirement *(ii)* above for coincidence detectors. The found that random trial–to–trial variations in the locations of the noise targets did not significantly affect discrimination threshold for the separation of the two test targets or for the verticality of the two targets.

These early studies did not fully test the hypothesis of coincidence detectors as set out above. First, the stimulus duration was 1000msec in the Morgan and Regan (1987) study and was probably not greatly shorter in the self–paced Morgan et al (1990) study. Such long presentation durations leave open the possibility that the discriminations were performed by shifting attention from one test target to the other. A second possibility is that observers paid attention to two locations simultaneously.

Methods

Stimulus and Apparatus:

Stimuli were generated by a PC containing D/A converters (Cambridge Instruments D300) and displayed on a large-screen electrostatically controlled monitor (Hewlett-Packard model 1321A) with green P31 phosphor. Optically superimposed on the monitor via a beam-splitting pellicle was a uniformly illuminated green screen which masked the slow phase of the phosphor afterglow of the line stimuli. The stimuli were presented in a darkened room on a large monitor and viewed from a distance of 290cm.

Fig. 10 illustrates the stimulus. There were two test lines and two "noise" lines. The noise lines were always placed between the test lines. The length of any given line was 0. 25 deg plus a random jitter of ± 20%. The line thickness was 0. 02 deg. Refresh rate was greater than 1000Hz.

When the four-line stimulus was presented in isolation a briefly lived afterimage was just detectable when the total energy delivered by the lines was 15 times (for author R. P. K.) or 25 times (for author D. R.) higher than the energy levels used in the experiment. Nevertheless, to curtail the effective duration of the stimulus we presented a 100msec masker immediately following each stimulus presentation. The width of the masker pattern was 1. 5 times the maximum width of the four-line pattern. Each of the 20 masker lines had an orientation that was selected randomly from the range of orientations of the test and noise lines. The location of each masker line was assigned randomly. Ten different masker patterns were pre-calibrated, and a random selection from the 10 was made after each presentation.

DC voltages controlled the separation, mean location, orientation difference and mean orientation of both the test and noise lines. The voltages were generated by digital-to-analog (D/A) converters within a second PC that controlled the psychophysical procedure. Responses were recorded through a button box connected to the second PC via A/D converters. Feedback was provided following each response.

EXPERIMENT 1

Purpose

The aim of Expt.1 was to find whether observers can compare two test lines so as to discriminate trial–to–trial variations in both their orientation difference and their mean orientation while ignoring trial–to–trial variations in the orientation difference and mean orientation of two noise lines located between the two test lines in a situation that rules out the following strategies: (a) shift attention from one test line to the other during the presentation; (b) attend to the locations of the test lines simultaneously.

Procedure

Fig.10A,B shows how M_T, S_T, α_T, β_T, M_N, S_N, α_N and β_N were defined. There were six values of each of the following variables, all symmetrically placed about zero: α_T; β_T; α_N; β_T. The range of variation of all four angles was ± 9 deg.

The set of 180 stimuli consisted of 5 subsets, each of 36 stimuli. Pairs of variables were rendered orthogonal within subsets as follows: (*i*) α_T, β_T; (*ii*) α_T, α_N; (*iii*) α_T, β_N; (*iv*) β_T, α_N; (*v*) β_T, β_N. Within any given subset the values of the two non–orthgonal variables were selected randomly from the six possible values. This ensured that it was not possible for an observer to know from which subset any given stimulus was drawn. Observers were instructed that, following each trial, they should signal whether the test lines were turned out (as in Fig. 10A) or turned in, and whether β_T was clockwise or anticlockwise of vertical. Discrimination thresholds (75% correct) were estimated by subjecting the response data to Probit analysis (Finney, 1971).

The separation of the noise lines was varied randomly by up to ± 0.2 deg (about a mean of 0.28 deg), and the separation of the test lines was randomly varied by up to ±0.2 deg (about a mean of 0.84 deg). The mean location of the test lines and the mean location of the noise lines coincided and was randomly varied by up to 0.25 deg. The resulting trial–to–trial jitter of line location ensured that the observers could not predict the location of either test line ahead of any given brief presentation. Indeed, either test line could fall on the location occupied by a noise line in the previous presentation.

For observer 1 all four lines were presented simultaneously for 20 ms. For the less experienced observers 2 and 3, presentation duration was 40ms rather than 20ms. To curtail the effective duration of the four–line presentation a 20–line masker pattern was presented immediately following (Fig. 10D).

Results and Discussion

In principle, two tasks and five stimulus subsets gives 20 possible graphs, but the design of the subsets meant that only the 12 graphs obtained from the following 12 combinations of subset and task–relevent variable were of interest:

Fig.9

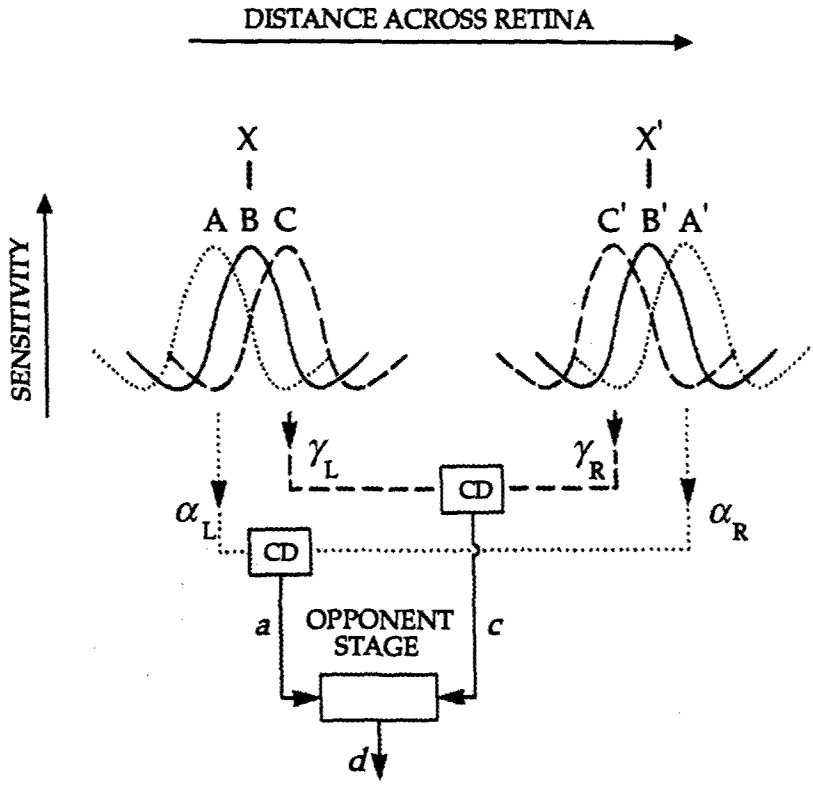

Coincidence detector model of line separation discrimination. Narrow spatial filters with strictly local receptive fields are connected in pairs to coincidence detectors (CD). If the separation of two lines (X & X') increases slightly, the outputs of the two most excited first–stage filters (B & B') change negligibly. But the outputs of less–strongly excited filters A & A' (i.e. α_L & α_R) will rise while the outputs of less–strongly excited filters C & C' (i.e. γ_L & γ_R) will fall. Consequently, coincidence detector output a will rise and coincidence detector output c will fall, thus producing output d from an opponent stage. Output d would assume the opposite sign if the separation of lines X and X' decreased. This arrangement unconfounds a change in the separation of the lines from a change in the contrast of one or of both lines. From Morgan, M.J. & Regan, D. (1987). Opponent model for line interval discrimination: interval and vernier performance compared. Vision Research, 27, 107–118.

Fig.10

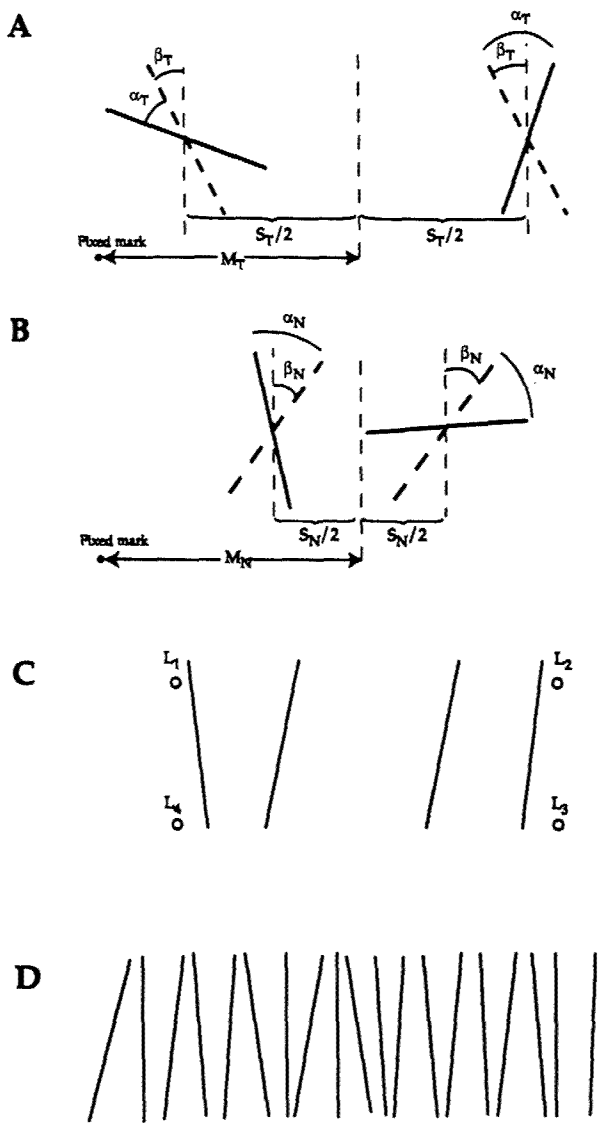

A: The mean orientation of the two test lines was bT deg, the difference between their orientations was $2\alpha_T$ deg, the separation between their midpoints was S_T deg of visual angle, and their midpoint was located M_T deg of visual angle from a fixed mark. B: Corresponding labels for the two "noise" lines were β_N, $2\alpha_N$, S_N and M_N. C: The four lines were combined to create the stimulus depicted; L_1–L_4 were LEDs. D: Following each 20 (or 40) msec presentation of stimulus C, a 20–line masker pattern was presented for 100msec.

Fig. 11

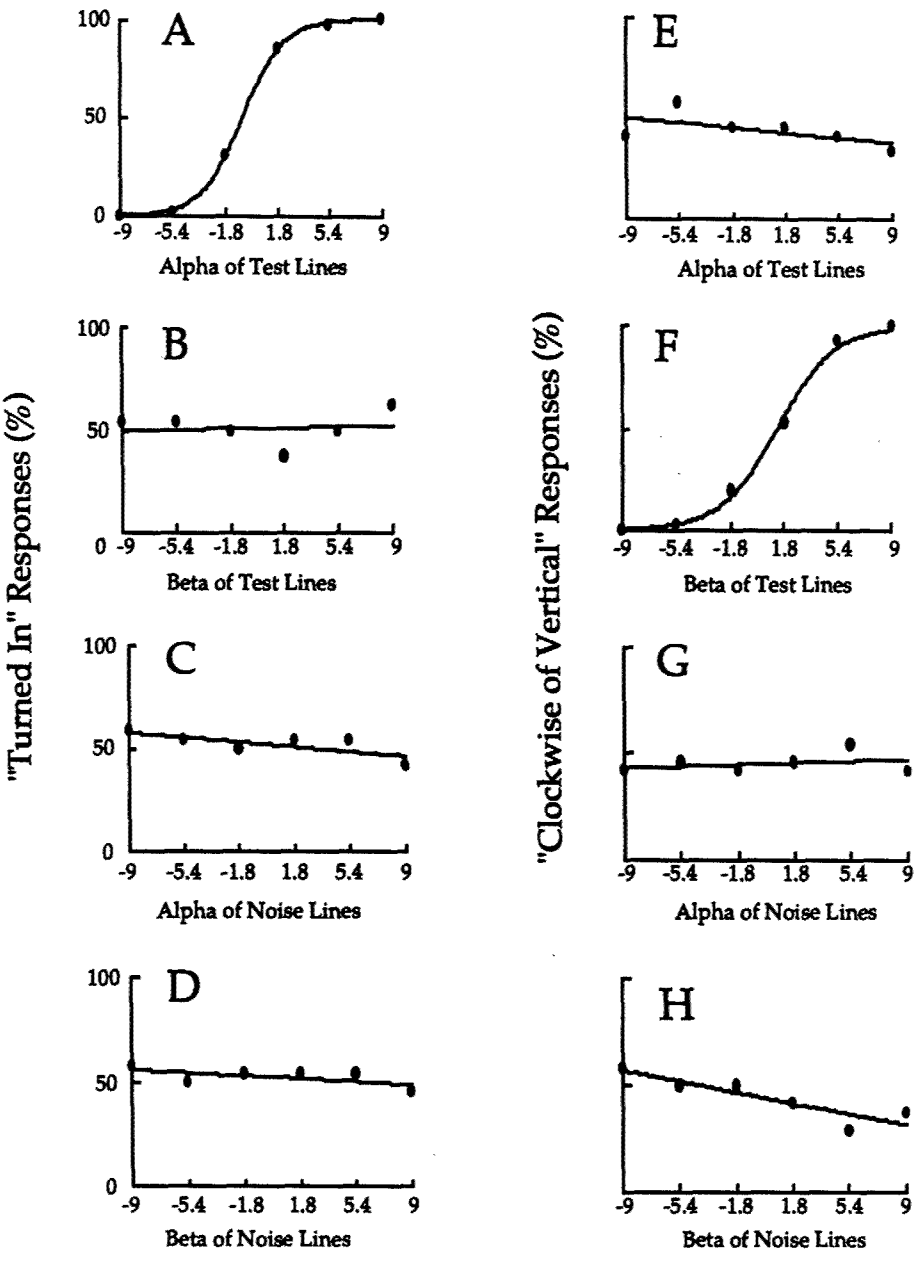

A total of 8 psychometric functions was obtained in experiment 1 where, following each presentations of the stimulus, the observer was required to discriminate both the difference between the orientations of the two test lines depicted in Fig.2 and their mean orientation. The data shown are for an SOA of zero. In this condition the observer based her discriminations of orientation difference on the task–relevant variable (steep slope in A) while ignoring trial–to–trial variations in the mean orientation of the test lines and the mean orientation and orientation difference of the noise lines (near–zero slopes in B, C & D respectively). Similarly, when discriminating mean orientation the observer based her responses on the task–relevant variable and ignored the noise lines. Observer 1.

Fig.12

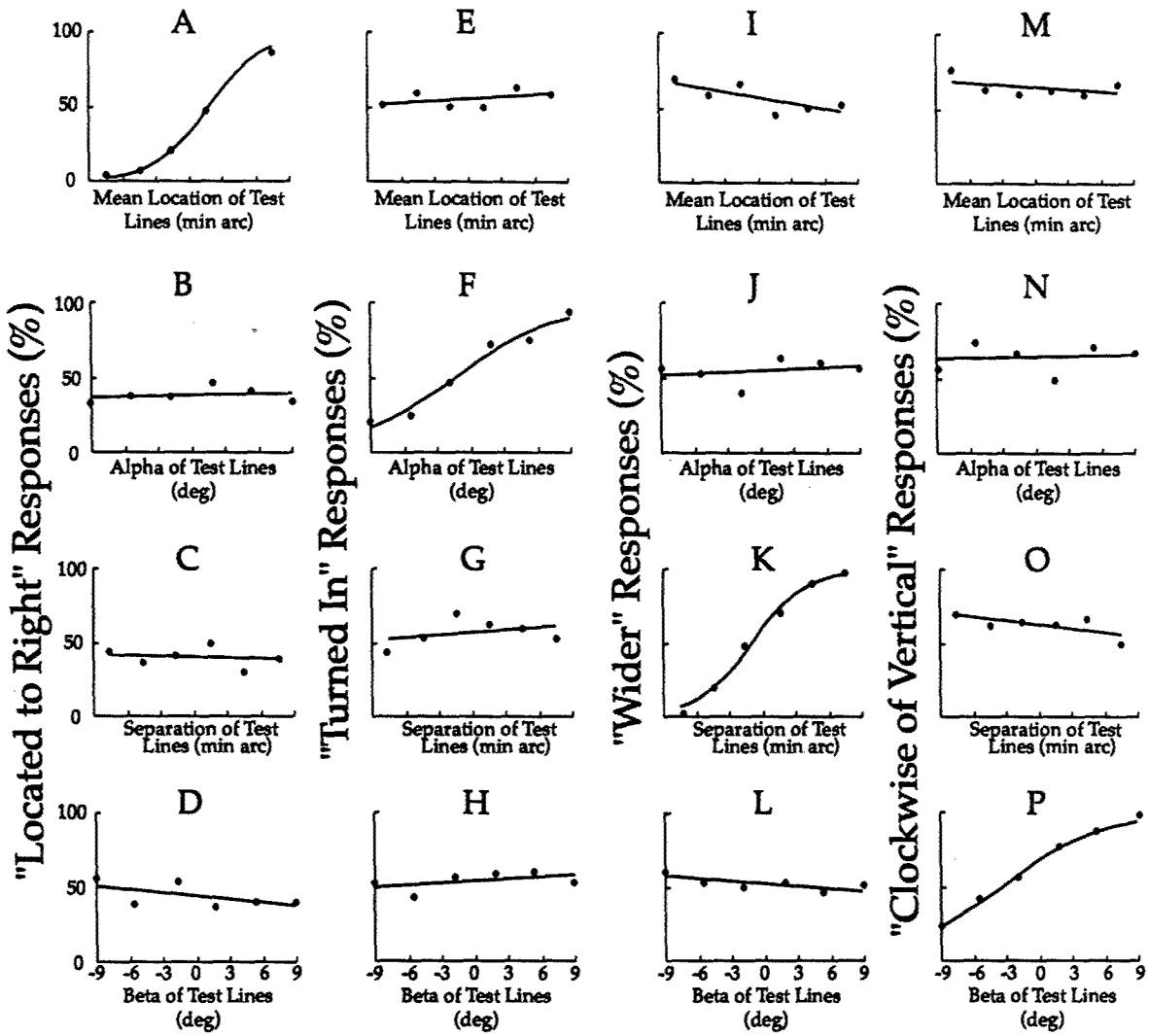

A total of 16 psychometric functions was obtained in Expt.2 where, following each presentation of the stimulus, the observer was required to discriminate four relationships between the two test lines. For each of the four discriminations (four columns) the plot with the task–relevant variable with abscissa was steep and the slopes with the three task–irrelevant variables were almost zero, indicating that the observer based her responses on the task–relevant variable while ignoring task–irrelvant variables for all four discriminations. Observer 1.

task–relevent variable α_T, subsets α_T β_T, α_T α_N, α_T β_N; task–relevent variable β_T, subsets α_T β_T, β_T α_N, β_T βN. When α_T was the task–relevent variable, the three plots of response probability vs. α_T were the same. (This confirmed that the observer's criterion from discriminating α_T was constant across the three subsets). Therefore, we collapsed these three psychometric functions so as to condense to 4 curves the data for which α_T was the task–relevent variable. Findings were similar when β_T was the task–relevent variable, so the data for Expt. 1 could be expressed in the form of 8 curves.

Fig. 11A–H shows these 8 curves obtained with zero SOA for observer 1. In Fig. 11A–D the observer's task was to discriminate the orientation difference of the two test lines ($2\alpha_T$). Discrimination threshold, estimated from the data shown in Fig. 11A, was 3.4 deg. Eyeball inspection shows that trial–to–trial variations of the task–relevent variable strongly influenced the observer's responses (Fig.11A) while simultaneous trial–to–trial variations of β_T had little or no effect (Fig. 11B). In Fig. 3E–H the observer's task was to discriminate the mean orientation of the two test lines (β_T). Discrimination threshold, estimated from the data shown in Fig. 11F, was 2.1 deg. Eyeball inspection shows that trial–to–trial variations in the task–relevent variable strongly influenced the observer's responses (Fig. 11F) while simultaneous trial–to–trial variations in α_T had little effect (Fig. 11E).

We conclude that the observer ignored β_T when discriminating α_T, and ignored α_T when discriminating β_T, a performance that could only be achieved by comparing the two test lines. (By reference to Fig. 10A it can be seen that the choice of equal range of variation for α_T and β_T ensured that simultaneous independent trial–to–trial variations in these two angles could only be unconfounded by comparing the orientations of the two test lines).

Because the presentation duration was only 20 msec, the comparison of the two test lines could not have been carried out by shifting either ocular

fixation or the focus of attention from one test line to the other: the shortest reported saccadic latency is 100–150ms (Kowler, 1990), and a shift of focal attention could not be achieved within 20ms (Reeves & Sperling, 1986; Sperling & Weichselgartner, 1995). Neither could the two lines have been compared by paying attention to two locations simultaneously because, as stated earlier, the random variations in the locations of the test and noise lines would have rendered ineffectual such a strategy. Our proposed explanation (Kohly & Regan, 2000) is that rather than attending to the outputs of first–stage spatial filters at two locations, either simultaneously or in succession, observers attended to the outputs of second–stage coincidence detectors and, in particular, to the population of coincidence detectors that signaled the widest separation of a line pair. (This would select the two test lines from the six possible combinations of the test and noise lines).

A comparison of Fig.11A, C & D shows that when discriminating the orientation difference of the test lines ($2\alpha_T$), trial–to–trial variations in neither the orientation difference ($2\alpha_N$) nor the mean orientation (β_N) of the noise lines had any appreciable influence on the observer's responses. The same was true when the observer discriminated the mean orientation (β_T) of the test lines (Fig. 11F, G & H).

The findings just reported can be explained in terms of a second–stage mechanism that compares the orientations of the two separated test lines while being insensitive to stimuli between the two test lines, this fulfilling requirements (*i*) and (*ii*) above for a coincidence detector. We assume that this second–stage mechanism encodes orthogonally the mean orientation and the orientation difference of the two test lines within 20ms (though the further processing of these encoded data that culminates in the observer's responses extends over a considerably longer duration).

Similar results were obtained from the two naïve observers.

EXPERIMENT 2

Purpose

The aim of Expt.2 was to find whether the human visual system can encode simultaneously four relationships between two separated test lines while ignoring stimuli located between the test lines.

METHODS

The range of variation in the lines' parameters were as follows: separation, 64-94 arc min (test), 8-38 arc min (noise); midpoint, ± 7.5 arc min (test and noise); α & β, ± 6 deg (test and noise, observer 1), ± 9 deg (test and noise, observer 2). Following each presentation of the four–line pattern (20 msec for observer 1, 40msec for observer 2) a 20–line masker was presented for 100 msec.

Observers had 4 tasks. They were instructed to signal after each presentation whether the midpoint (M_T) of the test lines was to the left of the mean of the stimulus set, whether the separation of the test lines (S_T) was larger than the mean of the stimulus set, whether the test lines were turned out or turned in, and whether their mean orientation was clockwise of vertical. The variation of M_T and S_T and the variations of α_T and β_T were such that the two discriminations could be carried out only by comparing the two test lines; the tasks could not be performed by attending to only one of the test lines, and we checked experimentally that this was correct.

In a subsidiary experiment observers carried out the four discrimination tasks one at a time. Observers 1 and 2 carried our Expt.2.

RESULTS

Eyeball inspection of the 16 psychometric functions shown in Fig. 12 indicated that, for each of the four discriminations, the responses of observer 1 were based on the task–relevant variable while she ignored all three task–irrelevent variables. We quantified this impression as follows. The first horizontal row of numbers in Table 1 were obtained by dividing the slopes in Fig. 12A, E, I & M respectively by the slope in Fig. 12A. They indicate that the responses of observer 1 were 6.8 times less affected by trial–to–trial variations in M_T when the task was to discriminate α_T than when the task was to discriminate

Table 1

			DISCRIMINATION TASK			
			M_T	α_T	S_T	β_T
OBSERVER 1	VARIABLE	M_T	1.0	0.15	0.06	0.16
		α_T	0.07	1.0	0.07	0.14
		S_T	<0.05	<0.05	1.0	<0.05
		β_T	0.11	0.10	0.14	1.0
OBSERVER 2		M_T	1.0	<0.05	0.15	0.07
		α_T	<0.05	1.0	<0.05	<0.05
		S_T	<0.05	0.08	1.0	0.11
		β_T	0.13	0.08	0.09	1.0

Normalized slopes of the 16 psychometric functions shown in Fig.12 for observer 1, and corresponding data for observer 2.

M_T, 16 times less than when the task was to discriminate S_T, and 6.4 times when the task was to discriminate β_T. (A value below about 0.3 in Table 1 means that the task–irrelevent variable was effectively ignored). Similarly the second row of numbers in Table 1 was calculated by dividing the slopes in Fig. 12B,F,J & N respectively by the slope in Fig. 12F and so on.

For observer 1 the ratio (4–task threshold)/(1–task threshold) was 0.90, 1.2, 0.85 and 1.1 for the M_T, α_T, S_T and β_T tasks respectively. Corresponding ratios for observer 2 were 0.79, 1.4, 0.88 and 1.2.

GENERAL DISCUSSION

In Expt. 1, the very brief presentation duration (20 or 40 msec) precluded any role of saccadic eye movements or shifts of locally–focussed attention in the immediate encoding of the four relationships between the two test lines, and the spatial jitter ruled out the possibility that observers compared the two test lines by attending to two spatial locations. If, as described above, we assume that observers selected the unique task–relevent population of second–stage coincidence detectors from the six activated populations by attending to the population that signaled the largest line spacing, our finding in Expt. 3 that observers could discriminate the mean orientation, orientation difference, separation, and mean location of the two test lines while ignoring all task–irrelevent variables implies that the output of any given coincidence detector signals these four orthogonally labeled relationships.

We assume that each discrimination threshold is determined by the pattern of activity among coincidence detectors, perhaps by an opponent process as proposed earlier in the case of line separation discrimination threshold (Morgan & Regan, 1987, see Fig.9).

The long–distance comparator proposed by Morgan and Regan (1987)—their 'coincidence detector'—as an explanation for the psychophysical characteristics of line separation discrimination received inputs from two distant first-stage spatial filters that preferred the same orientation (Fig.9). This arrangement does not account for the findings of Expt.1, because the

Fig.13

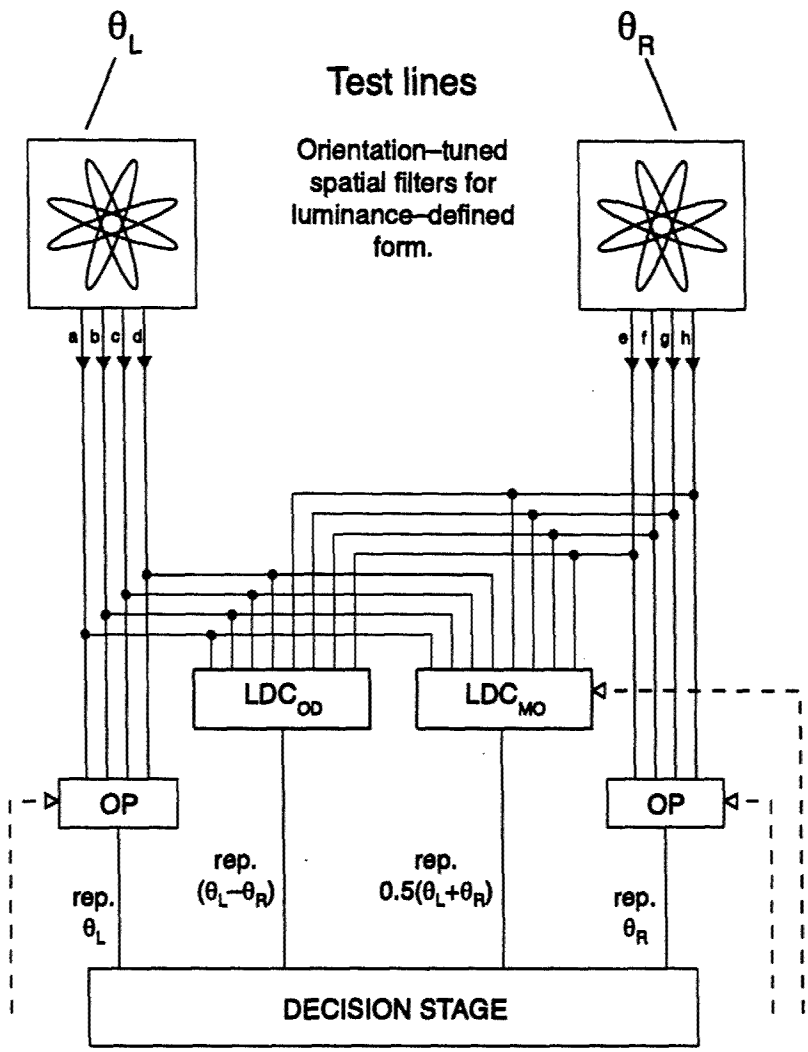

Schematic of a model of the discrimination of the orientation difference and mean orientation of two separated lines in Expt. 1. Key: LD_{COD} and LD_{CMO}, long distance comparator whose outputs neurally–represent the orientation difference and mean orientation of the test lines respectively; OP, a stage that is sensitive (perhaps through opponent–processing) to the pattern within the outputs of the first–stage filters. The results of Expt.3 are consistent with the hypothesis that the two long-distance comparators illustrated are merged, into one, whose output is a line labelled for line separation and mean location as well as for $(\theta_L - \theta_R)$ and $0.5(\theta_L + \theta_R)$.

orientations of the left and right test lines are generally different. This means that the two inputs to our proposed long–distance comparator must carry information as to the orientation of the left test line and of the right test line, and that both the accuracy and precision of this information are better than ca. 2–3 deg—much finer than the bandwidths of the most sharply–tuned neurons in striate cortex (DeValois, Yund & Hepler, 1982).

We note here a related problem. It is well known that orientation discrimination threshold for a foveally–viewed grating or line is (at ca. 0.3–0.6 deg) considerably finer than the bandwidths of the most sharply–tuned neurons in striate cortex. A proposed explanation is that orientation discrimination threshold is determined by the pattern of activity among a population of orientation–tuned neurons (Westheimer et al., 1976). Regan and Beverley (1985) reported the following empirical support for this suggestion. After viewing a high–contrast adapting grating, orientation discrimination threshold for a test grating was elevated, but this elevation was not at the adapting orientation but at orientations 11–17 deg to either side of the adapting orientation. The explanation they offered for this finding was that the most important neurons for discriminating the orientation of a test grating were not those most excited by the test grating, but rather those whose sensitivity profiles were steepest at the orientation of the test grating. As to a possible mechanism they suggested opponent processing (opponent–orientation).

In our present context, and for the purpose of argument, we follow the proposal of Regan and Price (1986) that the number of spatial filters that are served from any given small area of the retina and that are sharply tuned to orientation is small—possibly comprising two inclined at about 15 deg to the vertical, and two inclined at about 15 deg to the horizontal. (This arrangement causes the lowest discrimination thresholds to be for near–vertical and near–horizontal targets). In Fig. 13 we show four orientation–tuned filters at this first stage. The outputs (*a*, *b*, *c*, & *d*) of these filters are each labelled for the filter's preferred orientation (Thomas & Gille, 1979). Following stimulation by the left test line, fine–grain information about its orientation (θ_L) (carried in terms of the pattern within signals *a*, *b*, *c*, & *d*) reaches a stage sensitive to this pattern (an

opponent–process stage, OP) where, in our particular task, it is compared with a template neural representation of vertical. One way in which this template might be created is that a task–dependent descending signal (dashed line) would represent equal outputs from first–stage filters that prefer orientations symmetrically inclined about the vertical. We suppose that orientation discrimination for the right test line alone can be explained analogously.

As already mentioned, signals that carry information about the left and right test lines from all 8 first–stage filters reach a long–distance comparator, where the fine–grain information about the left line's orientation (carried in terms of the pattern within signals *a*, *b*, *c* & *d*) is compared with fine–grain information about the right line's orientation (carried in terms of the pattern within signals *e*, *f*, *g*, & *h*). The outputs of the long–distance comparators (LDC_{OD} and LDC_{MO}) neurally–represent (θ_L–θ_R) and $0.5(\theta_L$ & $\theta_R)$ respectively with degree–level accuracy and precision.

Our finding that orientation discrimination threshold for the left or for the right test line alone was *higher* than threshold for mean orientation rejects the hypothesis that the information that supports discrimination of the orientation (θ_L) of the left line alone and the information that supports discrimination of the orientation (θ_R) of the right line alone pass directly to a long–distance comparator that computes the mean orientation $0.5(\theta_R+\theta_L)$. (The long–distance comparator could not lose a negative amount of information). One possible explanation is that more information is lost in the processing stages marked OP in Fig. 13 than in the stage marked LDC_{MO}.

As far as the orientation difference [(θ_L–θ_R)] signal is concerned ,one possible explanation is that comparing the orientations of two physically present lines might lose less information than comparing the orientation of a physically–present line with an internal template of the vertical.

These findings leave us with the question of what role coincidence detectors might play in everyday vision. Our suggestion is based on findings that our eyes examine the visual environment by successively foveating different

locations, resting for perhaps 200 msec on each location, and moving from one location to the next by executing a rapid saccade (Kowler, 1990). We propose that, following each saccade, coincidence detectors provide a near–instantaneous 'snapshot' of an object, an initial 'snapshot' that provides a full description of the object's boundaries while ignoring its internal structure.

Summary

Within a duration of 20msec humans can encode the mean orientation and orientation difference of two test lines while ignoring stimuli in the space between the test lines. Furthermore, performance is not impaired by randomly varying the location of each test line from trial to trial. We conclude that the two test lines are not compared by shifting eye fixation or attention from one to the other, nor by attending to two spatial locations. This evidence is consistent with the proposal that the human visual system contains coincidence detectors that respond to simultaneous stimulation of two conventional first–stage spatial filters located some distance apart and are insensitive to stimuli that fall between these two filters. We suggest that our observers performed discriminations by attending to the outputs of coincidence detectors rather than by attending to two spatial locations. In addition to their mean orientation and orientation difference, humans can simultaneously encode the separation and mean location of the two test lines while ignoring stimuli in the space between the lines. We suggest that, following each of the eye's exploratory saccades, coincidence detectors , in effect, take a snapshot of the retinal image so as to encode the shape of an object's boundaries.

Our proposal that the human visual system contains long–distance comparator mechanisms whose outputs orthogonally signal the mean orientation of the two test lines independently of their difference in orientation might account for the finding reported by Li & Westheimer (1997) that observers can discriminate the implicit orientation of a crossed pair of lines or the implicit orientation of an ellipse.

Our finding that observers can dissociate and discriminate simultaneous trial-to-trial variations in both the separation and the difference in orientation of

two lines provides independent evidence in support of the hypothesis put forward by Wilson and Richard (1989) that the curvature of a line is encoded in terms of the separation and difference in preferred orientation of two narrow spatial filters that are fed from distant locations.

Our proposal that the human visual system contains long–distance comparator mechanisms that signal the difference in the orientations of a pair of lines independently of their mean orientation might account for our finding that observers can make acute discriminations of both Vee angle and the angle contained by crossed lines even when there are large random trial-to-trial rotations of the Vee or cross (Regan & Hamstra, 1992; Regan et al. , 1996; Chen & Levi, 1996).

Long–distance comparator mechanisms that signal the mean location of two test lines independently of their separation, orientation difference and mean orientation would encode the local location of what has been termed the *core* of a shape (Burbeck & Pizer, 1995).

Finally, the long–distance comparator mechanisms for contour separation could account for the finding that the aspect-ratio aftereffect caused by inspecting a solid sharp-edged rectangle transfers to an outlined ellipse (Regan & Hamstra, 1992). It might also explain why we can recognize a given shape whether it is the shape of a solid or the shape of an outlined figure - a problem of historical interest to the Gestaltists (Ellis, 1967; Koffka, 1935).

2.2(b) Long–distance interactions in the early processing of cyclopean form

One paper has been published: Kohly, R. & Regan, D. (2001). Long–distance interactions in cyclopean vision. Proceedings of the Royal Society of London, B, 268, 213–219.

Background

Although, in the years following Wheatstone's paper in 1838 the vivid depth created by a stereoviewer was commonly attributed to binocular disparity, the stereo line drawings that he used contained monocular as well as binocular cues to depth as do almost all stereo photographs. A demonstration

that binocular disparity alone can support the perception of spatial form by breaking camouflage was not available until Julesz isolated neural processing that occurs after signals from the left and right eyes have converged. He did this by creating patterns that contain no monocularly–available cues to the camouflaged form (Julesz, 1960). A Julesz random dot stereogram consists of randomly located texture elements such as dots. One eye views such a pattern that is identical to the pattern viewed by the other eye except that one or more parts of the pattern are shifted bodily to the left or right. The resulting empty areas are filled in with more random dots. In monocular view the shifted area(s) are perfectly camouflaged: each pattern looks like a flat array of random dots. In binocularly–fused vision, however, normally sighted individuals see the camouflaged form. Furthermore, the camouflaged form is perceived in vivid depth. Many dramatic illustrations are to be found in Julesz (1971). Julesz called this kind of vision *cyclopean* and the kind of form seen in random dot stereograms *cyclopean form*. The spatial properties of cyclopean perception have been recently reviewed (Regan, 2000,, pp.343-374). In this paper we used random dot stereograms, one of which is illustrated in Figure 14.

Current models of the early processing of cyclopean form are chiefly based on experimentally–measured changes in detection threshold caused by adaptation or masking. The stimuli used in these experiments were either cyclopean gratings or more localized stimuli such as a cyclopean difference of Gaussians (DOG). The resulting models are framed in terms of a parallel array of first–stage cyclopean spatial filters, each of which has a strictly local receptive field and is tuned to both spatial frequency and orientation. Each small area of the retina feeds a small number of filters that prefer different spatial frequencies and orientations (Julesz, 1975; Schumer & Ganz, 1979; Tyler, 1983, 1991, 1995; Yang & Blake, 1991; Cormack et al., 1993).

The contrast sensitivity curve for cyclopean gratings falls off from 0.5–1.0 cycles/deg to give a grating acuity of only about 4 cycles/deg (Tyler, 1974). If the cyclopean visual system were linear, this low acuity would conflict with the findings that cyclopean vernier acuity is 40 arc sec. (Morgan, 1986) and aspect ratio discrimination threshold for a cyclopean rectangle of mean area 1.0 deg^2

can be as low as 3% (Regan & Hamstra, 1994). A proposed explanation for these findings, and for the observation that a cyclopean boundary can appear sharp (for a demonstration, see Fig.2A in Regan & Hamstra, 1994), is that the subjective sharpness of a cyclopean edge as well as threshold for the relative position of the edge is determined by the pattern of activity among an array of cyclopean filters that serve different locations along a line that straddles the edge (Regan, 1991). This proposal can be reconciled with the finding that cyclopean grating acuity is low if we assume that the cyclopean visual system exhibits the following nonlinear behaviour: the second–stage edge–sharpening spatially–integrative process that supports high sensitivity for the relative position of an isolated cyclopean edge is disrupted when there is more than one disparity gradient within its summation field (Regan, 1991).

Not only is orientation discrimination threshold for a cyclopean bar (0.6–1.5 deg according to Mustillo et al., 1988 and Hamstra and Regan, 1995) far lower than the orientation tuning bandwidth for cyclopean filters, it is even lower than the orientation tuning bandwidth for the most sharply–tuned striate cortical neurons that respond to luminance–defined gratings (DeValois et al., 1982). A proposed explanation for this conflict is that orientation discrimination threshold is determined by the pattern of activation within a population of neurons that are tuned to the orientation of cyclopean targets, each of which prefers a different orientation.

So far we have discussed models that seek to explain spatial discriminations in terms of the relative activity of first-stage cyclopean filters, each of which is driven from a small area of the binocular visual field. Such models could be couched in a line–element format analogous to the Wilson and Gelb (1984) line–element model of spatial discriminations for luminance–defined form in which the outputs of cyclopean filters would be represented in a multidimensional filter–output space. Alternatively, an opponent–process approach could be adopted in which, as already mentioned, discrimination thresholds are determined by the relative activation of cyclopean filters driven from a small area of the binocular visual field (Regan, 1991). (The so–called

combinational objection to the opponent–process approach is discussed in the Appendix to Kohly and Regan, 2000).

In this paper we report findings that do not fit within the framework of current models of cyclopean vision. In particular, these new findings cannot be described fully in terms of the pattern of activity within the outputs of first–stage cyclopean filters, each of which is driven from a small area of the visual field. These findings require a second stage of processing that involves long–distance cyclopean interactions.

Methods

Stimulus and apparatus

Cyclopean stimuli were generated by a PC that contained 16 bit D/A converters (Cambridge Instruments model D300) and displayed on a large–screen electrostatically driven monitor (Hewlett–Packard model 1321A) with green P31 phosphor. This arrangement gave a maximum of approximately 65,000 x 65,000 (i.e. $4x10^9$) possible locations within the display. A complete stereopair was displayed every 27.4 msec. The monitor was viewed through a pair of high–speed goggles (Cambridge Instruments model FE1) that was switched in synchrony with the presentations of the left and right eye's components of a stereopair. The pattern subtended 12 x 12 deg. Each test bar had a constant width of 0.64 deg, and the mean width of the noise bar was 0.80 deg. Each eye saw 3500 dots. Any given dot subtended 2.4 arc min. Stimuli were presented in a darkened room and viewed from a distance of 143 cm.

Fig. 15 explains the meaning of α_T, β_T, S_T, M_T, β_N, W_N and M_N. Fig. 13 allows the reader to experience a typical test stimulus.

To constrain the effective duration of the stimulus by curtailing neural persistence and abolishing iconic memory, a masker was presented for 112msec immediately after each test presentation. The masker was 8 cyclopean bars, each of whose orientation was selected randomly from within the range of test bar orientations. Masker bars were 0.64 deg wide. The location of any given masker bar was assigned randomly within a region 1.5 times wider than the widest three–bar test display. Ten different masker patterns were pre–computed, and

each masker presentation was a random selection from the ten. The disparities of the test bars, noise bar and masker bars were equal. The purpose of the masker was to allow us to test whether the early processing and encoding of the four relationships between the two test bars was carried out in parallel.

EXPERIMENT 1

Purpose

The purpose of Expt. 1 was to find whether observers can, following each single presentation, discriminate trial–to–trial variations in the orientation difference, mean orientation, separation and mean location of a pair of cyclopean test bars while ignoring all task–irrelevent variables including trial–to–trial variations in the orientation, width and location of a central noise bar.

METHODS

Rationale

We varied α_T and β_T simultaneously and orthogonally with the maximum variation of α_T exactly the same as the maximum variation of β_T. This ensured that neither bar alone provided a reliable cue to either angle discrimination task. Our purpose was to force observers to base their responses on a comparison of the two test bars (see Fig. 15 for an explanation of symbols).

We varied M_T and S_T simultaneously and orthogonally with the maximum variation of M_T exactly half the maximum variation of S_T. This ensured that neither bar alone provided a reliable cue to discriminating either M_T or S_T. Our purpose was to force observers to base discriminations of M_T and S_T on a comparison of both lines.

We ensured that the output of any first–stage cyclopean filter with a strictly local receptive field that responded to both test lines would be corrupted by randomly varying the orientation (β_N), width (W_N) and location (M_N) of the central noise bar on a trial–to–trial basis. The maximum variation of β_N was

Fig.14

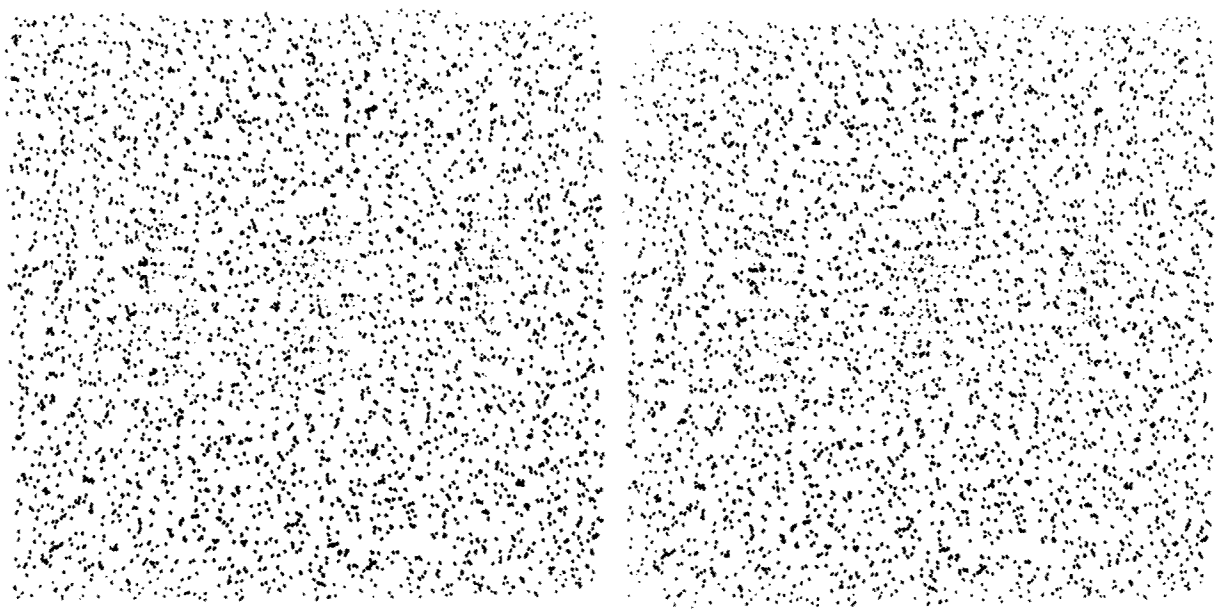

Photograph of a typical test stimulus. Place a pencil point above the page at such a height that it appears to be centred on the right half of the stereopair when the right eye is closed and centred on the left half of the stereopair when the left eye is closed. Now stare at the pencil point. The cyclopean bars will slowly emerge. The faint dots in the plane of the background that can be seen within the bars in the photograph were not visible to the eye during the experiment and, therefore, provided no monocular cue to the bars.

Fig.15

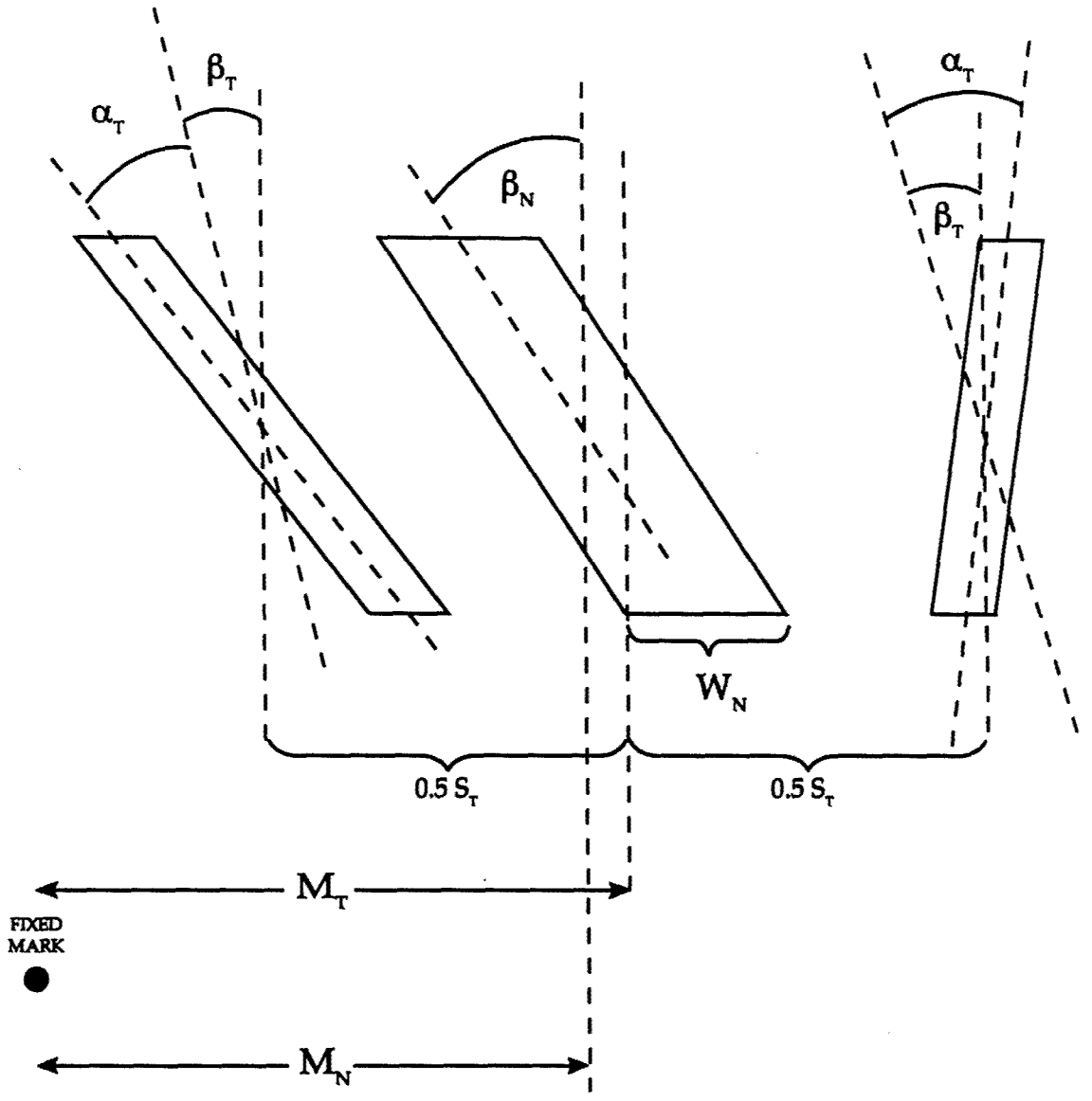

Key to symbols. The figure depicts two test bars with mean orientation b_T, orientation difference $2\alpha_T$, separation S_T and mean location M_T. B: Between the two test bars is a "noise" bar of orientation β_N, width W_N, and location M_N. Note that angles α_T, β_T and β_N are exaggerated for clarity.

equal to the maximum variation of β_T. The maximum variation of M_N was equal to the maximum variation of M_T.

Stimulus organization

The mean value of β_T was vertical (0 deg). In the set of 216 stimuli there were six values of α_T and six values of β_T, all symmetrically placed about zero. The range of values for α_T and β_T was ±9 deg. In the set of 216 stimuli there were six values of M_T and six values of S_T. The range of values of M_T was ± 24 arc min, and the range of values of S_T was 5.7 to 7.3 deg (i.e. ± 48 arc min).

Test stimuli were divided into six subsets. Within any given subset two of the variables α_T, β_T, M_T and S_T were orthogonal (i.e., had zero correlation). Having 6 subsets allowed every possible pair of these four variables to be rendered orthogonal within at least one subset. In any given subset the values of the non–orthogonal variables were randomly selected from the possible six values. This procedure ensured that an observer could not know from which subset any given stimulus were drawn and, therefore, could not vary his or her criterion according to subset.

Procedure

Each trial consisted of a single presentation of one of the 216 test stimuli. For observer 1 the presentation duration was 82.3 msec in most experiments, but some data were collected with a 54.9 msec presentation duration. For technical reasons, when the shorter duration was used only three variables were discriminated (α_T, β_T and S_T). The less practiced observers 1 and 2 were unable to provide low–noise data when the presentation duration was 82.3 msec. Presentation duration was set at 192 msec for the observer 2, and 247 msec for observer 3. The observer was required to make four different classifications after each trial. In particular, the observer's task was to signal after each trial whether: (a) the test bars were configured like an inverted Vee (as in Fig. 2) or like a Vee; (b) whether the mean orientation of the two test bars was clockwise or

anticlockwise of vertical; (c) whether the mean location of the two test bars was to the left or to the right of the mean of the stimulus set; (d) whether the separation of the test bars was larger or smaller than the mean of the stimulus set. Feedback was provided.

RESULTS

Each run of 216 trials produced 16 psychometric functions. For the condition that M_T was the task–relevent variable we plotted the percentage of "mean location of the two test bars to the right of the mean of the stimulus set" responses versus all four variables, giving four psychometric functions. The 0%–100% plot versus the task–relevent variable was steep, indicating that trial-to–trial variations of M_T strongly affected the observers' responses. In contrast, the plots of "mean location to the right responses" versus each of the three task–irrelvent variables (i.e., S_T, α_T, and β_T) were approximately flat, indicating that the observers ignored trial-to-trial variations in α_T, S_T and β_T when discriminating trial–to–trial variations in M_T.

Next we describe how we quantified this qualitative impression. First, by subjecting each of the 4 sets of response data to Probit analysis (Finney, 1971), we estimated the distance along each abscissa between the 25% and 75% response points. Then, following the standard procedure, each of the 16 distances was divided by two. These data (in degrees) are set out in the third column of Table 2 for observer 1 using an 82 msec presentation duration.

Analogously, when β_T was the task-relevant variable each observer's 0%–100% plot of the percentage of "mean orientation of the two test bars was clockwise" versus β_T was steep, while the three plots of the same response data versus the three task–irrelvent variables (α_T, M_T and S_T) were approximately flat. We analyzed these response data in the same way as the response data for M_T discriminations, and the results are set out in the sixth column of Table 2. The

fourth and fifth columns of Table 1 show corresponding data for discriminating trial–to–trial variations in α_T and S_T.

When the task was to discriminate M_T and the variable was M_T, the number given in Table 2 was the *discrimination threshold* for M_T. Similarly, when the task was to discriminate α_T and the variable was α_T, the number given in Table 2 was the discrimination threshold for α_T, and so on for S_T and β_T.

To compare data on dimensionally–dissimilar variables (orientation and distance) we normalized the numbers set out in Table 2 by dividing all the numbers with M_T as variable with the number when M_T was both the task and the variable. Similarly, we divided all the numbers with α_T as variable with the number when α_T was both the task and the variable, and so on for the remaining variables S_T and β_T. This converted all the numbers set out in Table 2 to dimensionless ratios. Table 3 sets out these normalized data for observer 1. We used this table as follows. The smallest ratio for the three task–irrelevent variables in column 3 of Table 2 is 29. We take this number (the *confidence ratio*) as a measure of our confidence that, when instructed to discriminate M_T, observer 1 ignored all task–irrelevent variables. A similar argument applies when the task–relevent variable was α_T, S_T or β_T (columns 3–6 respectively in Table 2). We have used a closely related statistic in previous studies (Kohly & Regan, 1999, 2000). When observer 1 used the 55 msec presentation duration her thresholds were a little higher than for the 82 msec condition, but she still based her responses on the task–relevent variables. Confidence ratios and discrimination thresholds for all three observers are listed in Table 4. The thresholds listed in Table 4 are higher than are obtained with presentation durations of one sec. or longer. We used the shortest presentation duration compatible with a tolerable signal–to–noise ratio in our data.

We repeated the experiment just described with the central noise bar removed, and compared the four thresholds in the "with noise bar" and "without noise bar" conditions by subjecting each threshold to a two–tailed

Fig.16

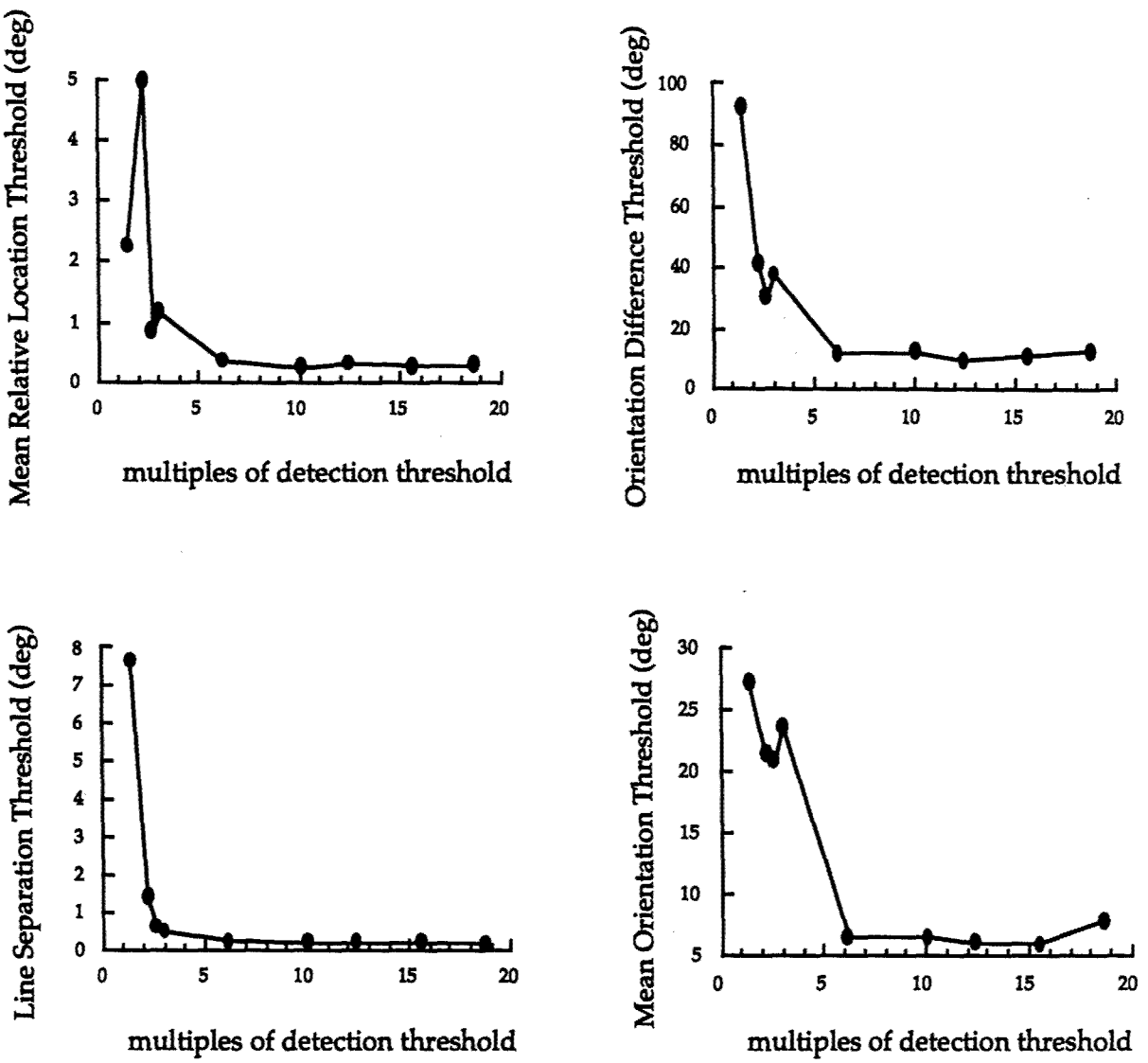

Effect of the relative disparity of the bars (abscissae) on the four discrimination thresholds (ordinates). Disparity is expressed as a multiple of the relative disparity at bar detection threshold.

Table 2

		TASK			
		M_T	α_T	S_T	β_T
VARIABLE	M_T	0.34	13	7.7	542
	α_T	171	5.9	306	102
	S_T	12.3	3.7	0.37	7.4
	β_T	194	171	35	6.5

Estimates, obtained by Probit analysis, of the distances (in deg.) between the 25% and 75% response points on the 16 psychometric functions derived from the four–task response data. Observer 1 (author R.P.K., presentation duration 82 msec).

Table 3

		TASK			
		M_T	α_T	S_T	β_T
VARIABLE	M_T	1.0	38	23	>100
	α_T	29	1.0	52	17
	S_T	33	10	1.0	20
	β_T	30	26	5.0	1.0

The data shown in Table 2 normalised to dimensionless ratios. Observer 1 (author R.P.K.)

Table 4

OBSERVER	DISCRIMINATION TASK	THRESHOLD (S.E.)	CONFIDENCE RATIO
1	Mean location	0.34 (0.03)	29
	Orientation Difference	12 (1)	10
	Separation	0.37 (0.04)	5
	Mean Orientation	6.4 (0.6)	17
2	Mean location	0.26 (0.03)	2.6
	Orientation Difference	14 (2)	3.3
	Separation	0.32 (0.04)	2.9
	Mean Orientation	5.5 (1)	4.7
3	Mean location	0.25 (0.03)	4.2
	Orientation Difference	14 (2)	5.1
	Separation	0.23 (0.02)	7.2
	Mean Orientation	7.0 (0.8)	4.6

Discrimination thresholds (in degrees) and confidence ratios for the four tasks. Results shown for three observers.

dependent t-test. The pairs of thresholds for M_T, α_T, S_T and β_T respectively gave the following results. Observer 1: p>0.41, >0.43, >0.99, >0.20; observer 2: p>0.07, >0.68, >0.23, >0.26; observer 3: p>0.54, >0.12, >0.14, >0.04. Thus, the presence of the noise bar had no significant effect on 11 of the 12 thresholds for the three observers; for observer 3 one of his four thresholds showed a significant difference at the 0.05 level for observer 3.

EXPERIMENT 2

The purpose of Expt. 2 was to find how the four discrimination thresholds were affected by the relative disparity of the test bars.

METHODS

In the first part of Expt. 2 we used a one–interval yes–no psychophysical design to measure the disparity required to just detect the cyclopean test bars (Macmillan & Creelman, 1991). Each trial consisted of a single presentation of the same duration as was used in Expt. 1. There were two classes of stimuli: the test bars were either presented or not presented. However the noise bars and the masker bars were always presented. Equal numbers of the two classes were presented during any given run. The observer's task was to signal whether the test bars had been presented. In the second part of Expt. 2 the stimuli set and procedures were as the first part of Expt. 1, but we varied the relative disparity of the bars over a wide range. Observer 1 carried out Expt. 2.

Results

Experiment 2

Relative disparity is expressed In Fig. 16 as a multiple of the 1.4 arc min test bar detection threshold. Fig. 16 shows that all four discrimination thresholds were independent of relative disparity for relative disparities more than about 2–5 times above bar detection threshold. The onset of diplopia was at about 20 min arc relative disparity.

EXPERIMENT 3

The purpose of Expt. 3 was to compare the discrimination threshold for the cyclopean bars used in Expt. 1 with corresponding thresholds for luminance–defined bars. The procedure was the same as in Expt. 1 except that all dots outside the three bars were switched off. Observer 1 carried out Expt. 3.

Results

The thresholds for M_T, α_T, S_T and β_T were 0.41, 6.2, 0.24 and 4.6°, respectively. These thresholds were little different from those listed in table 1.

Discussion

How did observers compare the two cyclopean test bars? In principle, one way would be to shift fixation (i.e. saccade) from one to the other bar. For observer 1, however, this would not be possible within an 82 msec presentation duration (Tables 1&2), and certainly not within a 55 msec presentation duration: the shortest reported saccade latency is 100-150 msec (Kowler, 1990). In any case, the location of one or other test bar varied unpredictably over a range of 96 arc min so that, in general, a successive–fixation strategy would require a saccade to one test bar followed by a second saccade to the other test bar. We conclude that, at least for observer 1, information about relations between the two test lines was processed in parallel.

Our observers ignored trial–to–trial variations in the orientation, width, and location of a third cyclopean bar that was placed between the two test bars. First–stage cyclopean filters with strictly local receptive fields that responded to both test bars must necessarily have been stimulated by the third bar also. Our findings can be understood of the visual systems of at least some individuals contain long–distance cyclopean second–stage mechanisms that compare information about a pair of cyclopean bars but are insensitive to cyclopean stimuli located between the two bars.

Our finding that the four kinds of discrimination thresholds did not change when the central noise bar was removed is consistent with the idea that the proposed long–distance comparators determine discrimination threshold

even when first–stage cyclopean filters driven from a single area of the retina could, in principle, provide reliable task–relevent information.

Now we turn to the question of orthogonality. To distinguish between trial–to–trial variations of α_T and β_T it was necessary to compare the two test bars. With one test bar removed, the ratio between the slopes of the psychometric functions whose abscissae were, respectively, α_T and β_T would not be affected by changing the task from discriminating α_T to discriminating β_T. But with both test bars present, when the task was changed the ratio changed by a factor of 448, 21 and 27 respectively for observers 1–3. Again, to distinguish between trial–to–trial variations in M_T and S_T it was necessary to compare the two test bars. With one test bar removed, the ratio between the slopes of the psychometric functions whose abscissae were, respectively, M_T and S_T would not be affected by changing the task from discriminating M_T to discriminating S_T. But with both bars present, when the task was changed the ratio changed by a factor of 1680, 16, and 126 respectively for observers 1–3. One these grounds, and on the basis of the data in Table 3, we conclude that the proposed long–distance cyclopean comparator mechanisms encode, near–orthogonally, the mean orientation, orientation difference, mean location, and separation of a pair of bars: crosstalk can be considerably less than 1%.

There is a sizeable literature on the theoretical construct *focal spatial attention*. Some authors have suggested that visual attention acts like a spotlight focussed on some discrete location (Posner et al., 1980), while others have used the metaphor of a zoom lens (Eriksen & James, 1986). Still other authors have proposed the concept of *feature–based* or *object–based* attention (Treisman & Gelade, 1980; Roelfsema et al., 1998).

It seems unlikely that our observers performed their four assigned tasks by attending simultaneously to two focal locations, because it was not possible to predict accurately the future location of either one of the two test bars. Our proposed explanation is that observers attended to the outputs of the population of cyclopean long–distance comparator mechanisms that, of the possible three

pairings of bars, signaled the widest separation. The effect of this stratagem would be to attend to the population of comparators that were driven by the two test bars. Although this stratagem might give the impression of attending simultaneously to two remote locations some distance apart, it was in fact a quite different thing and is better described as attending to a stimulus feature (here "outermost pair").

Following the algebra set out in the Appendix of Morgan and Regan (1987) we can understand why the four discriminations measured were independent of relative disparity for relative disparities more than about 2–5 times above bar detection threshold. We assume that (1) the two test bars activated a population of cyclopean long–distance comparators, each of which preferred a different test bar separation and (2) that discrimination threshold for the separation of the test bars was determined by the relation between the "separation" labelled outputs of this population of comparators. We further assume that (3) each of the long–distance comparators activated by the test bars preferred a different mean orientation of the test bars and (4) that discrimination threshold for the mean orientation of the test bars was determined by the relation between the "mean orientation"–labelled outputs of this population of comparators. We suppose that discrimination threshold for mean location and orientation difference were determined along analogous lines.

We have recently reported evidence that the human visual system contains long–distance comparators that process luminance–defined form in a similar way to that in which the cyclopean long–distance comparators proposed here process cyclopean form (Kohly & Regan, 2000). However, the discrimination thresholds obtained using our luminance–defined targets (sharp, narrow bright lines) were considerably lower than those obtained using our dotted cyclopean bars. But this is not a fair comparison because the spatial sampling of the two kinds of target was not matched. The results of Expt. 3 show that discrimination thresholds for the two kinds of target are little different when the spatial sampling of the luminance–defined and cyclopean targets is identical. We conclude that, in our experimental context, long–distance processing of spatial information is not inherently superior for luminance–defined form than

for cyclopean form. This issue is discussed more generally in Regan (2000, pp.164-169).

What might be the role of the mechanisms proposed here? Suppose that the evolution of forward–facing eyes in predators was driven by a competitive advantage of binocular stereopsis over the greater security offered by the near–panoramic view offered by side–facing eyes. In this context the role of the mechanisms proposed here might be to encode information about the boundaries of prey whose bodies are matched to their surroundings in luminance, colour, texture and motion, and whose camouflage is broken by means of binocular stereopsis.

Summary

We report evidence for selective long–distance interactions in cyclopean binocular vision. When presented with a pair of cyclopean test bars observers could discriminate trial–to–trial uncorrelated variations in the mean orientation, orientation difference, separation and mean location of the test bars while ignoring random variations in the orientation, width and location of a third bar placed between the two test bars. We propose that the human visual system contains cyclopean long–distance comparators that: (1) compare the outputs of two narrow receptive fields some distance apart while being insensitive to stimuli located between those receptive fields and (2) whose outputs carry orthogonally–labelled indicators of orientation difference, mean orientation, separation and mean location. In the evolutionary context, one role for the proposed mechanisms might be to encode information about the silhouettes of animals whose camouflage is broken by the binocular vision of predators.

2.2(c) Long–distance interactions in the early processing of motion–defined form and of combinations of motion–defined, luminance–defined, and cyclopean form.

One paper has been published, title as above: Kohly, R & Regan, D (2002). Vision Research, 42, 969–980.

EXPERIMENT 1

Purpose

The aim of Expt. 1 was to find whether observers can compare two motion–defined test bars so as to discriminate trial–to–trial variations in both their orientation difference and their mean orientation while ignoring trial–to–trial variations in the orientation and width of a motion–defined 'noise' bar located between the two test bars in a situation that rules out the following strategies: (a) shift attention from one test bar to the other during the presentation; (b) attend to the locations of the two test bars simultaneously.

Rationale

In order to force observers to compare the orientations of the two test lines we varied α_T and β_T simultaneously and orthogonally, with the maximum variation of α_T exactly the same as the maximum variation of β_T. This ensured that the orientation of neither test bar alone provided a reliable cue to either discrimination task.

Methods

Motion–defined bars were created by moving the dots within a bar vertically downwards while the dots immediately outside the bar moved in the opposite direction at the same speed ($0.87^{\circ}\ sec^{-1}$) as the dots within the bar. This equal–and–opposite motion was used rather than unequal speeds or different directions of motion to avoid providing texture contrast cues for bar visibility (Regan, 1986; Regan et al., 1992). The appearance and disappearance of dots at the bar's edge would contribute negligibly to bar visibility (Regan & Hamstra, 1992) so that bar visibility would be entirely created by motion contrast. The dotted lines at the bar's edges represent the resulting perceived sharpness. In Fig. 17 the two outer bars are the test bars and the central bar is the noise bar.

There were 6 values of the following variables, all symmetrically placed about zero: α_T; β_T; β_N. The range of variation of all three angles was $\pm 8^{\circ}$. The choice of equal range of variation for α_T and β_T meant that simultaneous

trial–to–trial variations in the orientation difference and the mean orientation of the two test bars could be unconfounded only by comparing the two bars. Bar width was 0.75°. The mean separation of the two test bars was 4.1°. The midpoint of the two test bars coincided with the centre of the noise bar, i.e. $M_T = M_N$.

For observer 1 presentation duration was 106 ms (i.e. 4 frames). For the naïve observer 2 presentation duration was 133 ms (i.e. 5 frames). The masker bars were motion–defined and their orientations were selected randomly from the range of orientations used in the experiment.

In a subsidiary experiment carried out by observer 1 we compared (a) discrimination thresholds for orientation difference and mean orientation of the test bars measured using a two–bar configuration (with masker) with (b) orientation discrimination threshold for a single motion–defined test bar (with masker). The separation of the two bars were varied randomly so as to remove the distance between either the upper or lower ends of the bars as a reliable cue to their orientation difference. The values of α_T and β_T were varied orthogonally by ± 5.0° about zero, and in the two–bar experiment the observer discriminated both α_T and β_T after each presentation. In the one–bar experiments a fixation mark was placed between the two bars, the noise bars were removed, and either the left or right bar was occluded. Orientation discrimination threshold was measured separately for the right and the left test bar.

Results

In principle, the combination of three stimulus subsets and two tasks would give 12 plots of response probability vs. one of the three variables, but only the following stimulus subsets were of interest: when α_T was the task–relevent variable $\alpha_T\beta_T$ orthogonal and $\alpha_T\beta_N$ orthogonal; when β_T was the task–relevent variable $\alpha_T\beta_T$ orthogonal and $\beta_T\beta_N$ orthogonal. This left only 8 plots of interest. When α_T was the task–relevent variable the two plots of

Fig.17

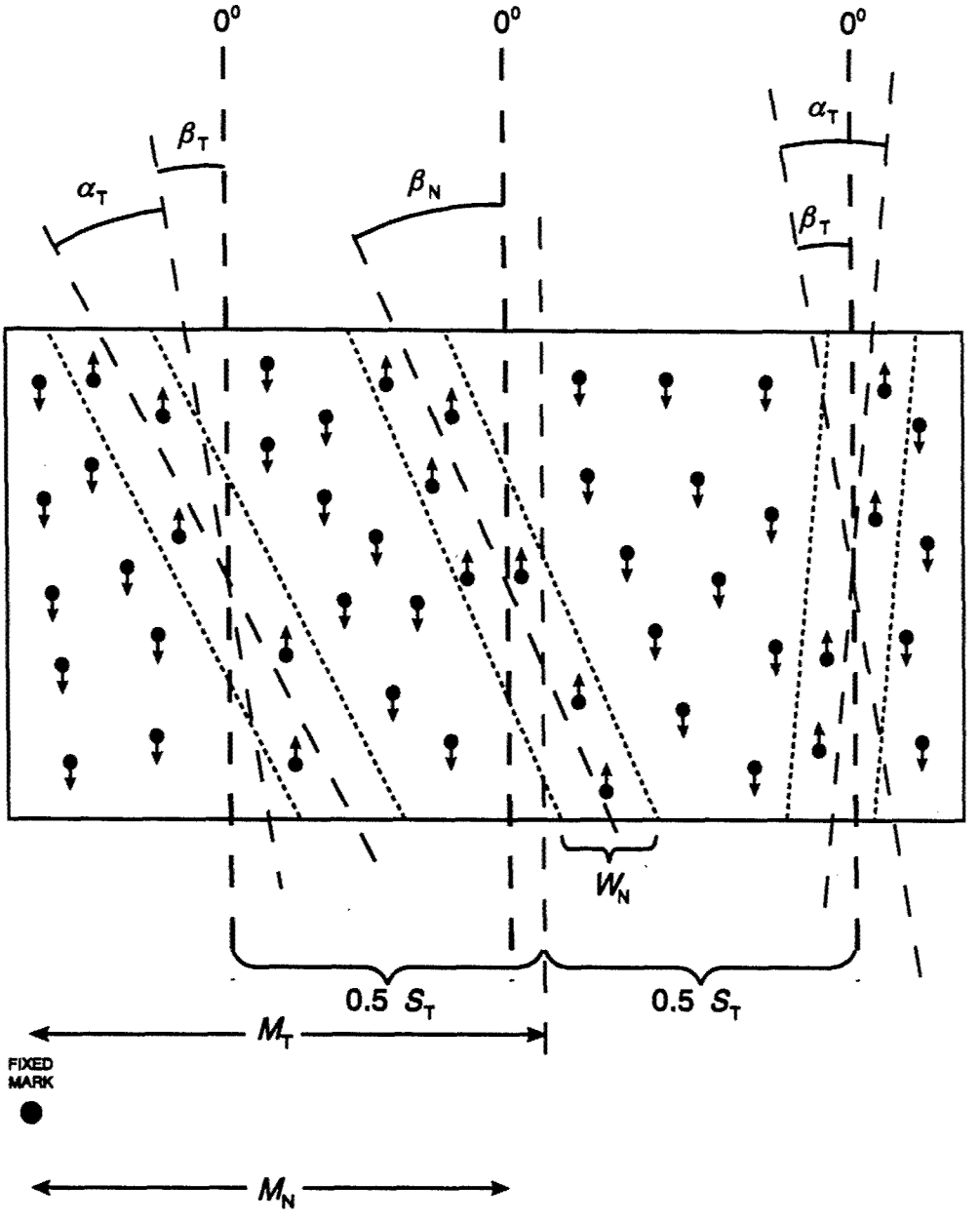

The stimulus used in Expts.1 and 2. The figure depicts two motion–defined test bars with mean orientation bT, orientation difference aT, separation ST and mean location MT. Between the two test bars is a motion-defined 'noise' bar of orientation bN, width WN and location MN, Dots inside and outside the bars moved at the same speed but in opposite directions. The dotted lines depict the illusory sharp boundaries of the motion–defined bars. Note that the dot density was much higher than shown here, and that all dots were bright rather than dark as shown here.

Fig.18

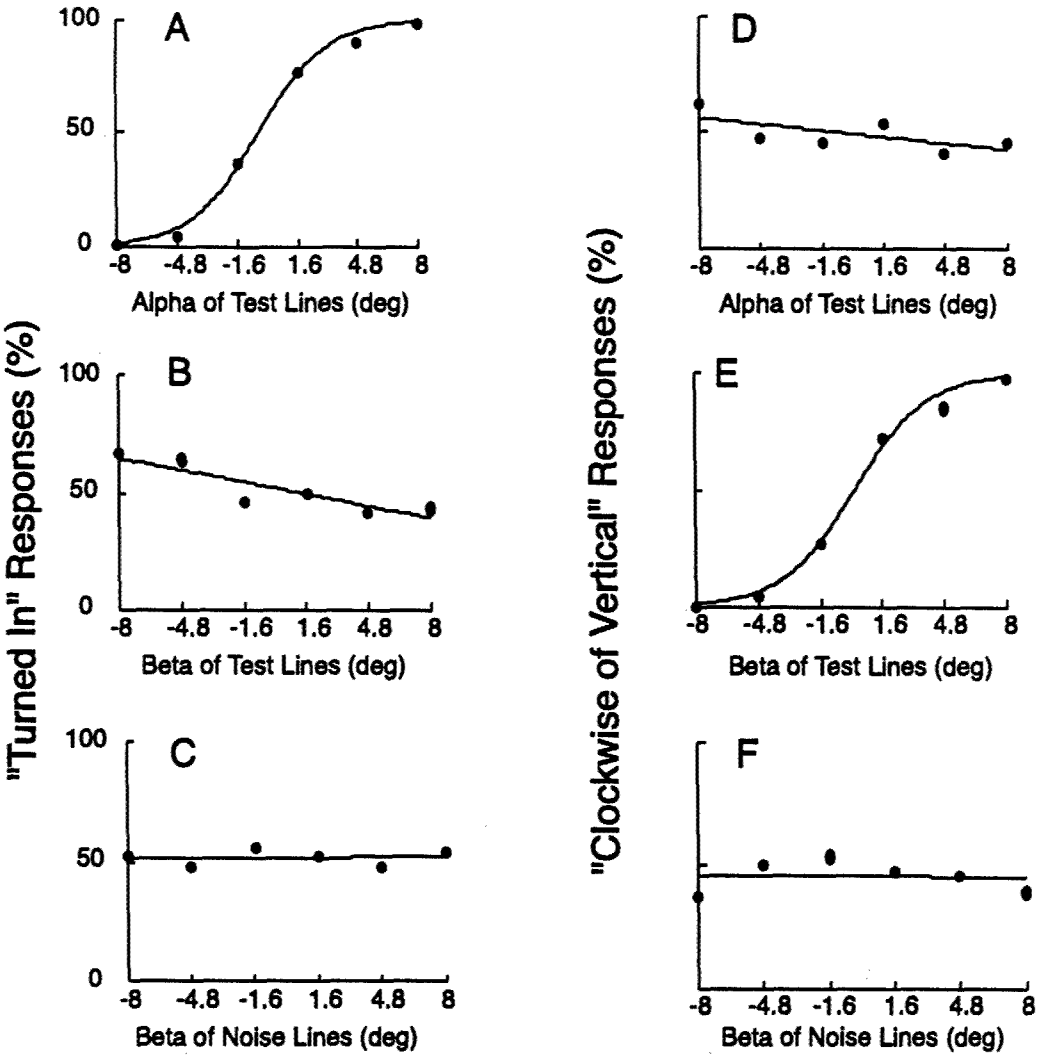

Following each presentation in Expt.1 observers were required to discriminate both the difference between the orientations of the two test bars (A–C), and their mean orientation (D–F). The observer based her discriminations of orientation difference on the task–relevant variable (steep slope in A), while ignoring trial–to–trial variations of the mean orientation of the test bars and of the orientation of the 'noise' bar (shallow slopes in B & C respectively). Similarly, when discriminating mean orientation, the observer based her responses on the task–relevent variable and ignored both task–irrelevent variables (D–F). Observer 1 (R.P.K).

response probability vs. α_T were similar, thus confirming that the observer's criterion for discriminating orientation difference was the same in both subsets. Therefore we collapsed the two plots, thus condensing to three plots the data collected when α_T was the task–relevent variable. Following a parallel argument we condensed to three plots the data collected when β_T was the task–relevent variable.

Fig 18A–F shows the 6 curves obtained in Expt.1 for observer 1. In Fig.18A–C the observer's task was to discriminate the orientation difference of the two test lines ($2\alpha_T$). Eyeball inspection shows that trial–to–trial variations of the task–relevent variable strongly influenced the observer's responses (Fig.18A), while simultaneous trial–to–trial variations of β_T had little effect. In Fig.18D–F the observer's task was to discriminate the mean orientation of the test lines (β_T). Eyeball inspection shows that trial–to–trial variations in the task–relevent variable strongly influenced the observer's responses (Fig.18E), while simultaneous trial–to–trial variations in α_T had comparatively little effect (Fig. 18D). All this indicated that the observer ignored β_T when discriminating α_T, and ignored α_T when discriminating β_T, a performance that could only be achieved by comparing the two test lines. (As mentioned earlier, by making the range of variation of α_T equal to the range of variation of β_T, we ensured that simultaneous trial–to–trial variations in α_T and β_T could only be unconfounded by comparing the two test lines).

A comparison of Fig. 18A & C shows that, when discriminating the orientation difference of the test lines ($2\alpha_T$), trial–to–trial variations in the orientation of the noise line had essentially no effect on the observer's responses. The same was true when the observer discriminated the mean orientation (β_T) of the test lines. (Fig. 18E & F).

Discrimination threshold for orientation difference ($2\alpha_T$) was 4.8° (SE=0.3°) and discrimination threshold for mean orientation (β_T) was 2.3 ° (SE=0.3°)

These findings were confirmed for a naïve observer for whom discrimination thresholds for $2\alpha_T$ and for β_T were, respectively, 4.5° (SE=0.4°) and 1.7 (SE=0.2°).

In the subsidiary experiment thresholds for $2\alpha_T$ and β_T respectively were 6.3° (SE=0.8°) and 2.8° (SE=0.3°). Single–bar orientation thresholds were 3.7° (SE=0.4°) and 2.8° (SE=0.3°) for the left and right bars respectively.

Discussion

By analogy with previous proposals for luminance–defined form and cyclopean form (Morgan & Regan, 1987; Kohly & Regan, 1999, 2000, 2001a,b) we here put forward the hypothesis that the human visual system contains fast long–distance comparators sensitive to motion-defined form.

Our findings can be understood in terms of the hypothesis that the visual system of at least some individuals contains a second–stage comparator mechanism that can compare the orientations of two motion–defined bars while being insensitive to a third motion-defined bar located between the two bars. We assume that this long–distance comparator encodes orthogonally and then places in memory the mean orientation and orientation difference of the two motion–defined test bars within 106 ms. (though the further processing of these encoded data that culminates in the observer's response extends over a considerably longer duration).

Suppose that the neural representation of bar orientation that supports discrimination of the orientation (θ_L) of the left line alone and the neural representation of bar orientation that supports discrimination of the orientation (θ_R) of the right line alone pass directly to a long–distance comparator that computes the mean orientation $0.5(\theta_R+\theta_L)$. In which case, and assuming that the

Fig.19

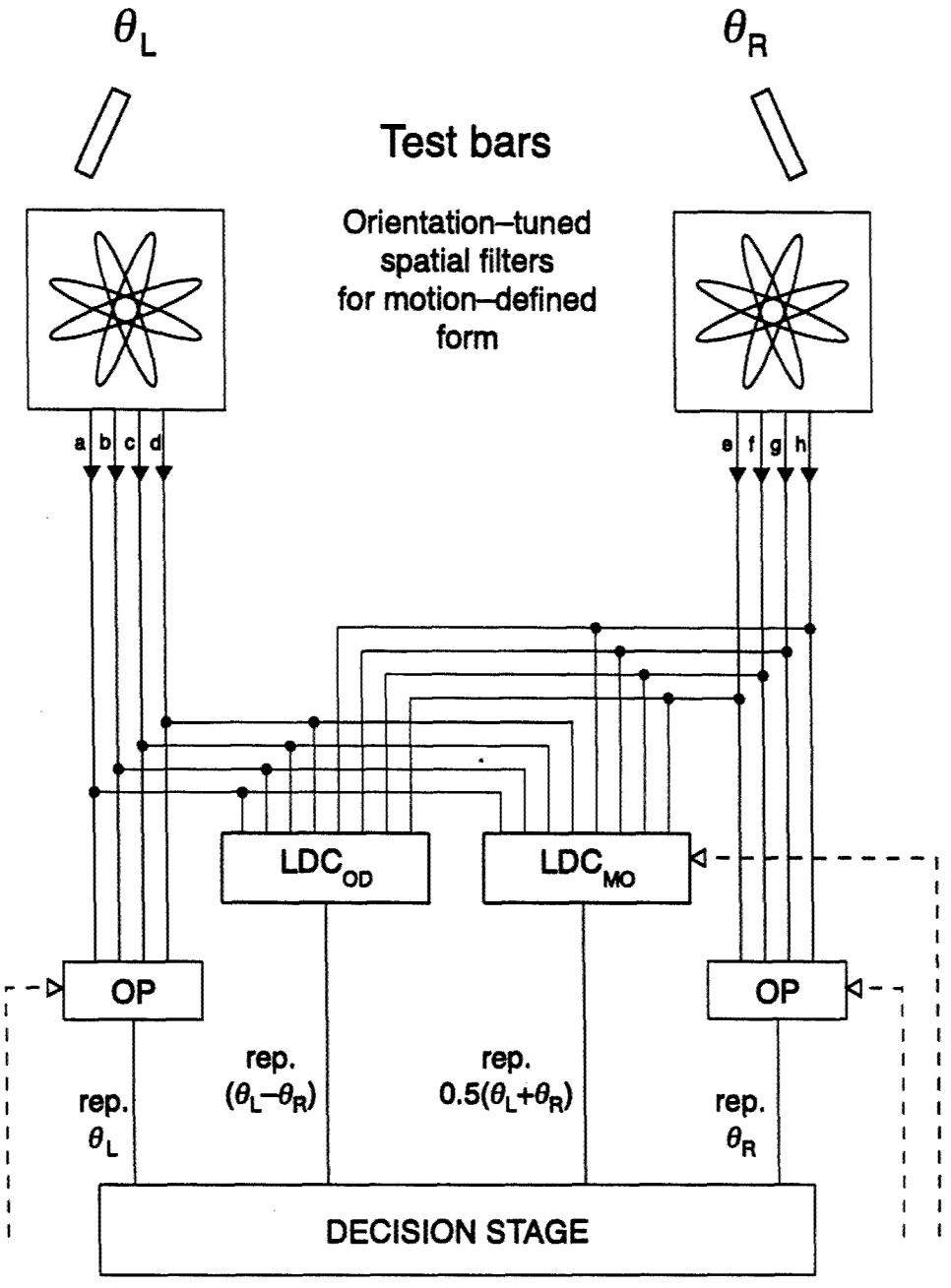

Schematic of a model of the discrimination of the orientation difference and mean orientation of two motion-defined bars in Expt. 1. Key: LDCOD and LDCMO, long–distance comparators driven by orientation–tuned spatial filters for motion-defined form whose outputs neurally–represent the orientation difference and mean orientation of the two test bars; OP, a stage that is sensitive to the pattern within the outputs of the spatial filters for motion–defined form, perhaps through opponent–processing.,

long–distance comparator loses no information, the results of the subsidiary experiment lead to the prediction that discrimination thresholds for mean orientation (in degrees) could be no lower than $[(3.7)^2 + (2.8)^2]^{\frac{1}{2}}$, i.e. 4.6° (SE=0.5°). The experimentally measured threshold however, [2.8° (SE=0.3°)] was lower than this prediction. This implies that our hypothesis was invalid.

The schematic in Fig.19 illustrates our proposed explanation. As suggested elsewhere (Regan, 1989), following stimulation by the left test bar, fine–grain information about its orientation (θ_L) is carried in terms of the pattern within the outputs of the orientation–tuned filters excited by the bar. (For purpose of explanation we show four signals *a*, *b*, *c*, & *d*), and a representation of θ_L is extracted at an opponent–process stage. We suppose that the value of θ_L with respect to vertical is obtained by comparing the pattern of filter outputs with a neural representation of vertical. One way in which this internal template might be created is that a task–dependent descending signal (dashed line) would represent equal outputs from first–stage filters that prefer orientations symmetrically inclined about the vertical. We suppose that orientation discrimination for the right test bar alone can be explained analogously.

We suppose that the outputs of all first–stage filters excited by the two test bars reach the long–distance comparator LDC_{MO} where the fine–grain information about θ_L (carried in terms of the pattern within signals *a*, *b*, *c*, & *d*) is compared with the fine–grain information about θ_R (carried in terms of the pattern within signals *e*, *f*, *g*, & *h*) to obtain the mean orientation, and this mean orientation is compared with a neural template of vertical. The output of LDC_{MO} neurally–represents $0.5(\theta_R + \theta_L)$ with degree–level accuracy and precision. One possible explanation for our finding that the measured threshold was lower than the predicted threshold is that more information is lost in the processing stages marked OP than in the stage marked LDC_{MO}.

In Fig. 19 the output of the long-distance comparator LDC_{OD} neurally-represents the difference in the orientations of the two test bars. To explain our finding that the measured threshold [6.3° (SE=0.8°)] was lower than the predicted threshold [9.2° (SE=1 °)] we suppose that comparing the orientations of two physically–present lines loses less information than comparing the orientation of a physically–present line with an internal template.

EXPERIMENT 2

Purpose

The aim of Expt. 2 was to find whether, following each presentation, observers can discriminate trial–to–trial variations in the orientation difference, mean orientation, separation, and mean location of a pair of motion-defined bars while ignoring task–irrelevent variables.

Methods

We varied M_T and S_T simultaneously and orthogonally with the maximum variation of M_T exactly half the maximum variation of S_T. This ensured that neither bar alone provided a reliable cue for discriminating either M_T or S_T. Our purpose was to force observers to base discriminations of M_T and S_T on a comparison of the two test bars. As in Expt. 1 we varied both α_T and β_T simultaneously and orthogonally, both through exactly the same range of variation, to ensure that α_T and β_T could be unconfounded only by comparing the two test bars.

By randomly varying the orientation (β_N), width (W_N), and location (M_N) of the central noise bar on a trial–to–trial variations basis (see Fig. 17) we corrupted the output of any first stage filter for motion–defined form with a strictly local receptive field that responded to both test bars.

The rectangular display subtended 11.6° (horizontal) x 5.8°, and contained 1000 dots. The ranges of variation in the bars' parameters were as follows:

Fig.20

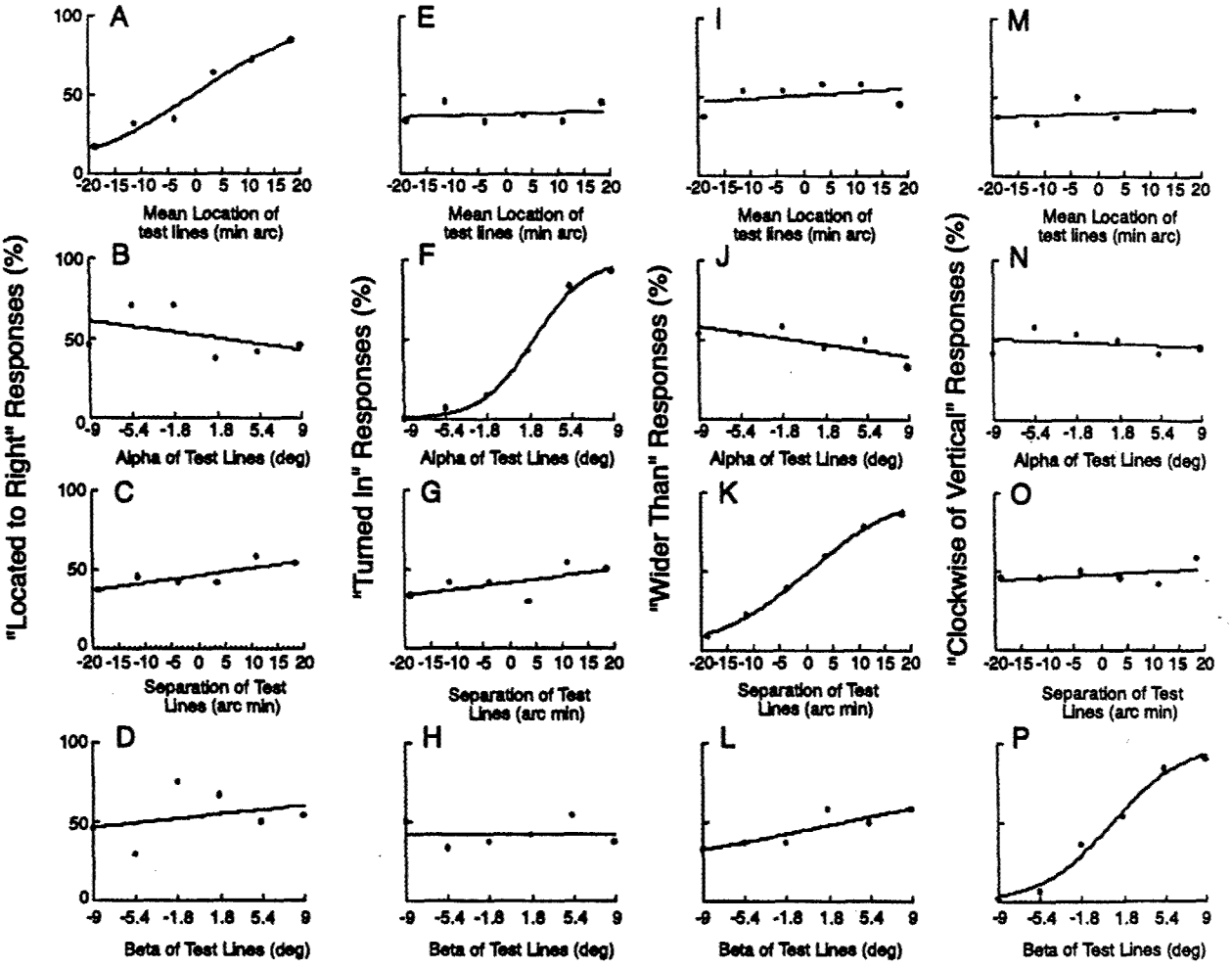

A total of 16 plots was obtained in Expt.2 where, following each presentation, the observer was required to discriminate four relationships between the two test bars. For each of the four discriminations (four columns) the plot with the task–relevent variable as abscissa was steep, and the slopes of the three plots with task–irrelevent variables as abscissas were almost zero, indicating that for all four tasks the observer based her responses on the task–irrelevent variable while ignoring task–irrelevent variables. Observer 1 (R.P.K.).

midpoint ± 17 arc min (test bars and noise bar); separation of test bars, 5.1–6.2 arc min, width of noise bar 19–86 arc min; α_T, β_T, and β_N, ± 9°. Following each 123 ms presentation of the three bars a masker pattern of motion-defined bars was presented for 200 ms.

The observer (R.P.K.) had four tasks. She signaled after each presentation whether the midpoint (M_T) of the test bars was to the left of right of the mean of the stimulus set, whether the separation of the test bars (S_T) was larger or smaller than the mean of the stimulus set, whether the test bars were turned in or turned out, and whether their mean orientation was clockwise or anticlockwise of vertical.

Results

The combination of six subsets (each of which contained two orthogonal variables) and four tasks meant that each run of 216 trials produced 48 possible plots of response probability versus one of the four variables. Of these 48 possible plots 24 were uninformative. Of the remaining 24 plots, 12 were of response probability versus the task–relevent variable (3 for each of the 4 variables). We first compared the 3 samples of discrimination threshold for each of the 4 variables to ensure that they were similar. This comparison confirmed that the observer's criteria was constant over subsets. Then we combined the three psychometric functions for each of the 4 variables so that our data were expressed in the form of the 16 plots shown in Fig. 20A–P.

Eyeball inspection of the 16 plots shown in Fig. 20A–P indicated that, for each of the four discriminations, the responses of observer 1 were based on the task–relevent variable while she almost completely ignored the three task–irrelevent variables.

We quantified this impression as follows. First, by subjecting each of the four subsets of response data to probit analysis (Finney, 1971), we estimated the distance along each abscissa between the 25% and 75% response points. Then, following the standard procedure, each of the 16 distances was divided by two. These data (expressed in degrees) are set out in Table 5. When the task was to

Table 5

VARIABLE	TASK			
	M_T	α_T	S_T	β_T
M_T	0.21	3.9	2.0	3.4
α_T	28	2.9	26	102
S_T	0.97	1.0	0.17	2.6
β_T	35	790	18	3.5

Estimates obtained by probit analysis of half the distance (in degrees) between the 25% and 75% response points on the 16 plots derived from the four–task response data. Observer 1 (R.P.K.)

Table 6

VARIABLE	TASK			
	M_T	α_T	S_T	β_T
M_T	1.0	19	9.5	16
α_T	9.7	1.0	9.0	35
S_T	5.7	5.9	1.0	15
β_T	10	>20	5.1	1.0

The data shown in Table 5 expressed as dimensionless ratios.

discriminate M_T and the variable was M_T, the number given in Table 5 is the discrimination threshold for M_T. Similarly, when the task was to discriminate β_T and the variable was β_T, the number given in Table 5 was the discrimination threshold for β_T, and so on for S_T and α_T.

In order to compare data on dimensionally dissimilar variables (orientation an distance) we normalized the numbers set out in Table 5 by dividing all the numbers with M_T as variable by the number for which M_T was both the task and the variable. Similarly, we divided all the numbers for which α_T was the variable by the number for which α_T was both the task and the variable, and so on for the remaining variables S_T and M_T. This converted all the numbers in Table 5 to dimensionless ratios in Table 6. The top row indicates that the observer's responses were 19 times less affected by trial–to–trial variations in M_T when the task was to discriminate α_T than when the task was to discriminate M_T, 9.5 times less when the task was to discriminate S_T, and 16 times less when the task was to discriminate β_T. (A value above *ca.* 3-4 means that the task–irrelevent variable was effectively ignored). Similarly, the second row of ratios in Table 6 was calculated by dividing the second row of numbers in Table 1 by 2.9, and so on.

In the subsidiary experiment (in which only one discrimination was carried out after each trial), the observer's responses were based on the task–relevent variable for each of the four discriminations, and all task–irrelevent variables were ignored. The four discrimination threshold were as follows: M_T, 0.23° (SE=0.3°); α_T, 2.8° (SE=0.2°); S_T, 0.20° (SE=0.02°); β_T, 2.4° (SE=0.2°). Corresponding thresholds in the four–task case [M_T, 0.21° (SE=0.02°); α_T, 2.9° (SE=0.3°); S_T; 0.17° (SE=0.02°); β_T, 3.5° (SE=0.3°)] were similar except for β_T, which was slightly higher. This finding indicates that carrying out four tasks places little greater load on attentional resources than carrying out only one task.

Fig.21

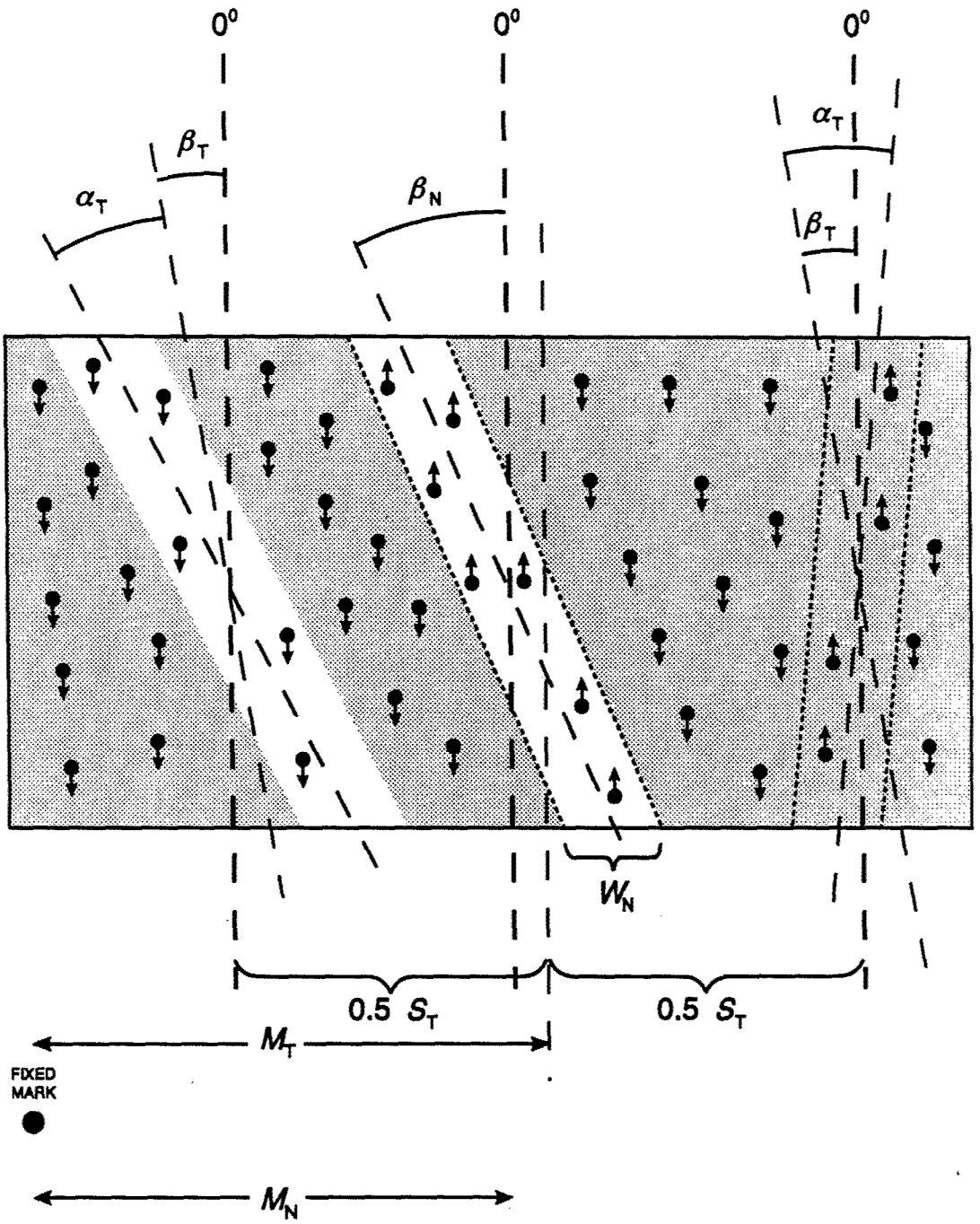

The stimulus used in Expt. 3A. One test bar was rendered visible entirely by relative motion while the other test bar was rendered visible entirely by luminance contrast. The central 'noise' bar was rendered visible by a combination of relative motion and luminance contrast. Note that the dot density was much higher than shown here and that all dots were bright on a uniform dark background.

Discussion

One explanation for our finding that observer 1 could, following each trial, discriminate S_T and M_T as well as $2\alpha_T$ and β_T is as follows. The long–distance comparators LDC_{OD} and LDC_{MO} in Fig. 19 are merged into one long–distance comparator whose output carries the following four independent labels: separation (S_T), mean location (M_T), orientation difference ($\theta_L - \theta_R$), and mean orientation $0.5(\theta_L - \theta_R)$. Of these four labels, only one is at all closely related to the following three independent labels carried by the output of a first–stage filter: location, i.e. local sign (Lotze 1885, cited in White et al., 1992); preferred orientation (Thomas & Gille, 1979); preferred spatial frequency (Watson & Robson, 1981). Following Morgan and Regan (1987) we assume that discrimination thresholds for mean location (M_T) as well as for separation (S_T) are determined by the pattern of activity among long–distance comparators driven from different pairs of locations, perhaps via opponent processing.

EXPERIMENT 3

Purpose

The purpose of experiment 3 was to determine whether, following each single presentation, observers can compare the orientations of two test bars that are rendered visible by different sub–modalities so as to discriminate trial–to–trial variations in their orientation difference and mean orientation while ignoring trial–to–trial variations in the orientation of a noise bar located between the two test bars.

Methods

Figure 21 depicts the combination of motion–defined and luminance–defined bars used in experiment 3A. The rightmost bar is rendered visible by motion contrast: dots within the bar move vertically upwards while dots outside the bar move vertically downward at the same speed (0.87° sec^{-1}). The dotted lines at the bar's edges represent the resulting perceived sharpness.

Fig.22

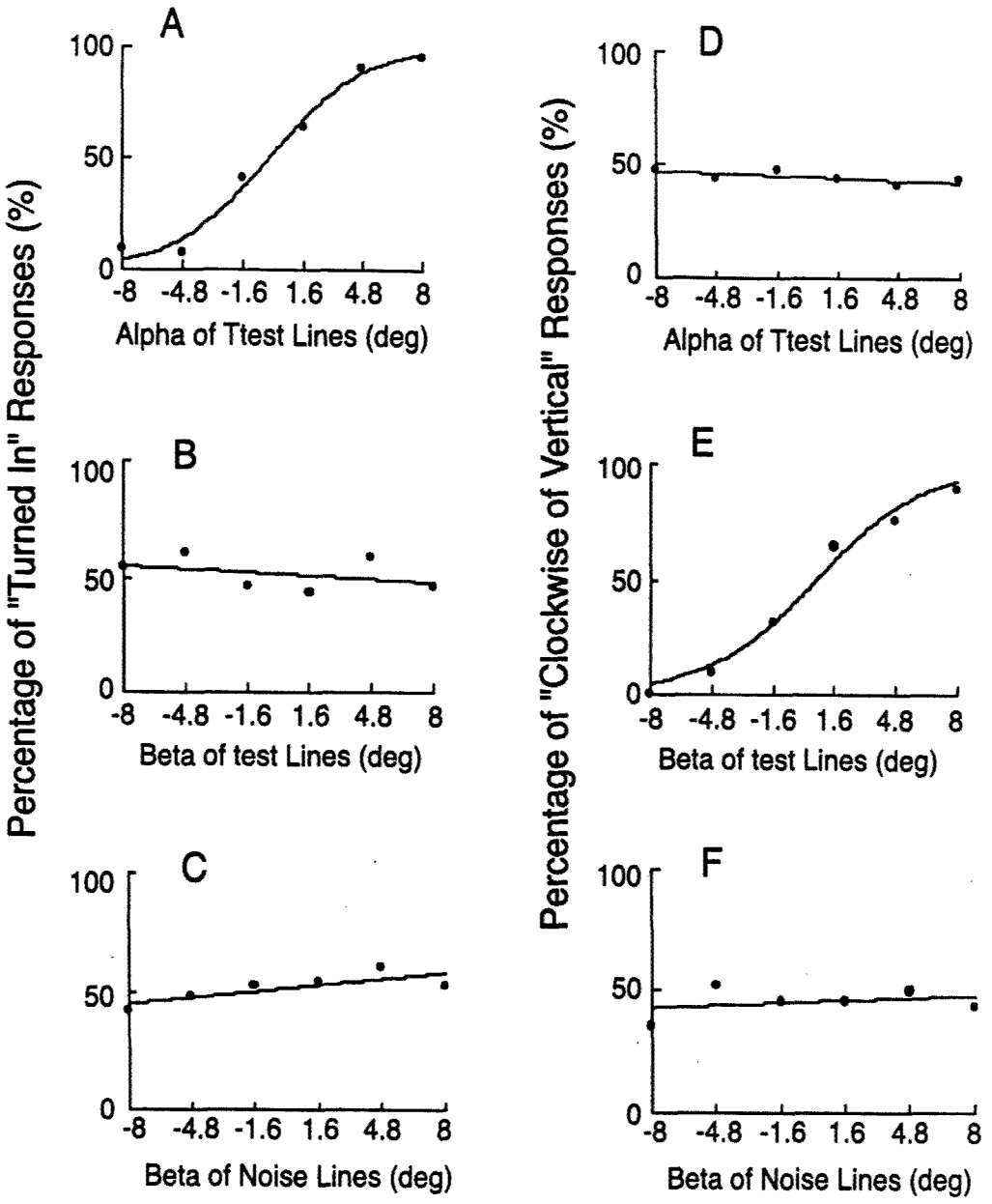

Following each presentation in Expt. 3A observers were required to discriminate both the difference between the orientations of the two test bars (A-C), and their mean orientation (D–F). Compare with Fig.18. Observer 1 (R.P.K.)

Table 7

	VARIABLE	OBSERVER 1		OBSERVER 1	
		TASK			
		α_T	β_T	α_T	β_T
MD + LD	α_T	3.1	100	2.8	40
	β_T	61	3.2	100	2.8
	β_N	33	84	>100	2.8
MD + LD	α_T	5.3	58	4.2	81
	β_T	27	5.7	>100	4.4
	β_N	25	24	>100	10
DD + LD	α_T	4.7	24	4.1	>100
	β_T	38	4.8	14	4.4
	β_N	21	34	27	14

Estimates obtained by probit analysis of half the distance (in degrees) between the 25% and 75% response points on the 6 plots derived from the two-task response data in Expts. 3A, B & C.

and Fig. 18 indicates that similar conclusions can be drawn from the results of Expts. 3A and 1.. Discrimination thresholds for orientation difference ($2\alpha_T$) and mean orientations (β_T) were, respectively 6.2° (SE= 0.8°) and 3.2° (SE= 0.2°) for observer 1, and 5.7° (SE= 0.4°) and 2.8° (SE-= 0.3°) for observer 2. For conciseness we will present the remaining findings numerically as was done in Table 5. Table 7 shows that results obtained from observer 2 confirmed the conclusions just described.

In experiment 3B (the MD/cyclopean combination) discrimination thresholds for $2\alpha_T$ and for β_T were, respectively, 10.6° (SE= 0.9°) and 5.7° (SE= 0.5°) for observer 1, 8.5° (SE= 0.6°) and 4.4° (SE= 0.3°) for observer 2. Table 7 shows that both observers based each discriminations on the task-relevant variable, and ignored all task-irrelevant variables.

In experiment 3C (the cyclopean/LD combination) discrimination thresholds for $2\alpha_T$ and β_T were, respectively 9.4° (SE= 0.8)° and 4.8° (SE= 0.4°) for observer 1, 8.3° (SE= 0.7°) and 4.4° (SE= 0.4°) for observer 2. Table 7 shows that both observers based each discrimination on the task–relevant, and ignored all task–irrelevant variables.

General Discussion

The pattern of results in each of Expts. 3A-C are similar to the pattern of results in Expt.1, and can be understood along the same lines. In particular, we conclude that the human visual system contains second–stage mechanisms that can compare the orientations of a motion–defined test bar and a luminance–defined test bar, or a motion–defined test bar and a cyclopean test bar, or a luminance–defined test bar and a cyclopean test bar so as to signal their mean orientation and orientation difference while being insensitive to a noise bar located between the two test bars.

As in Expt. 1 the tasks could not have been performed by shifting either ocular fixation or the focus of attention form one test bar to the other, nor by paying attention to two locations simultaneously. We suggest that, rather than

attending to the outputs of the two spatial filters that detected the test bars either in succession or simultaneously, observers attended to the outputs of the second–stage comparators that signaled "widest separation". This would select the two designated test bars from the three possible combinations of test and noise bars. In this way "largest separation" would neurally–represent "outermost pair" and thus provide a physiological basis for this particular Gestalt.

A possible general explanation for our findings with combinations of sub–modalities (Expt.3), motion–defined stimuli (Expt.1), and previous findings for luminance–defined (Kohly & Regan, 2000, 2001a) and cyclopean stimuli (Kohly & Regan, 2001b) is that the human visual system contains a comparator mechanism that mediates fast long–distance interactions for each of the six combinations of sub–modalities (i.e., LD/LD, cyclopean/cyclopean, MD/MD, and the three combinations). A more parsimonious proposal, however, is that any given comparator mechanism compares the orientation of two separated test bars independently of whether one or other test bar is luminance–defined, cyclopean, or motion–defined to at least for LD/LD, cyclopean/cyclopean, and MD/MD combinations. Extrapolating from our findings with luminance–defined, cyclopean, and motion–defined stimuli we suggest that any given comparator also compares the locations of the two test bars so as to signal their separation and mean location.

As mentioned earlier, an object can be rendered visible when it differs from its surroundings sufficiently in any one of the following sub–modalities: luminance, motion, depth, colour or texture. In everyday life several of these differences may exist simultaneously yet, with few exceptions, normally–sighted individual's see a single object at a single location rather than several objects, each rendered visible by a different sub-modality. We suggest that one possible role of our proposed second-stage comparators in everyday vision is, following each saccade, to rapidly bind the spatial aspects of the retinal image across sub-modalities.

The entire boundary of an object's retinal image is often defined by a difference in a single sub–modality (though this is not always the case). We have previously suggested that, for an object whose image is rendered visible entirely

by luminance contrast or by disparity contrast, long–distance comparators operating within a single sub-modality (luminance or disparity) could rapidly provide a complete description of the object's boundaries following any given saccade (Kohly & Regan, 2000, 2001a,b). On the basis of the results of Expts. 1 & 2 we here propose that the same holds for objects rendered visible entirely by motion contrast. In some situations, however, the boundary of part of an object's retinal image might be rendered visible by one kind of spatial contrast while the remaining boundary is rendered visible by another kind of spatial contrast. For example, the upper boundary of an object that is tilted in depth may be rendered visible by disparity contrast and the lower boundary by luminance contrast. The results of Expt.3 might explain how the boundaries of such objects were encoded.

2.2(d) Spatial frequency discrimination in cyclopean vision

One paper has been published, title as above: Grove, P.M. & Regan, D (2002). Vision Research, 42, 1837–1846.

EXPERIMENT 1

Purpose

The aim of Expt. 1 was to find the number of spatial samples (dots) per cycle of a cyclopean grating above which the effect of spatial sampling on spatial frequency discrimination can be ignored.

Methods

At the viewing distance of 114 cm the display subtended 15° (horizontal) x 15°. The mean number of cycles across the display was 9, and mean spatial frequency was 0.58 cycles/$^{\circ}$. The mean number of dots seen by each eye ranged from 90 to 7100. A complete stereopair was displayed every 27 ms for 90 dots, and every 29 ms for 7100 dots. Spatial frequency discrimination threshold was measured as a function of the mean number of dots for both the quasi–random and the nonrandom arrangements of dots.

Fig.23

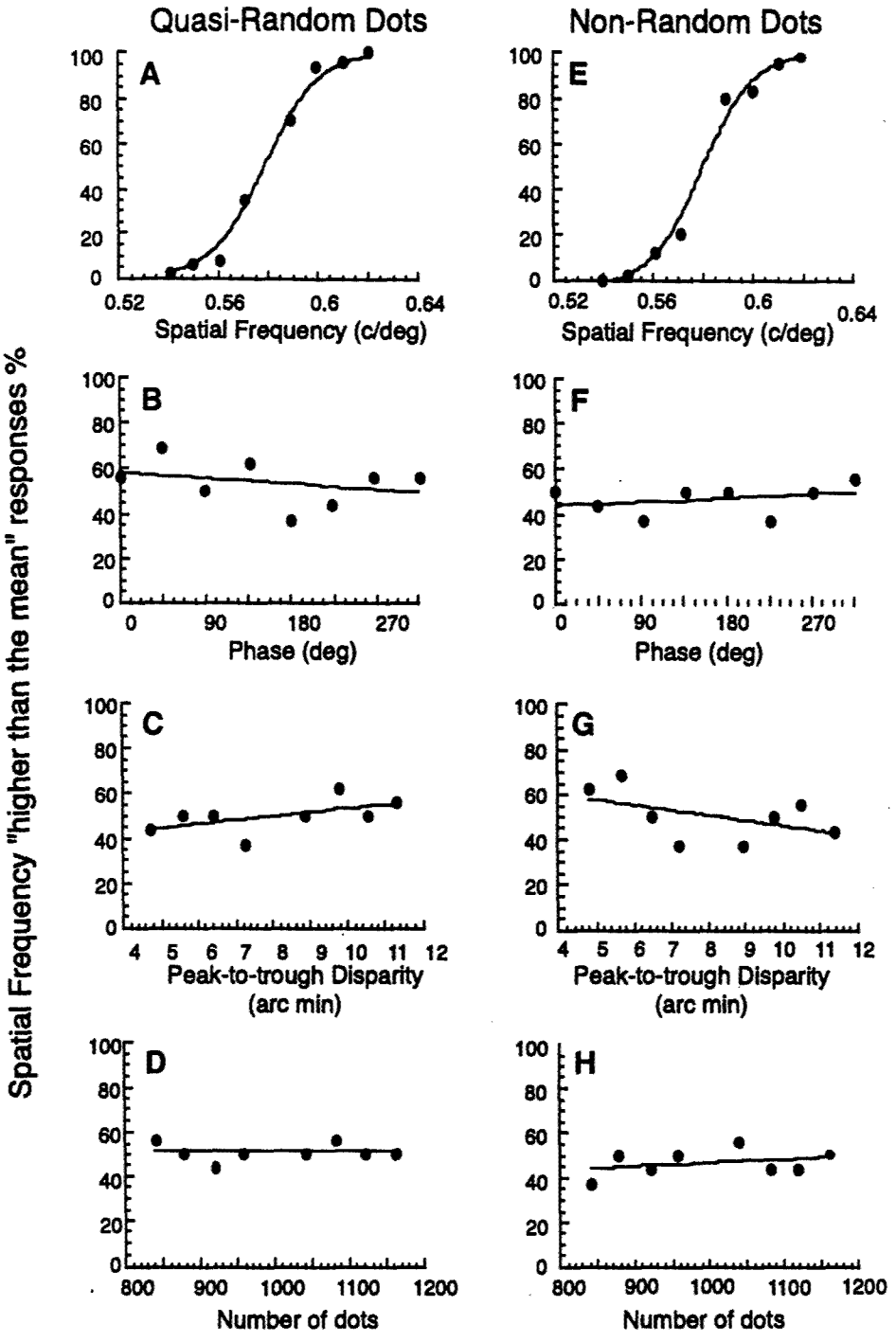

Spatial frequency discrimination for cyclopean gratings in a quasi–random pattern of dots (A–D) and in a nonrandom pattern of dots (E-H). The percentage of "spatial frequency higher than the mean of the stimulus set" response was plotted versus the spatial frequency of the test grating (the task–relevant variable) in panels A& E, versus the spatial phase of the test grating (task–irrelevant variable no.1) in panels B&F, versus the peak–to–trough disparity of the test grating (task–irrelevant variable no.2) in panels C&G, and versus the total number of dots in the pattern (task–irrelevant variable no.3) in panels D & H. The mean number of dots was 1000, giving 3 dots per grating cycle along a line at right angles to the bars of the grating. Observer 1.

Fig.24

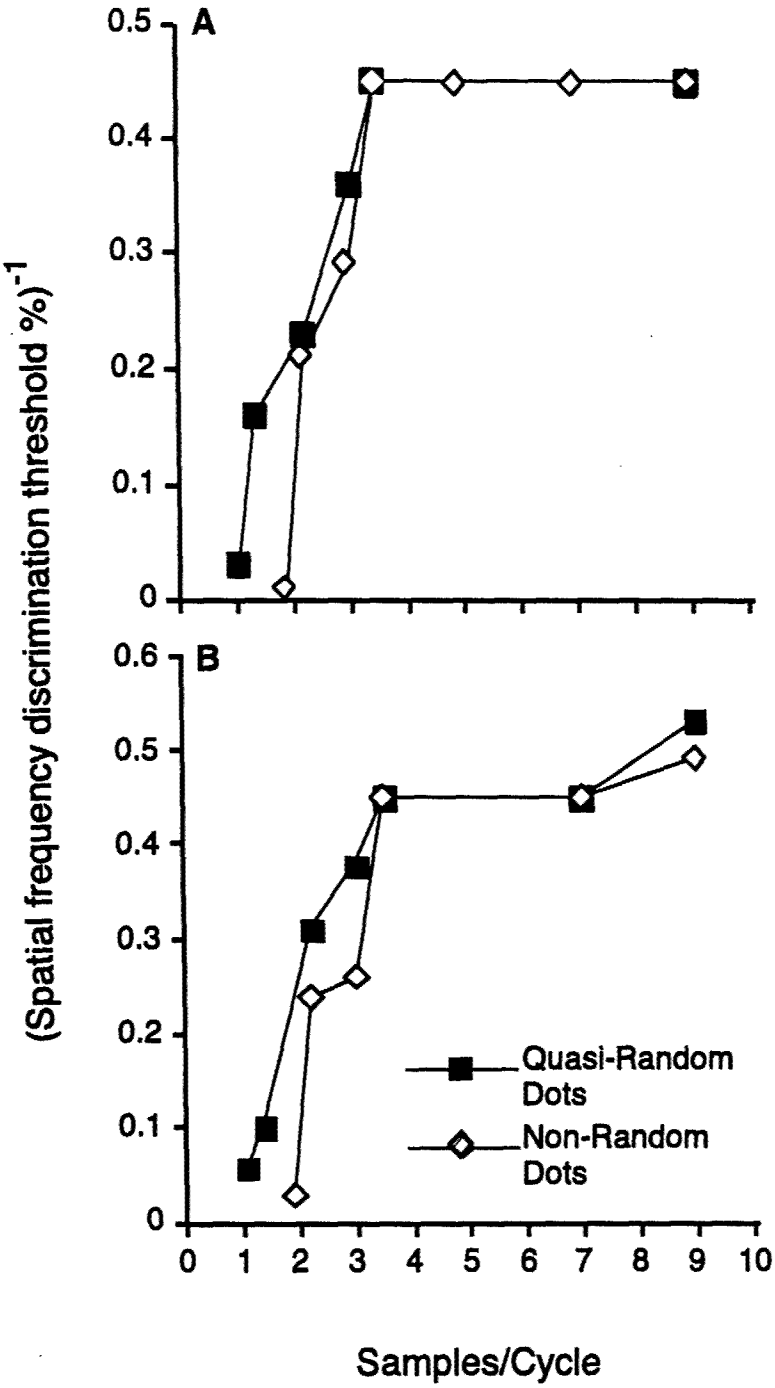

The reciprocal of spatial frequency discrimination threshold for a cyclopean grating was plotted as ordinate versus the number of dots per grating cycle along a line at right angles to the bars of the grating. The dots were arranged either quasi–randomly or nonrandomly. Standard error bars were smaller than the symbols. A: Observer 1. B: Observer 4.

Results

Fig., 23A–H shows data that were typical of the situation that the pattern contained sufficient dots to ensure a low discrimination threshold. Each run yielded three plots of response probability vs. spatial frequency. As would be expected if the observer's criterion was the same for each of the three stimulus subsets, the estimate of threshold was the same for each of the three plots. In Fig. 23A the three subsets of data have been combined and Fig.23E was generated similarly. Fig. 23A–D and E–H shows that the responses of observer 1 were based on the task-relevant variable: the Fig. 23A plot was steep while the Fig. 23B–D plots were flat, and the Fig.23E plot was steep while the Fig.23F–H plots were flat. This steep/flat dichotomy indicated that the observer's responses were strongly influenced by the task-relevant variable while he ignored trial–to–trial variations in all three co-varying task–irrelevant variables. We confirmed that this was the case for both observers when the mean number of dots in the display totalled 1000 or more. When the total number of dots was progressively reduced below *ca.* 1000 a pattern of results different to that shown in Fig.23A–H was obtained. In particular the slopes in panels A&E were reduced (corresponding to an increase of threshold) and the slope in one or more of the other panels was increased (indicating that a task–irrelevant variable influenced the observer's responses).

In Fig. 24A,B the reciprocal of spatial frequency discrimination threshold was plotted as ordinate *vs.* the mean number of spatial samples per grating cycle as abscissa. For the nonrandom arrangement of dots this number is the number of dots per grating cycle along any vertical column of dots at right angles to the horizontal bars of the grating. For the quasi–random arrangement of dots the number is the mean number along a line at right angles to the bars.

Fig. 24A,B shows that discrimination threshold fell to an asymptotic value when the number of dots per grating cycle exceeded *ca.* 3 Threshold rose steeply when the number of dots per cycle was reduced below 3, and the rise was steeper for the non-random arrangement then for the quasi–random arrangement.

Discussion

When the non–random dot pattern was used, the discrimination task became essentially impossible when the number of samples per cycle fell below two. (This was because the number of samples per cycle was varied independently of spatial frequency. Had this not been done, measured sensitivity to differences of spatial frequency would not have fallen to near–zero at two samples per cycle, because a reliable—though spurious—cue to the discrimination task would have been provided by depth corrugations caused by interactions between the grating's nominal spatial frequency and the number of samples per cycle.)

Our proposed explanation for the difference between the curves for non-random and quasi–random dot patterns is as follows. Even if the visual system integrated information parallel to the grating's bars no further sampling information would have been provided in the non–random case because the horizontal rows of dots were parallel to the bars. In contrast, spatial integration parallel to the bars would, in effect, increase the number of samples per grating cycle in the quasi–random case. The data shown in Fig. 24A,B allows us to estimate the spatial extent of integration. Sensitivity to differences in spatial frequency fell to zero at *ca.* 1.0 samples per cycle in the quasi–random case and at *ca.* 1.9 samples per cycle in non–random case, indicating that the spatial integration along the bars renders one sample per cycle in the quasi–random case effectively equal to *ca.* 1.9 samples per cycle. Given that the mean horizontal distance between dots was 1.56 deg when the number of samples per cycle was 1.0, we concluded that the cyclopean visual system integrates over a distance of *ca.* 1.6° along the length of a depth corrugation. The advantage given by this spatial integration diminishes progressively as the number of samples per cycle is increased beyond 1 until, at 3 samples per cycle, no advantage remained.

We conclude that cyclopean gratings should contain at least 3 dots per grating cycle along a line perpendicular to the bars.

EXPERIMENT 2

Fig.25

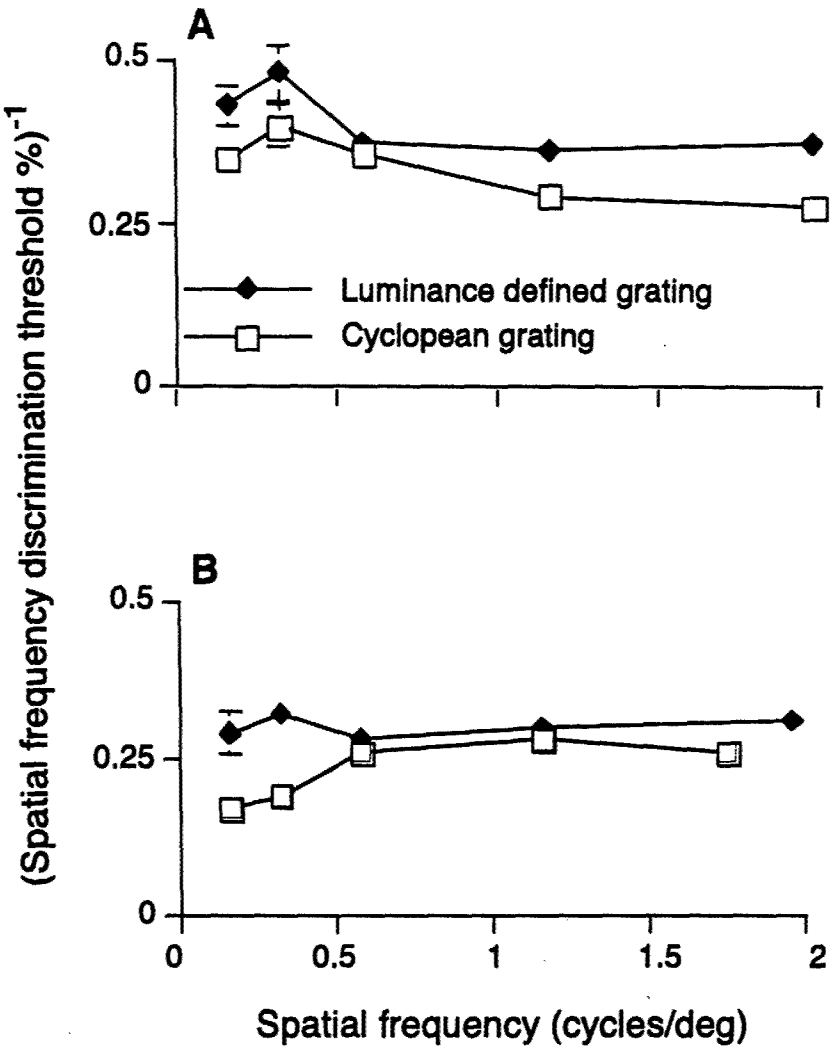

The reciprocal of spatial frequency discrimination threshold was plotted as ordinate for cyclopean (open symbols) and luminance–defined (filled symbols) gratings versus grating spatial frequency. A: Observer 1. B: Observer 2.

Purpose

The aim of Expt. 2 was to compare discrimination threshold for the periodicity of depth corrugations in a cyclopean grating with discrimination threshold for the periodicity of luminance modulation in a luminance–defined grating of matched spatial sampling.

Methods

Each eye saw a mean number of 7100 dots. The display was masked to subtend 15° (horizontally) x 12° at a viewing distance of 114 cm. A complete stereo pair was presented every 29ms. Dots were arranged quasi–randomly.

To avoid undue spread of power in the frequency spectrum the lowest number of cycles in the display was 5. (In this situation power fell to half of its maximum value at spatial frequencies ± 20% to either side of the nominal spatial frequency, see Regan, 2000, pp.418–420). Measurements were made in the following conditions: viewing distance 57cm, 5 cycles displayed; viewing distance 114cm, either 5 or 9 cycles displayed; viewing distance 228 cm, 9 cycles displayed. This gave a spatial frequency range of 0.16–2.0 cycles/$^{\circ}$. Beyond the highest spatial frequency (2 cycles/deg) the visibility of the cyclopean grating fell sharply.

The mean disparity of the cyclopean grating was zero, and peak–to–trough disparity was 4.2 arc min. The mean disparity of the luminance–defined grating was zero, and the luminance contrast was varied between 70% and 95%.

Results

Set of curves similar to Fig. 23A,D were obtained for both cyclopean and luminance–defined gratings. In every case the curves showed that observers based their responses entirely on the task-relevant variable. Fig. 25A, B compares sensitivity to a difference in the periodicity of depth corrugations (open symbols) with sensitivity to the periodicity of luminance modulation (filled symbols) as a function of the spatial frequency of the grating. Except where shown, standard errors were smaller than the symbols. For observer 1 (Fig. 25A)

and 2 (Fig.25B) sensitivity was almost independent of grating spatial frequency over the range 0.16 to 2.0 cycles/°. This was the case for both cyclopean and luminance–defined gratings. At every spatial frequency tested, discrimination threshold was lower for the luminance grating than for the cyclopean grating, though the difference was only slight. This was the case for both observers.

For observer 1 the lowest value of spatial frequency discrimination threshold was 2.5% for the cyclopean grating and 2.1% for the luminance–defined grating. Corresponding thresholds for observer 2 were 3.5% and 3.1%.

Discussion

We conclude that spatial frequency discrimination threshold is only slightly higher for a cyclopean grating than for a luminance–defined grating of matched sampling. Cyclopean discrimination thresholds were considerably lower than the psychophysically–estimated spatial frequency bandwidth of cyclopean channels, or of channels for luminance–defined form (Graham, 1989) or of the most sharply–tuned neurons in monkey striate cortex (DeValois, Albrecht and Thorell, 1982).

We suggest that this discrepancy can be explained by analogy with the corresponding discrepancy for luminance–defined form (Campbell, Nachmias & Jukes, 1970; Regan et al., 1982; Regan & Beverley, 1983). In particular, we propose that discrimination threshold for cyclopean gratings is determined by the pattern of activity among cyclopean channels that prefer different spatial frequencies. In Expt.4 we will subject this hypothesis to experimental test.

EXPERIMENT 3

Purpose

The purpose of Expt. 3 was to find how spatial frequency discrimination threshold for a cyclopean grating was affected by the peak–to–trough disparity of the grating.

Methods

Fig.26

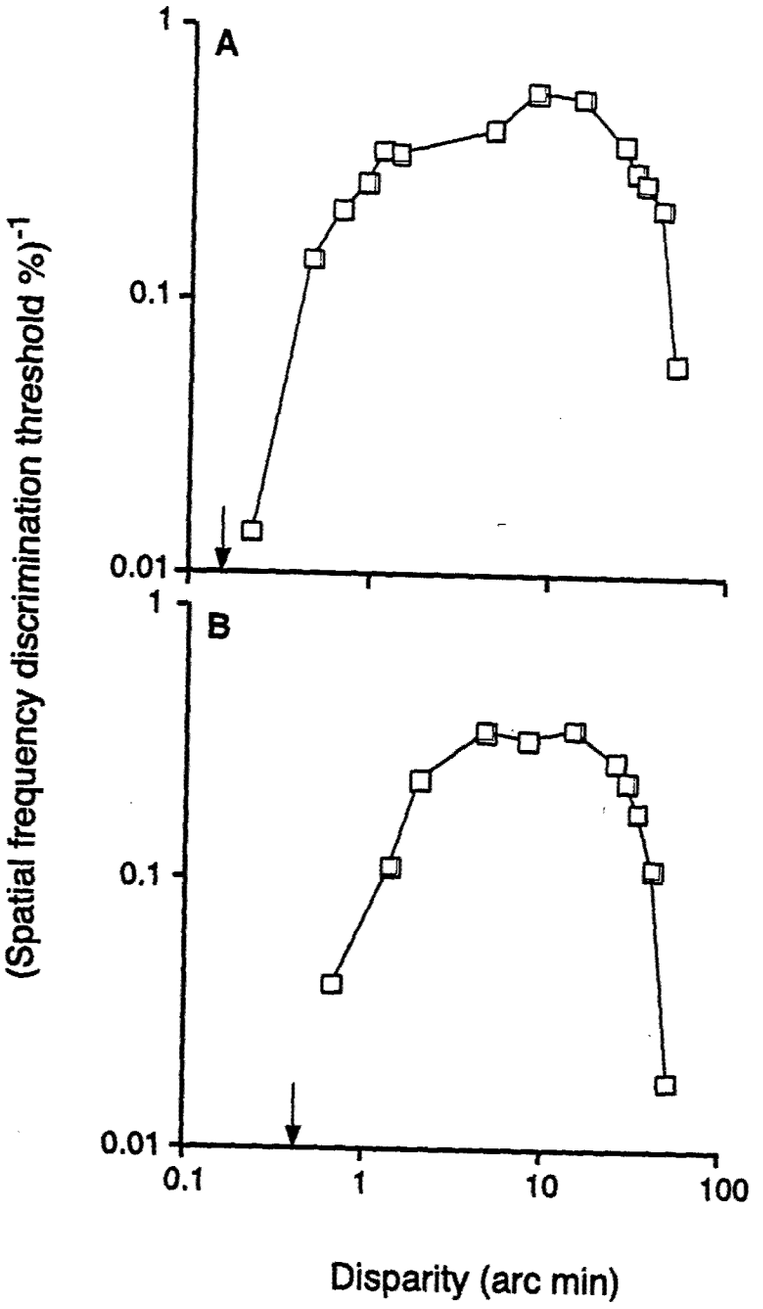

The reciprocal of spatial frequency discrimination threshold for a cyclopean grating was plotted as ordinate versus the peak-to-trough disparity of the grating. Note that both axes are logarithmic. Grating detection thresholds are arrowed. The dots were arranged quasi-randomly. Standard error bars were smaller than the symbols. A: Observer 1, B: Observer 3.

From the viewing distance of 228 cm the display subtended 7.7° (horizontal) x 7.7°. There were 9 cycles across the display, so that the spatial frequency was 1.16 cycles/°. Each eye saw a mean number of 7100 dots. A complete stereopair was presented every 29 ms. Discrimination thresholds were measured over a *ca.* 500:1 range of peak-to–trough disparities from 0.1 to 49 arc min. The procedure in the main experiment was as described in General Methods.

In a subsidiary Expt. we measured grating detection threshold. The stimulus set contained two values of peak–to–trough disparity, namely zero and a value that gave a d' near 1.0. For each value of peak–to–trough disparity there were 8 values of spatial phase, giving 16 stimuli in all. Observers were instructed to signal which of the two possible values of peak-to–trough disparity had just been presented. The value of d' was calculated conventionally (Macmillan & Creelman, 1991).

Results

Grating detection threshold ($d'=1.0$) for observer 1 was estimated as 0.18 arc min peak–to–trough and, for observer 3, 0.41 arc min peak–to–trough. Fig. 26A,B shows that, as the peak–to–trough disparity was progressively increased above grating detection threshold, spatial frequency discrimination threshold fell steeply to *ca.* 1.7% for observer 1 (4.4% for observer 3), and thereafter remained approximately independent of peak–to–trough disparity over a range of *ca.* 45:1 for observer 1 and *ca.* 17:1 for observer 3. Binocular fusion became difficult when peak–to–trough disparity was increased further, and discrimination threshold rose correspondingly.

Discussion

It is not surprising that spatial frequency discrimination threshold rose sharply when the peak–to-trough disparity approached grating detection threshold nor when peak–to–trough disparity was so large that it rendered binocular fusion intermittent: one would expect that the curves in Fig.26A,B

would have the shape of an inverted U. The interesting aspect of Fig. 26A,B is the 45:1 and 17:1 ranges over which discrimination threshold is approximately independent of peak-to–trough disparity. It has previously been reported the spatial frequency discrimination threshold for luminance–defined form (and also orientation discrimination threshold and line separation threshold) are approximately independent of luminance contrast over a similarly wide range of contrasts (Regan et al., 1982; Skottun et al., 1987; Regan & Beverley, 1983, 1985; Morgan & Regan, 1987). The explanation proposed for these findings was that the discrimination thresholds were determined by the pattern of activation among tuned neurons, possibly by opponent–processing as discussed mathematically in the appendix in Morgan and Regan (1987) and Regan and Beverley (1985). We suggest that the approximately flat regions in Fig.26A & B can be explained analogously, and will test this hypothesis in Expt. 4.

EXPERIMENT 4

Purpose

The purpose of Expt.4 was to test the hypothesis that spatial frequency discrimination threshold for cyclopean gratings is determined by the pattern of activity among cyclopean neurons tuned to spatial frequency. Our procedure was to compare the effects of adaptation on spatial frequency discrimination threshold and on grating detection threshold (Regan 1982; Regan et al., 1982; Regan & Beverley, 1983, 1985).

Methods

From the viewing distance of 114 cm the display subtended 15^{o} (horizontally) x 15^{o}. Each eye saw a mean number of 7100 dots. A complete stereopair was displayed every 29 ms.

After viewing a cyclopean adapting grating for 5 minutes, a cyclopean test grating was presented, followed by a 10sec refresh of adaptation, followed by another test presentation, and so on. Test presentation duration was 400ms for observer 1 and 600ms for observer 4. Adaptation, refresh and test gratings all had zero mean disparity and 4.2 arc min peak-to–trough disparity. An

Fig.27

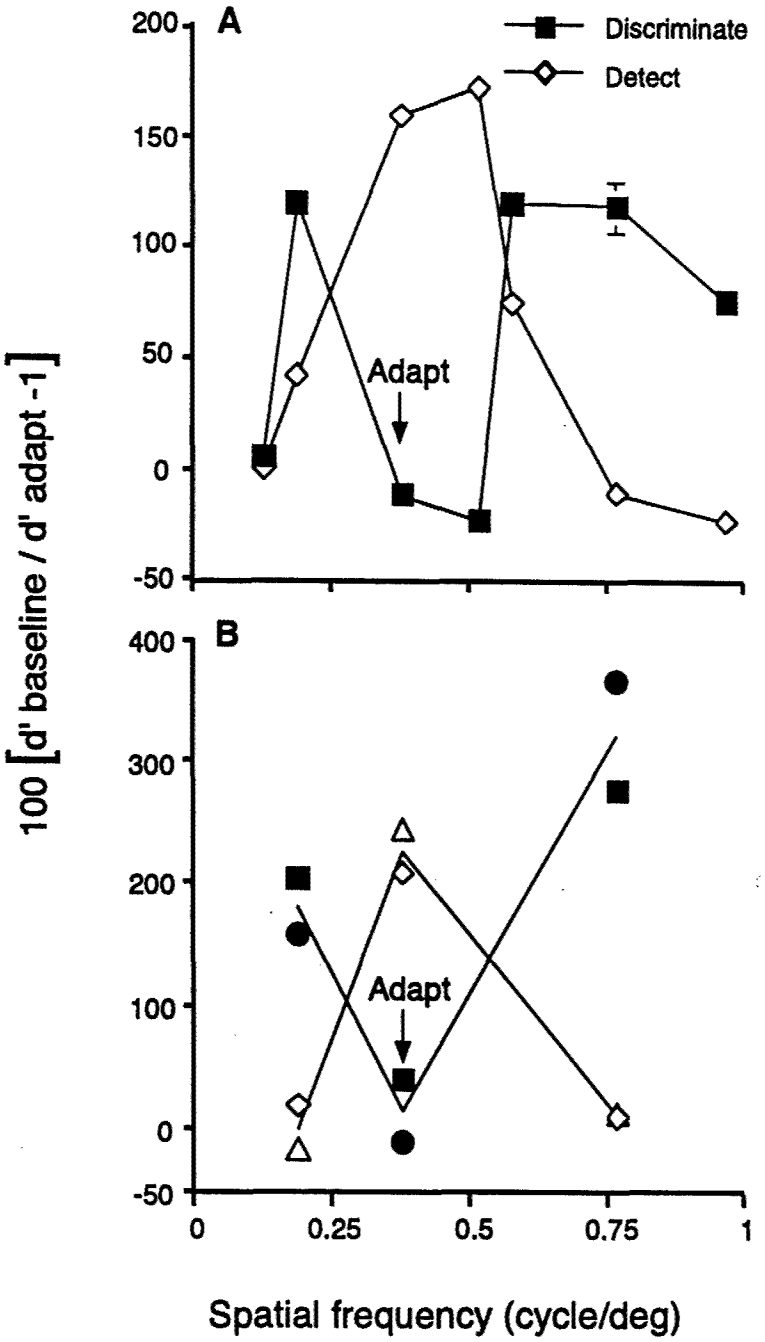

The effect of grating adapting to a cyclopean grating on detection threshold (open symbols) and spatial frequency discrimination threshold (filled symbols) for cyclopean test gratings. The ratio (baseline d l)/(postadaptation d l) was plotted as ordinate versus the spatial frequency of the test grating. Vertical arrows mark the spatial frequency of the adapting grating. A: Observer 1. B: Observer 4.

adapt/refresh grating had one of 8 equally–spaced spatial phases, and switched to a randomly–selected phase every 500ms. The phase of a test grating was selected randomly from the 8 possibilities. When measuring the effect of adaptation on spatial frequency discrimination, the test grating had one of two possible spatial frequencies that differed by 3.75%, each spatial frequency being paired with 8 spatial phases, giving 16 test stimuli in all. Following each presentation of a test grating, observers were instructed to signal whether the spatial frequency was high or low, and d' estimates were made conventionally (Macmillan & Creelman, 1991). Baseline values of d' were obtained using the same procedure except that the adapting grating had a peak–to–peak disparity of zero.

Baseline and postadaptation values of d' for detecting the grating were measured by combining the adaptation/refresh procedure just described with the test procedure used in Expt.3 with a 400ms (observer 1) or 600ms (observer 2) test presentation duration.

Results

The ratio (baseline d')/(postadaptation d') was plotted as ordinate in Fig. 27A,B versus the test spatial frequency as abscissa. Open symbols in Fig.27A confirm the previous finding (Schumer & Ganz, 1979) that, after inspecting a high–visibility cyclopean grating, detection threshold for a test grating is elevated maximally at the adapting spatial frequency, and that the detection threshold elevation falls off as the difference between the spatial frequencies of the test and adapting gratings is increased.

Our main finding is that adaptation produced the opposite effect on spatial frequency discrimination threshold. Filled symbols in Fig.27A,B show that discrimination threshold was, if anything, slightly improved at the adapting spatial frequency for observer 1 and unaffected for observer 4. The maximum postadaptation elevation of discrimination threshold occurred at test frequencies offset from the adapting frequency, where detection threshold was comparatively unaffected by adaptation. In Fig. 27A the data plotted as filled

Fig.28

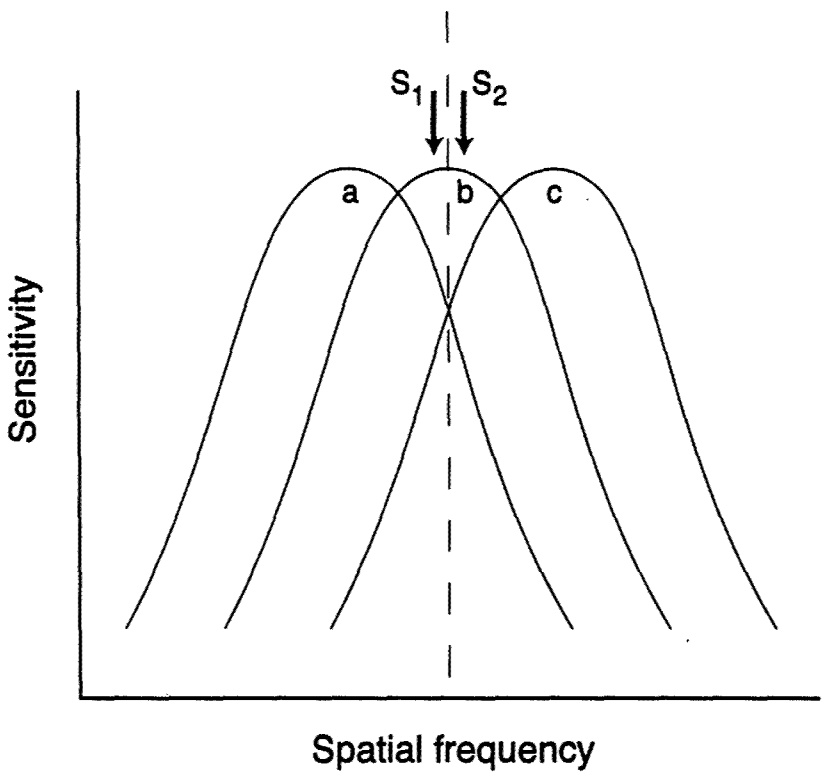

Proposed explanation for the postadaptation data of Fig. 27. A small change of test spatial frequency from S1 to S2 produces little change in the output of the cyclopean filter (b) that is most sensitive to the cyclopean test grating, but produces a large change in the balance between the outputs of the offset filters a and c.

symbols second and fifth from the right were subjected to a two–tailed t test. The difference was highly significant (t=-6.26, dF=4, p=0.003).

Discussion

The finding that grating detection threshold is elevated maximally at the adapting spatial frequency is conventionally taken to indicate that the most highly activated spatial frequency channel determines detection threshold (Graham, 1989). Our data can be understood if spatial frequency discrimination threshold is determined by comparatively weakly–activated channels.

Filled symbols in Fig.27A,B indicate that the effect of activation of the most sensitive channel was, if anything, deleterious to spatial frequency discrimination. As noted earlier (Regan & Beverley, 1983, 1985), slight postadaptation reduction in discrimination threshold at the adapting frequency would be expected if random noise from the channel most sensitive to the test grating reduces the signal–to–noise ratio of the "frequency change" signal.

Following a previous argument (Regan & Beverley, 1983) and referring to Fig.28, we assume that a small change of test spatial frequency from S_1 to S_2 traverses the almost–flat top of the most sensitive cyclopean channel (*b*) so that the output of this channel changes negligibly. The two most important cyclopean channels for spatial frequency discrimination, *a* and *c*, are those whose slopes differ most at the test frequency. It follows that, as shown in Fig.27A,B, the maximum effect of adaptation on discrimination threshold will be at frequencies offset from the adapting frequency. By analogy with out previous discussion of spatial frequency discrimination for luminance–defined form (Regan & Beverley, 1983), the hypothesis that spatial frequency discrimination threshold for cyclopean gratings is determined by the relative activity among cyclopean channels (we suggest by an opponent process) can, as discussed earlier, account for the findings that (1) discrimination threshold is far lower than the estimated bandwidth of cyclopean channels (Fig.25) and (2) that discrimination threshold is approximately constant over a wide range of peak–to–peak disparities (Fig.26).

Fig.29

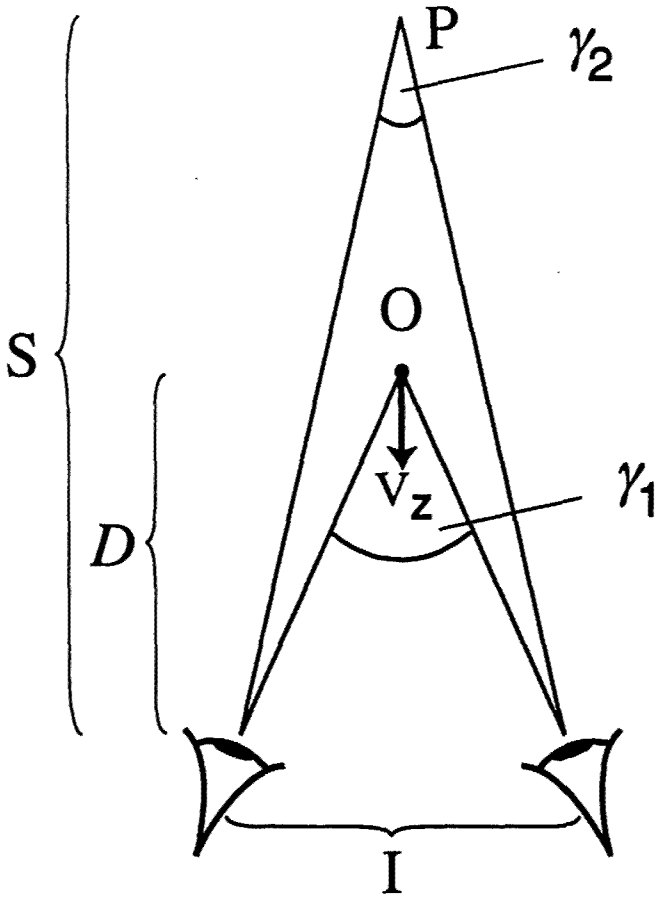

A point object O is moving at constant speed Vz directly towards a point midway between an observer's eyes. P is a stationary object.

2.2(e) Binocular information about time to collision and time to passage

A theoretical paper on visual psychophysics has been published, title as above: Regan, D. (2002). Vision Research, 42, 2479–2484.

In a recent paper, Rushton and Wann (1999) stated that TTC with an object that is approaching the observer's head at constant speed is approximated by the ratio (relative horizontal disparity)/(rate of change of relative horizontal disparity), and noted that, like *tau*, this ratio does not involve the object's distance. This equation and conclusion conflict with the equation previously derived by Regan (1995), namely that TTC is approximated by the ratio (angle γ_1 in Fig.29)/(rate of change of relative horizontal disparity). Angle γ_1 in Fig.29 is not, of course, the relative horizontal disparity of object O as in the Rushton and Wann (1999) equation.

The Rushton and Wann equation is correct only when the reference object is at infinity. In this case the approaching object is seen double when it is near. When the reference object is close to the moving object (giving maximum sensation of motion in depth) the Rushton and Wann equation gives an infinite error.

In Fig.29 O is an object moving in a straight line at constant speed V_z whose instantaneous distance from the observer is D. P is a stationary reference object whose distance (S) is fixed. The observer's interpupillary separation is I.

In Fig.29 the relative horizontal binocular disparity of O with respect to stationary point object P is δ, where

$$\delta = \gamma_1 - \gamma_2 \approx \frac{I}{D} - \frac{I}{S} \qquad \text{----------(4)}$$

provided that $D >> I$. Equation (4) is valid independently of the ocular vergence angle. I assume, however, that the vergence angle is such that the reference (P) and object (O) are both seen in binocular single vision.

Since I and S are constant, we have from equation (4)

$$\frac{d\delta}{dt} \approx \frac{d}{dt}\left(\frac{I}{D}\right) \qquad \text{----------(5)}$$

Hence

$$\frac{d\delta}{dt} \approx \frac{IV_z}{D^2} \qquad \text{----------(6)}$$

Fig.30

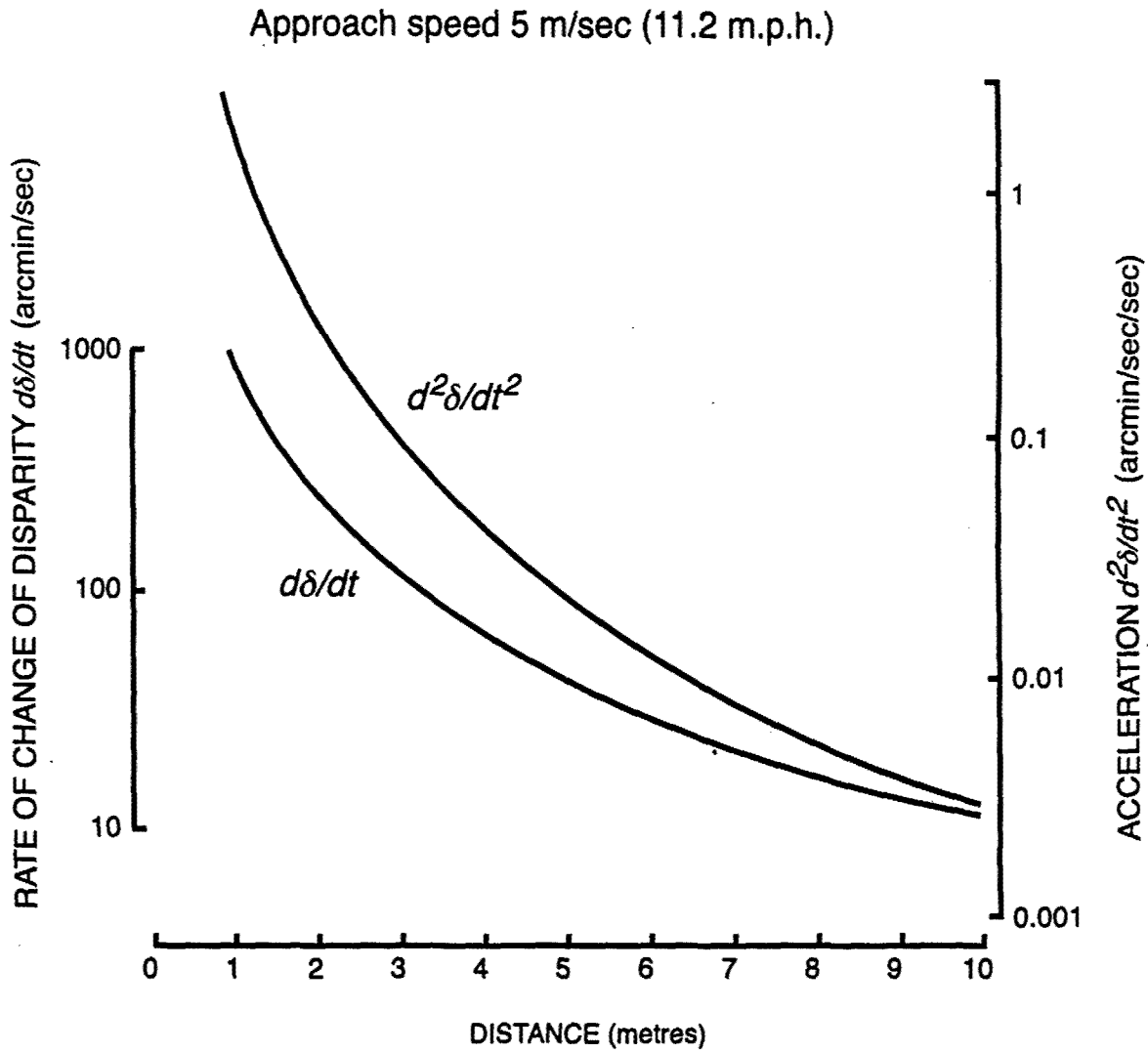

Timecourses of the first and second temporal derivatives of the horizontal disparity of the moving object O depicted in Fig.29. The ordinates are logarithmic to bring out the point that the ratio (d2d/dt2)/(dd/dt) increases progressively as the object approaches. As shown in the text this ratio is inversely proportional to time to collision.

since I is constant. Given that TTC=D/V_z, we have from equation (6)

$$TTC \approx \frac{I}{D(d\delta/dt)} \qquad \text{----------(7)}$$

Rewriting equation (7)

$$TTC \approx \frac{\gamma_1}{(d\delta/dt)} \qquad \text{----------(8)}$$

As mentioned earlier, equation (8) is quite different from equation (9) published by Rushton and Wann.

$$TTC \approx \frac{\delta}{(d\delta/dt)} \qquad \text{----------(9)}$$

(Note that in their paper they used α instead of δ to represent relative horizontal disparity). Using a different mathematical procedure, equations (7) & (8) were previously derived by Regan (1995). This derivation is replicated in Gray & Regan (1998).

Equation (7) leaves us with the unresolved problem of how the visual system might encode distance *D(t)* with sufficient accuracy to support estimates of TTC based entirely on binocular information that would be useful in everyday life. [In laboratory studies, errors in estimating TTC with a small target were reported by Gray and Regan (1998) to be only 2.6% to 3.0%[6]].

On the face if it, a plausible hypothesis would be that the angle of ocular convergence is used to estimate distance in equation (7), at least for distances less than a few m. This hypothesis, however, is not consistent with the finding that, for a target of constant mean angular size (θ), the effect of a large variation of ocular convergence (0 to 24 prism dioptres) on the rate of change of disparity required to cancel the sensation of motion in depth created by a fixed oscillation of θ was zero for observer and only twofold for a second observer (Regan & Beverley, 1979). A possible solution to this "distance estimation" problem is illustrated in Fig. 30.

By differentiating equation (6), we obtain

$$\frac{d^2\delta}{dt^2} \approx \frac{2IV_z^2}{D^3} \qquad \text{----------(10)}$$

and from equations (6) and (10) we have

Fig.31

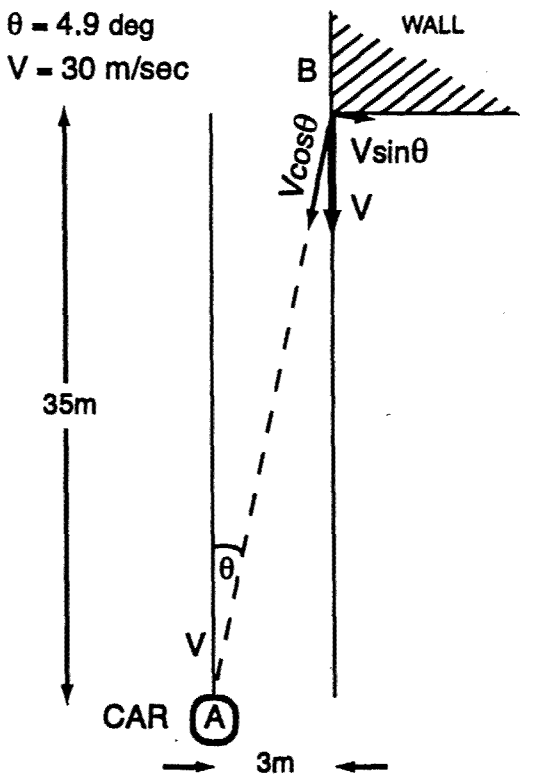

Time to passage and location at passage. A car (A) travelling at a speed of 30m/sec (ca. 67 m.p.h.) is steered so as to enter an underpass with the wall of the underpass (B) passing 3m from the driver's head. The time to passage and the 3m distance of object B at the instant of passage can be obtained from retinal image information with high accuracy.

$$\frac{d^2\delta/dt^2}{d\delta/dt} \approx \frac{2V_z}{D} = \frac{2}{\mathrm{TTC}} \qquad \text{----------(11)}$$

Equation (11) gives a value for TTC that does not involve object distance and is based entirely on retinal image variables. A signal proportional to $(d^2\delta/dt^2)/(d\delta/dt)$ would grow larger as TTC grew smaller, thus indicating the growing urgency for evasive or interceptive action.

Finally, I discuss time to passage (TTP). Fig. 31 depicts the case of a car (A) being driven at 30 m/sec so that a point midway between the driver's eyes will pass 3m from object B. In Fig. 31, a velocity **V** equal and opposite to that of the car has been impressed on both the car and object B. The $V\cos\theta$ component of relative motion will give $d\delta/dt$=0.0014639 radians/sec and $d^2\delta/dt^2$=0.0025005 radians/sec/sec at 35m from the underpass. From equation (11) this retinal image information gives a TTP to the side of the underpass of 1.171 sec. The correct TTP is 1.167, so the error in TTP given by equation (11) is *ca.* 0.4% at 35m from passage where θ=4.9º. The $V\sin\theta$ component of relative motion will give an angular speed across the retina of 0.0732 radians/sec (4.2 deg/sec). From equation (2) it can be seen that, providing the car's speed and direction of motion remain constant, the side of the underpass (B in Fig.31) will pass 3.000 m to the right of a point midway between the driver's eyes.

A second numerical example applies to catching a ball. In the game of cricket a so–called slip fielder is commonly stationed behind the batsman and, for a right–handed batsman, slightly to the right of the batsman. When a fast bowler is operating with a delivery speed of *ca.* 40 m/sec (90 mph) the slip fielder may stand 15m from the batsman. It the ball hits the edge of the batsman's bat the ball may fly towards the fielder, but the trajectory is not known until the ball leaves the bat's edge. The fielder faces the bat and fixates its outer edge rather than following the flight of the ball from the bowler's hand. If the ball deflects from the edge of the bat, the fielder has 0.375 sec to judge the flight of the ball and execute the catch (bare–handed). A catch is often made wide of the body. The correct location of the hand is given by equation (2). If the outstretched arm is 1.0 m long, the obliquity of the trajectory is 3.8 deg, and equation (11) gives the time to passage with an accuracy better than 0.4%.

2.3 Auditory Studies

2.3(a) Response of auditory hair cells to amplitude–modulated and quasi–frequency–modulated tones

Long–Term Aims: 4.1.3. Specific Aims: 4.2.16.

Relevance: This research is intended to advance understanding of the auditory processing of complex sounds. A paper has been published: Regan, M.P. & Regan, D. (2001). Simulated hair cell transduction of quasi–frequency–modulated and amplitude–modulated tones. *Hearing Research*, 158, 65-70.

There is controversy as to whether changes in the frequency and in the amplitude of a tone are processed by the same (Zwicker 1956, 1970: Maiwald 1967a, b) or by different (Feth 1972; Kay and Matthews 1972; Coninx 1977a, b; Regan and Tansley 1979; Tansley and Regan 1979; Hartmann and Hnath 1982; Demany and Semal 1986; Ozimek and Sek 1987) mechanisms. Evidence that, at least for low modulation frequencies, AM and quasi-FM tones are processed by different mechanisms includes the following. After adapting to a quasi-FM tone, threshold for detecting a quasi-FM tone was elevated considerably more than threshold for detecting an AM tone, both tones being modulated at 2.0Hz. Conversely, after adapting to an AM tone, threshold for detecting an AM tone was elevated considerably more than threshold for detecting a quasi-FM tone (Regan and Tansley 1979).

We model the hair cell transducer function as a linear filter followed by a frequency-independent asymmetric compressive rectifier. Hair cell transducer functions have been measured in several species by plotting the receptor current as a function of the mechanical deflection of the hair cell (Corey and Hudspeth 1983; Hudspeth 1983; Crawford and Fettiplace 1985; Russell et al. 1986; Assad and Corey 1992), and it has been found that, although the estimates of sensitivity vary between the species, the functions all show that the response is much greater for the preferred direction of displacement than that for the opposite direction and that large displacements cause saturation in the responses. In what

follows, the equation of the rectifier will be that proposed by Assad and Corey (1992) as a model for Bullfrog saccular hair cell transducer function.

Transduction of a quasi-frequency modulated sinusoid

Theory

The peripheral part of the auditory pathway is commonly modeled as a bank of overlapping bandpass filters (Fletcher 1940, see Plomp 1976 and Moore 1982 for reviews). Several authors have used psychophysical procedures to estimate the shapes and equivalent rectangular bandwidths (ERBs) of these filters. Moore and Glasberg (1983) plotted six authors, estimates of ERB versus center frequency and fitted the following curve to the data

$$ERB = 6.23f^2 + 93.39f + 28.52 \quad (1)$$

where *f is* the center bandwidth in kHz and ERB is expressed in Hz. For our present purpose we note that ERB is 47.5Hz when f = 0.2kHz, 128Hz when f = 1.0kHz and 651 Hz when f = 5.0kHz.

The frequency difference between adjacent components in the power spectrum of a quasi-FM or AM tone is equal to the modulation frequency. Because the psychophysical distinction between the putative mechanisms for quasi-FM and AM is greatest at low frequencies of modulation (Kay and Matthews 1972; Regan and Tansley, 1979) attempts to investigate possible differences between these putative mechanisms should utilize low modulation frequencies. If, for example, we consider a modulation frequency of 2.0 Hz and a carrier frequency 1.0 kHz, the 4.0 Hz range of the three spectral components of a quasi-FM or AM tone would easily fit within the estimated 128 Hz ERB of the auditory filter centered on 1.0 kHz (Moore and Glasberg 1983). More specifically, suppose that the auditory filter has the rounded exponential (roex) form proposed by Patterson et al. (1982) given by

$$W(g) = (1 + pg)e^{(-pg)} \quad (2)$$

where W(g) is the intensity weighting function, g is the deviation from the center frequency and p is a parameter defining the sharpness of the filter. If we set p = *31.22* (Moore and Glasberg, 1983), then if the amplitude of a sideband relative to

Fig.32

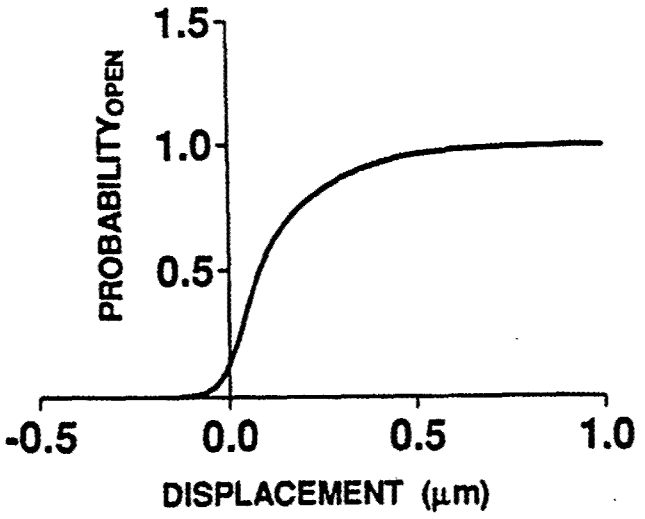

Experimentally–measured response characteristis of hair cells in bullfrog: tranduction frm sound to neural signal probability. Hair cell displacement in microns is plotted on the abscissa and the probability is plotted as ordinate. From Assad and Corey (1992).

Fig.33

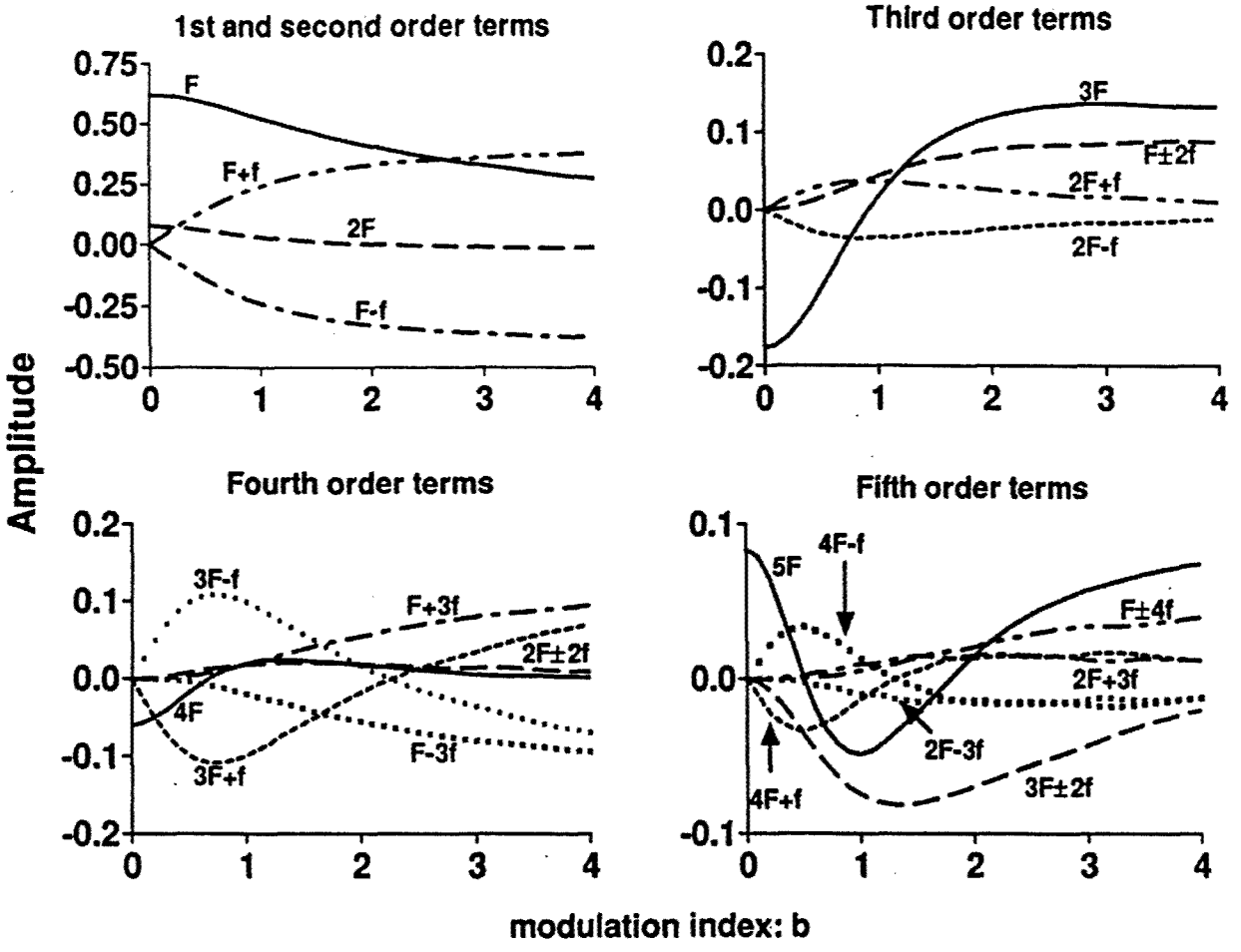

The family of curves for the output of the Figure 32 transducer function whose input is a quasi–FM waveform, $f(x,y,)=\cos x - b \sin x \sin y$ where $0<b<4$, $x=2\pi Ft$ and $y=2\pi ft$.

Fig.34

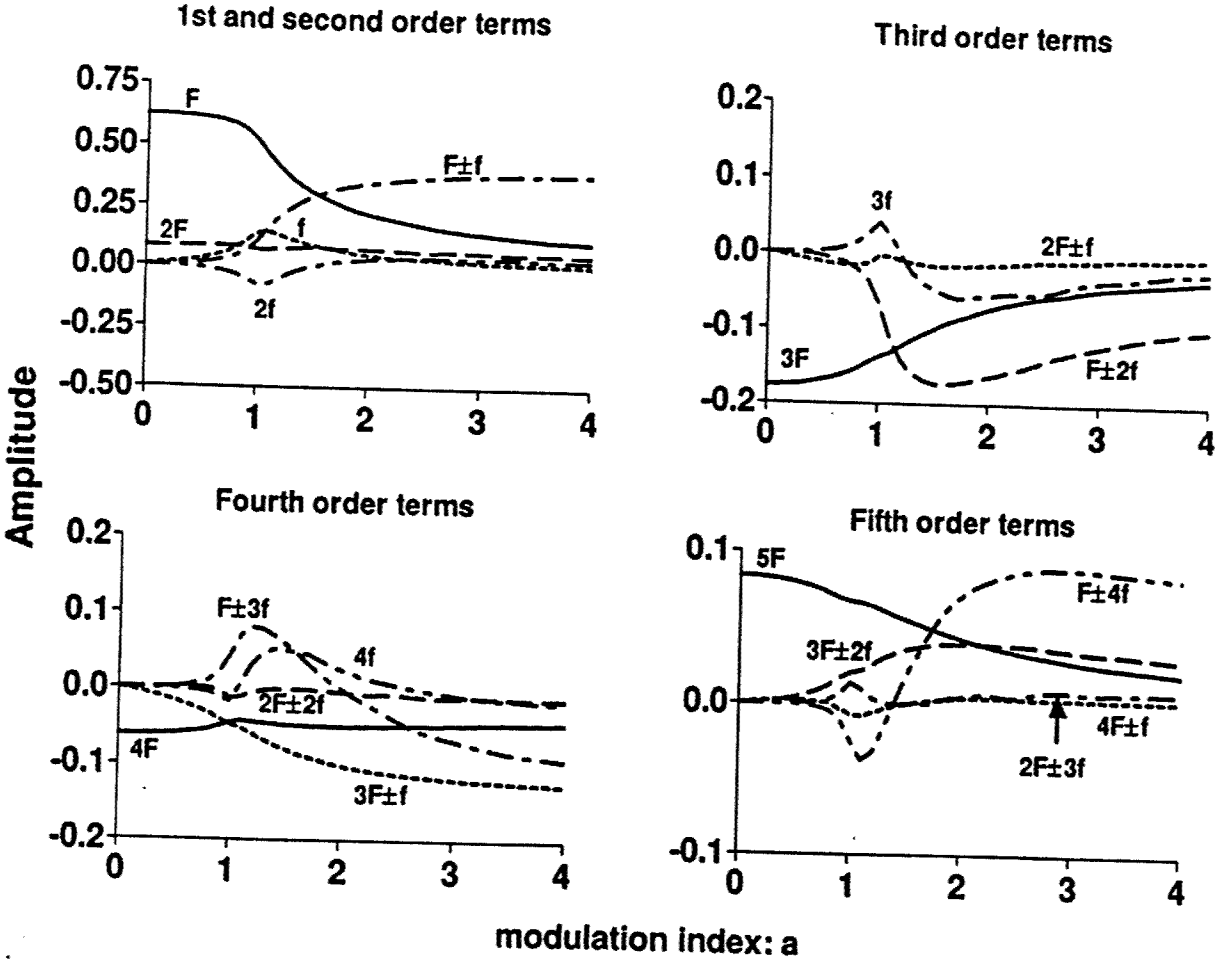

The family of curves for the output of the Figure 32 transducer function whose input is an AM waveform, $(1+a \cos y)\cos x$ where $0 \leq a \leq 4$, $x=2\pi Ft$ and $y=2\pi ft$.

the carrier was 1.0 before filtering, it would be approximately the same after filtering.

According to Assad and Corey (1992), the characteristic of an empirical hair cell transducer function fits the theoretical equation

$$H(r) = 1/(1+\exp[(g_2 - z_2 r)/kT]\{1+\exp[(g_1 - z_1 r)/kT]\}) \quad (3)$$

with g_1=6.1 x 10^{-21}, z_1=1.09 x 10^{-13}, g_2=7 x 10^{-22}, z_2=2.7x10^{-14} Newtons, r the hair cell displacement and $kT \approx h$ x 6 x 10^{12}sec^{-1} (Corey and Hudspeth,1983). This equation is shown graphically in Fig. 32. Suppose that the input to the transducer is a quasi-FM tone, in particular, a sinusoid whose amplitude is Q, of frequency F Hz and phase θF which is frequency modulated by a frequency f and phase θ_f.

A quasi-FM sinusoid can be expressed as the function $g(x,y)$ as follows,

$$\begin{aligned} g(x,y) &= Q\{\cos(2\pi Ft + \theta_F) + \frac{b}{2}\cos(2\pi(F+f)t + \theta_F + \theta_f) - \frac{b}{2}\cos(2\pi(F-f)t + \theta_F - \theta_f)\} \\ &= Q\{\cos(2\pi Ft + \theta_F) - b\sin(2\pi Ft + \theta_F)\sin(2\pi ft + \theta_f)\} \\ &= Q\{\cos x - b\sin x \sin y\} \end{aligned} \quad (4)$$

where x=$2\pi Ft$ + θ_F, y=$2\pi ft$ + θ_f and, for our present purpose, Q, b>0. In order to generate sidebands of the same amplitude as the sidebands for AM, the coefficient b in Eq. (4) corresponds to a in Eq. (14). As indicated by Equation 4, a quasi-FM sinusoid differs from an FM sinusoid in that its spectrum contains only two sidebands, while the spectrum of an FM sinusoid contains many sidebands. (In the time domain the envelope of a quasi-FM sinusoid is modulated, while the envelope of an FM sinusoid is unmodulated). These points are illustrated in Fig. 1.64 of Regan (1989).

If $g(x,y)$ is the input to a rectifier with characteristic given by Eq. (3), t the output $G(x,y)$ is given by

$$G(x,y) = H[g(x,y)] \quad (5)$$

The output from the rectifier is a periodic function of two variables with period 2π for both variables. $G(x,y)$ is bounded and its first derivatives are bounded in the rectangle $(-\pi,\pi) * (-\pi,\pi)$, so that $G(x,y)$ can be expressed as a

double Fourier series within this rectangle (Hobson 1926). Using the notation of Walker (1988), the Fourier series $G(x,y)$ is shown here where

$$G(x,y) = \sum_{m,n=0}^{\infty} \lambda_{mn} \{A_{mn} \cos mx \cos ny + B_{mn} \sin mx \cos ny + C_{mn} \cos mx \sin ny + D_{mn} \sin mx \sin ny\} \tag{6}$$

with

$$A_{mn} = \frac{1}{\pi^2} \int_{-\pi}^{\pi} \int_{-\pi}^{\pi} G(x,y) \cos mx \cos ny dx dy \tag{7}$$

$$B_{mn} = \frac{1}{\pi^2} \int_{-\pi}^{\pi} \int_{-\pi}^{\pi} G(x,y) \sin mx \cos ny dx dy \tag{8}$$

$$C_{mn} = \frac{1}{\pi^2} \int_{-\pi}^{\pi} \int_{-\pi}^{\pi} G(x,y) \cos mx \sin ny dx dy \tag{9}$$

$$D_{mn} = \frac{1}{\pi^2} \int_{-\pi}^{\pi} \int_{-\pi}^{\pi} G(x,y) \sin mx \sin ny dx dy \tag{10}$$

and

$$\lambda_{mn} = \begin{cases} \frac{1}{4}, & if \quad m = 0, n = 0 \\ \frac{1}{2}, & if \quad m = 0, n \neq 0 \; or \; m \neq 0, n = 0 \\ 1, & if \quad m \neq 0, n \neq 0 \end{cases} \tag{11}$$

Results- the quasi-FM waveform after nonlinear transduction

After hair cell transduction of quasi-FM, $B_{mn} = C_{mn} = 0$, for all values of m,r~ and, for all m, $A_{mn} = 0$ when n is odd and $D_{mn} = 0$ when n is even. For a quasi-FM input, the output of the rectifier can, from Eqs. (6) and (11) be expressed as follows.

$$\begin{aligned} G(x,y) &= \sum_{m,p=0}^{\infty} \lambda_{m(2p)} A_{m(2p)} \cos mx \cos 2py \\ &\quad + \lambda_{m(2p+1)} D_{m(2p+1)} \sin mx \sin(2p+1)y\} \\ &= \frac{1}{2} \sum_{m,p=0}^{\infty} \{\lambda_{m(2p)} A_{m(2p)} [\cos(mx + 2py) + \cos(mx - 2py)] \\ &\quad + \lambda_{m(2p+1)} D_{m(2p+1)} [\cos(mx + (2p+1)y - \pi) \\ &\quad + \cos(mx - (2p+1)y)]\} \end{aligned} \tag{12}$$

Hence, for all positive values of m, the amplitudes of the frequencies $mF \pm nf$ are given by

$$\begin{cases} \frac{1}{2}\lambda mn\, Amn, & n \quad \text{even} \\ \frac{1}{2}\lambda mn\, Dmn, & n \quad \text{odd} \end{cases} \tag{13}$$

The phases for the frequency components are shown in Table 1.

When $m = 0$, the amplitude of nf *is* zero when n *is* odd. When n *is* even, the amplitude of nf *is* far less than the amplitudes of the other frequency components. Thus, except for the fundamental and the harmonics of the modulating frequency f, all frequency components (i.e. the fundamental and the harmonics of the carrier frequency and the combination frequency components) are represented in the power spectrum.

We can represent the output of the rectifier as a spectrum for each of many discrete values of Q and b. Alternatively, for any amplitude Q, the amplitude of each frequency component can be plotted as a function of b. Fig.33 presents the data in this form for Q = 1.0.

Hair cell transduction of an amplitude-modulated sinusoid

Theory

It is well known that the difference between the time domain representations of an amplitude-modulated (AM) sinusoid and a quasi-FM sinusoid is reflected in the frequency domain only by a difference in the phase spectra: the two power plots are identical. An AM sinusoid can be expressed as the function g(x, y) as follows,

$$\begin{aligned} g(x,y) &= Q\{\cos(2\pi Ft + \theta_F) + a\cos(2\pi Ft + \theta_F)\cos(2\pi ft + \theta_f)\} \\ &= Q\cos x(1 + a\cos y). \end{aligned} \tag{14}$$

where $x = 2\pi Ft + \theta_F$, $y = 2\pi ft + \theta_f$ and Q, $a > 0$.

If $g(x, y)$ is the input to the rectifier, the output $G(x, y)$ can be expressed as a double Fourier series using Eqs. (7) to (10) as previously shown for quasi-FM.

Results: The AM waveform after nonlinear transduction

Unlike quasi-FM, $B_{mn} = C_{mn} = D_{mn} = 0$, for all values of m,n since $g(x,y)$ for AM is an even function. For AM, A_{mn}: is non-zero for all m, n.

Thus, in the case of AM and with the values for Amn as in Eq. (11), Eq. (6) can be rewritten in the following form.

$$\begin{aligned} G(x,y) &= \sum_{m,n=0}^{\infty} \lambda_{mn} A_{mn} \cos mx \cos ny \\ &= \frac{1}{2} \sum_{m,n=0}^{\infty} \lambda_{mn} A_{mn} \{\cos (mx + ny) + \cos (mx - ny)\} \\ &= \frac{1}{2} \sum_{m,n=0}^{\infty} \lambda_{mn} A_{mn} \cos (mx \pm ny) \end{aligned} \tag{15}$$

The amplitudes of the frequency components $mF \pm nf$ are given by $\frac{1}{2}\lambda_{mn}A_{mn}$ and the phases of all the frequency components are given by $m\theta_F \pm n\theta_f$ if A_{mn} is positive and by $m\theta_F \pm n\theta_f - \pi$ if A_{mn} is negative.

Thus, unlike quasi-FM, all frequency components (i.e. the fundamental and the harmonics of the carrier frequency and the modulating frequency and all the combination frequency components) are represented in the power spectrum or family of curves. As in the case of half-wave linear rectification of AM with an unsuppressed carrier (Regan 1994), the family of curves for AM changes its character rapidly around $a = 1$. For values of $a < 1$, the carrier frequency and its harmonics are clearly represented, but the amplitudes of the other frequency components (including the modulating frequency and its harmonics) are very small for small a.

Fig. 34 uses the same format as Fig. 33 to depict the output of the rectifier when fed with AM in the case that $Q = 1.0$. A comparison of Fig. 34 with Fig.33 brings out the point that the rectifier's output changes considerably when the input is switched from AM to quasi-FM with the value of Q held constant at 1.0.

Discussion

A comparison of Figs. 33 and 34 brings out the point that there is a marked difference between the power spectra of transduced quasi-FM and AM

signals for any given value of *b*. Furthermore, the phase spectra of transduced AM and quasi-FM differ by π for the sidebands $mF + (2p + l)f$, but the phases are the same for $mF - nf$ and for $mF + 2pf$, where $p = 1,2,3, \ldots$. This compares to the phases of the one pair of sidebands before transduction where there is a difference of π for $F - f$ and no difference for $F + f$. Since the two power spectra are identical before nonlinear transduction, we conclude that one effect of the nonlinear transduction is to translate a difference in phase spectra into a difference in amplitude spectra. This conclusion bears on the interpretation of the following findings: after adapting to a quasi-FM tone of $b = 1.0$, detection threshold for an FM tone was elevated more than detection threshold for an AM tone; after adapting to an AM tone of a = 0.5, detection threshold for an AM tone was elevated more than detection threshold for an FM tone.

Our proposed explanation for this differential adaptation is as follows. A comparison of Figs. 33 and 34 shows that transduced AM, but not transduced quasi-FM, includes terms at the modulating frequency *(f)* and its harmonics. The frequencies of these terms (e.g. $f = 2$Hz.) are far removed from the carrier frequency *(F)* (e.g. $F = 1000$Hz.). Considering the time-domain waveforms after transduction, although both are amplitude-modulated (the AM output much more strongly than the quasi-FM output), only for the quasi-FM does the point of maximum excitation on the basilar membrane oscillate at the modulation frequency. Suppose that two nearby locations on the basilar membrane feed an opponent-process element that, for example, subtracts the two inputs, and that there is an array of such opponent-process elements along the basilar membrane. For transduced quasi-FM, but not for transduced AM, the output of activated opponent-process elements would be a temporal waveform whose envelope was strongly amplitude-modulated at low frequency. Such opponent-process elements could be adapted by quasi-FM but not by AM, while the mechanisms sensitive to low temporal frequencies and to amplitude-modulation of the carrier frequency would be more strongly adapted by AM than by quasi-FM.

2.4 Evoked potential studies:

2.4(a) Orientation characteristics of a mechanism in the human visual system sensitive to cyclopean form.

Long term aim 1.1.4; Specific Aim 1.2.17. This project is completed and was reported to the 1999 and 2000 meetings of ARVO and has been published in Vision Research: M.P. Regan & D. Regan (2002). "Orientation characteristics of a mechanism in the human visual system sensitive to cyclopean form". Vision Research, 42, 661-668.

Background

Psychophysically based models of the detection of disparity–defined (DD) form have been reviewed by Tyler (1991, 1995). In brief, there is psychophysical evidence for an early visual processing stage that can be modeled in terms of a parallel array of spatial filters for cyclopean form, each of which is tuned to orientation and spatial frequency, and has a strictly local receptive field (Julesz & Miller, 1975; Schumer & Ganz, 1979; Tyler, 1983; Cavanagh, 1989; Yang & Blake, 1991; Cormack et al., 1993). However, although the existence of a tilt aftereffect for cyclopean form indicates that these early cyclopean filters are tuned to orientation (Tyler, 1975; Cavanagh, 1989), estimates of the orientation tuning bandwidth of cyclopean filters are lacking. In this study we attempted to measure orientation tuning bandwidths of cyclopean mechanisms in humans using an objective rather than a psychophysical approach.

Rationale

During the time that an observer views a temporally repetitive stimulus it may be possible to record a repetitive brain signal from scalp electrodes. A steady–state evoked potential is defined as a repetitive brain response whose constituent discrete frequency (Fourier) components remain constant in amplitude and phase throughout the stimulation (Regan, 1966, 1989). The Heisenberg–Pauli–Gabor equation states that the frequency resolution (ΔF Hz) within the spectrum of a steady–state evoked potential is equal to $(\Delta T)^{-1}$, where ΔT is the recording duration in sec. (Gabor, 1946; reviewed in Regan, 1989). Thus for example, a recording duration of 100 sec offers a maximum possible resolution of 0.01 Hz in the response spectrum. In the present study we used nondestructive zoom–FFT (Regan & Regan, 1988) to attain the maximum

possible resolution in the frequency domain. Each recording had a duration of 128 sec, giving a spectral resolution of 0.0078 Hz independently of the bandwidth of the frequency spectrum. In our case this gave 3800 frequency bins over the recording bandwidth of 0.3–30Hz. This procedure can display a signal frequency components at a high signal-to–noise ratio even when the power of the component is hundreds or even thousands of times less than the power of the corresponding averaged waveform (Regan, 1989, Fig. 1.70A; Regan & Regan, 1988, Fig.10, 1989, Fig.1). The reason is that a signal frequency component can lie within only one bin (Regan, 1989, pp. 95-96), while the noise is spread throughout all bins. We labelled or "tagged" the two gratings by assigning them different temporal modulation frequencies.

The rationale used in the experiment described below is as follows. It is well known that a grating that is counterphase–modulated at F_1 Hz and presented in isolation can generate steady–state evoked potential components at the pattern–reversal frequency $2F_1$Hz and at harmonics of that frequency (i.e., $4F_1$, $6F_1$, $8F_1$, etc). If this is so, a second grating of the same spatial frequency and orientation that is counterphase–modulated at F_2 Hz (where $F_1 \approx F_2$) will generate steady–state evoked potential components of $2F_2$Hz and harmonics when presented in isolation. However, if the two gratings are superimposed it is not necessarily the case that the resulting response will be the linear sum of the responses to the gratings presented in isolation. On the contrary, for luminance–defined gratings one may observe nonlinear suppression of pattern response components such as $2F_1$ and $2F_2$, coupled with the generation of nonlinear cross–modulation pattern response components of frequency ($2nF_1 + 2mF_2$), where n and m are integers and can be negative or positive. (Regan, 1983; Regan & Regan, 1986, 1987). The crucial point is that such nonlinear interactions between responses to the two grating patterns can occur only if the orientations of both gratings fall within the orientation tuning bandwidth of a single neural mechanism.. (In other words, the mechanism must "see" both gratings.) Thus, by progressively increasing the orientation difference between the two gratings, it is

possible to estimate the orientation tuning bandwidth of the mechanism sensitive to cyclopean form. In a previous study we used sinusoidal luminance–defined (LD) gratings. (Regan & Regan, 1986, 1987). In the present study on cyclopean form we use squarewave gratings because it is not possible to generate a sinusoidal cyclopean grating (without monocular cues) whose orientation is other than within the meridian that contains the eyes (horizontal in our case). This is because a nonhorizontal sinusoidal cyclopean grating necessarily contains variations of dot density at the periodicity of the cyclopean grating, and these, are visible to one or both eyes monocularly.

Methods

Referring to Fig.35, a vertical squarewave cyclopean grating was generated within dynamic random noise on monitor M1 and the disparity of adjacent bars was counterphase–modulated with an F_1 Hz sinusoidal waveform. The frame rate of M1 was 120 Hz and the sense of circular polarization of liquid crystal LC1 was switched on alternate frames. The observer wore passive circularly–polarizing goggles (CPG) so that the left and right eyes' components of each stereopair were routed to the appropriate eyes. A second squarewave cyclopean grating of variable orientation could be generated within dynamic random noise on monitor M2, the disparity of adjacent bars was counterphase–modulated at F_2 Hz with a sinusoidal waveform, and the left and right eyes' components of each stereopair were routed to the appropriate eyes by means of liquid crystal LC2. The two displays were optically superimposed by pellicle P (Fig.35). The square display was viewed at a distance of 70 cm and subtended 16x16 deg. Each cycle of the temporal sinusoid on either display was a series of 12 different stereopairs. A new stereopair was presented ca. every 40 msec. At any given instant 256 bright dots were visible to either eye on monitor M1 and also on M2. Each dot subtended 0.12x0.12 deg. The disparity of any given cyclopean bar oscillated between ± 0.98 deg (± 8 dot widths) with respect to the plane of the display. A fixation mark at zero disparity at the centre of the display was provided by a laser pointer (not shown in Fig.20).

Fig.35

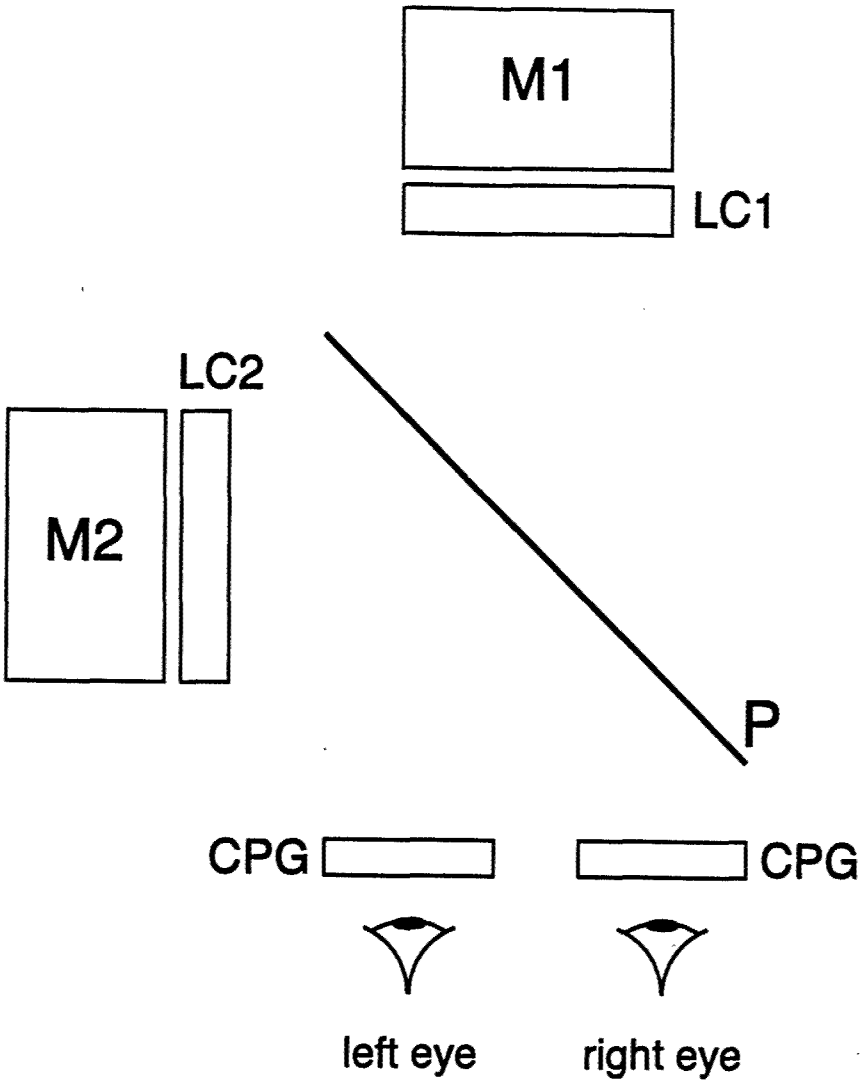

Schematic of the stimulus generator. M1–M2—monitors; LC1, LC2 — circularly polarizing liquid crystals; P–pellicle; CPG-circularly polarizing goggles.

Fig.36

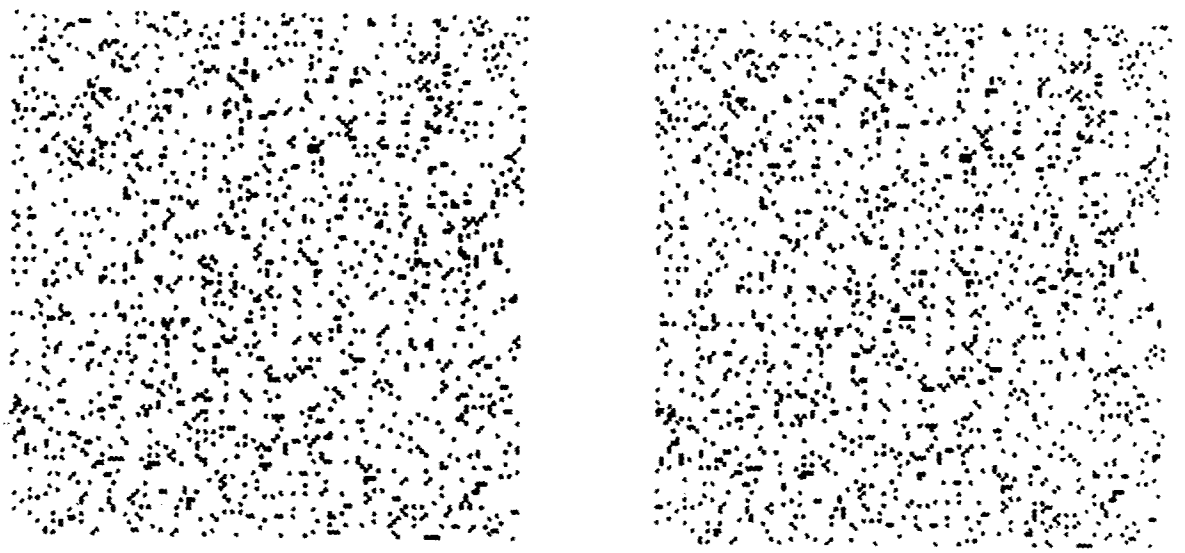

Negative photograph of one frame of the stereopair display of a single vertical cyclopean grating.

Fig.37

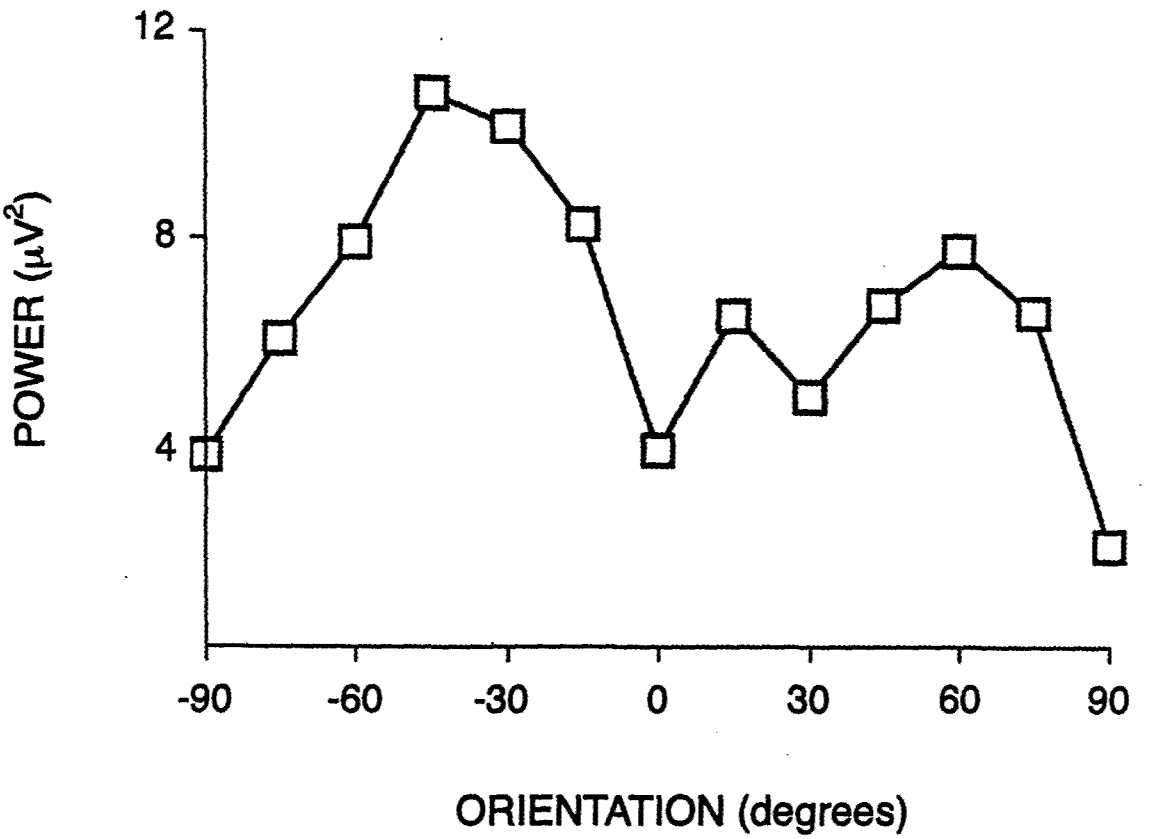

An inverse oblique effect. Data points show the effect of grating orientation on the 2*F*Hz response to a single cyclopean grating whose disparity was counterphase–modulated at fequency *F* (1.05 Hz). Bar width was 1.9°. Observer 1

The appearance of the display was as follows. Individual dots appeared and disappeared like the 'snow' on a detuned television set. When either of the two monitors was occluded the observer saw sharp–edged cyclopean bars within the dynamic random noise (Fig. 36). Adjacent bars oscillated forward and backward in depth in antiphase about a mean of zero disparity.

Experiment 1

The aim of Expt.1 was to determine the orientation selectively of the response to a single cyclopean grating.

Monitor M2 was occluded by a black card and power spectra were recorded for different grating orientations. This experiment was repeated for 6 bar widths from 0.5 deg to 3.5 deg.

Fig. 37 shows that for the 1.9 deg bar width used in Expt.1, the response at the pattern–reversal frequency was considerably stronger for both obliques than for either vertical or horizontal. This effect, however, depended on bar width. Oblique gratings gave the largest responses over a range of bar widths of about 1.2 to 1.9 deg, but were comparable to the responses produced by vertical or horizontal gratings for larger or smaller bar widths. The signal–to–noise ratio of the largest responses in Fig. 37 is typified by Fig. 39.

Experiment 2 Purpose and methods

The aim of Expt.2 was to find whether the orientation tuning curve shown in Fig. 37 represents the activity of a single orientation–tuned cyclopean mechanism.

The vertical cyclopean grating generated by monitor M1 (Fig.35) was modulated sinusoidally at 1.05 Hz (i.e. local disparity was modulated at 1.05 Hz and the modulation was in antiphase in adjacent bars). The optically–superimposed cyclopean grating generated by monitor M2 was counterphase–modulated sinusoidally at 1.35 Hz and was varied in orientation. Bar width was 1.9 deg for each of the two cyclopean gratings. The appearance of the display was as follows. A beating effect of frequency (F_1–F_2) Hz was evident when the display generated by monitor M2 was exactly superimposed on the M1

display and both sets of bars were vertical. The sinusoidal oscillation in depth slowly grew larger, then diminished to zero so that no bars were visible, then slowly grew large again, and so on. The percept was more complex when the bars displayed by monitor M2 were not vertical. For example, in the case that the bars generated by monitor M2 were horizontal the resulting percept was a pattern of cyclopean checks at the instant when the maximum amplitudes of the cyclopean bars generated by M1 and M2 occurred simultaneously (Fig.38). However, as the relative phases of the two oscillations slowly changed the spatial appearance of the pattern slowly changed with either horizontal or vertical bars predominating at different instants.

Experiment 2: Results

Fig. 39 shows the response to the cyclopean grating generated by monitor M1 while the M2 display was covered by black card. No response at the counterphase–modulation frequency F_1 nor at its odd harmonics (e.g. $3F_1$) was evident, but there was a strong response at the pattern–reversal frequency ($2F_1$Hz), i.e. the frequency at which near and far bars exchanged places (the signal-to–noise ratio was 10). This is also the frequency of reversal of the steep gradient of disparity across the edges of the bars. Similarly, when monitor M2 was covered by a blank card, there was a strong response at frequency $2F_2$Hz, a weaker response at $4F_2$Hz, and no response at odd harmonics. The $2F_2$ response as somewhat larger than the $2F_1$ response because of the difference in modulation frequency.

Fig.40(A) shows the result of superimposing the two cyclopean grating s with both gratings vertical. The $2F_1$ term in Fig. 39 was completely suppressed and the $2F_2$ term was almost completely suppressed. A strong nonlinear cross–modulation component of frequency $(F_1 + F_2)$ Hz appeared with a signal–to–noise ratio of 5. Fig. 40(B) shows that when the orientation of the variable grating was set at 45 deg the $(F_1 + F_2)$ component disappeared and,

Fig.38

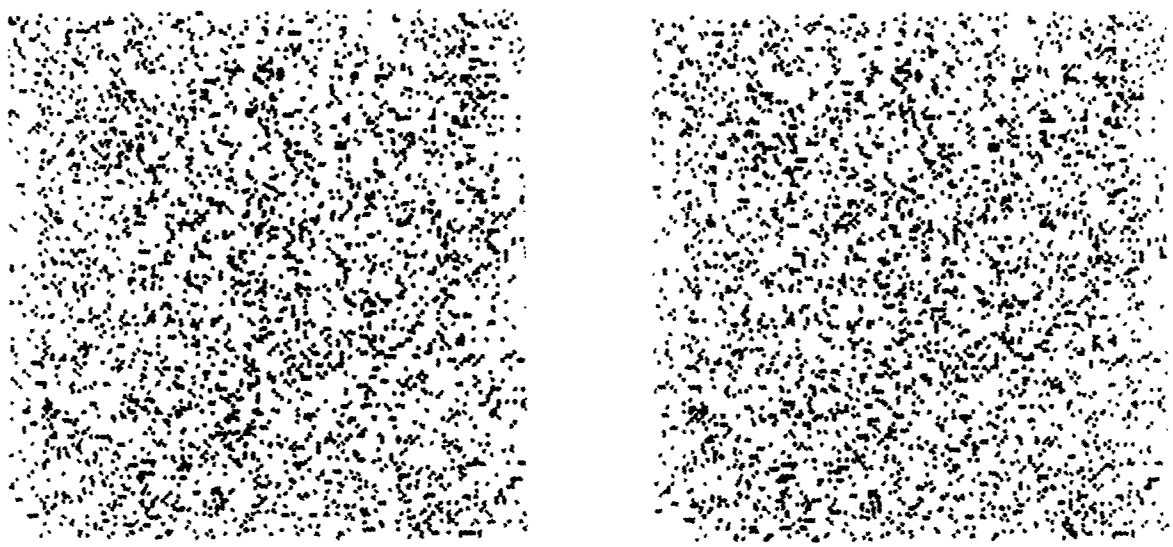

Negative photograph of one frame of the stereopair display of a horizontal cyclopean grating superimposed on a vertical cyclopean grating. This illustrates the instant during the temporal modulation when the observer saw a pattern of checks, neither grating predominating.

Fig.39

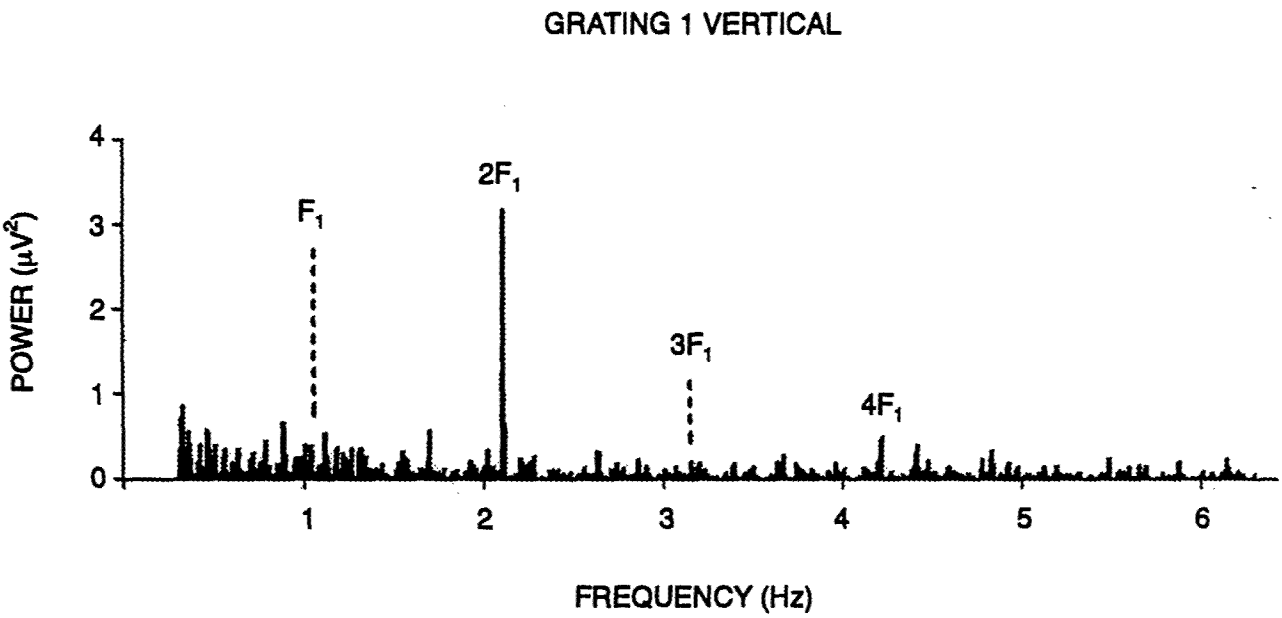

Power spectrum of the brain response evoked by a single vertical cyclopean squarewave grating of bar width 1.9° whose display was counterphase–modulated sinusoidally at frequency F_1 (1.05 Hz). The spectral resolution was 0.008 Hz. Recording between an electrode on the inion and an electrode on the vertex. The right earlobes were grounded. Observer 2.

Fig.40

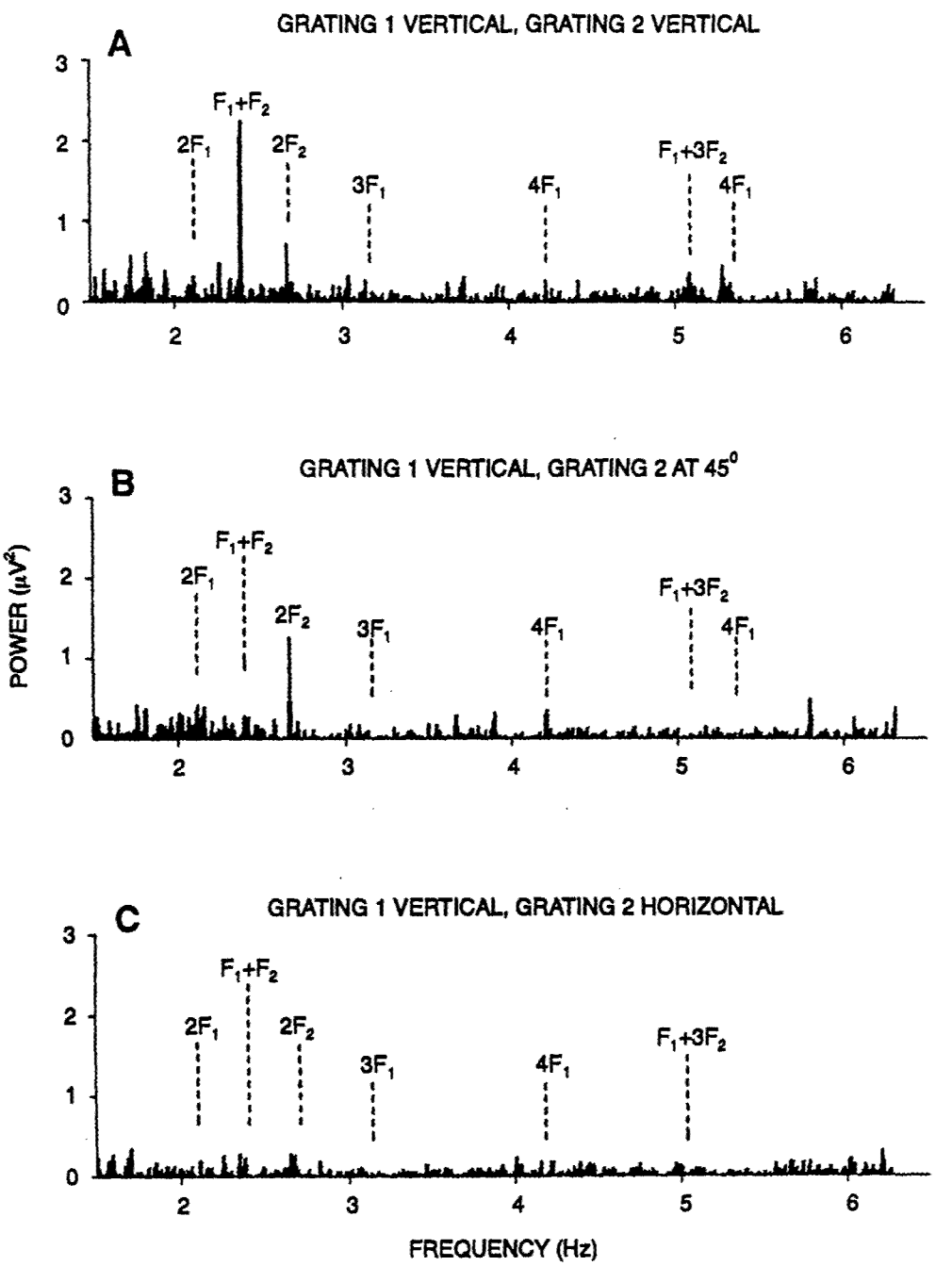

(A–C) Power spectra of the brain response recorded while the observer viewed a vertical cyclopean squarewave grating whose disparity was counterphase–modulated sinusoidally at frequency F_1 (1.05 Hz) on which was superimposed a second cyclopean squarewave grating whose disparity was counterphase–modulated at frequency F_2 (1.35 Hz) and whose orientation was variable. Bar width was 1.9 deg for both gratings. The spectral resolution was 0.008 Hz. Recording was between an electrode on the inion and an electrode on the vertex. Observer 2.

although the $2F_1$ Hz component remained completely suppressed, the $2F_2$ Hz component was somewhat larger than in Fig. 40(A) with a signal–to–noise ratio of 7. When the orientation of the variable grating was set at 90 deg (Fig. 40C) no response components were evident in the spectrum. Data from observer 2 were similar except that the (F_1+F_2) term was not evident.

Discussion

In a study on superimposed luminance–defined gratings that is analogous to the experiment just described, the $2F_1$ Hz component at the pattern–reversal frequency of the fixed vertical grating was strongly suppressed when the variable grating was either vertical or horizontal, but was much less strongly suppressed when the variable grating was inclined at 45 deg to the vertical (Regan & Regan, 1987, 1988). The following explanation was offered: (1) the neural mechanism responsible for the $2F_1$ Hz response to a luminance–defined grating is tuned to orientation. The half–height full bandwidth of the suppression was estimated as *ca*.30 deg; (2) there is a strong nonlinear interaction between mechanisms that prefer horizontal and vertical orientations. Our present data on cyclopean gratings can be discussed along these same lines.

Because both of the superimposed gratings were cyclopean, the nonlinear interactions we report here must have been between responses to the two gratings that occurred after signals from the left and right eyes had converged.

A major difference between our present cyclopean data and previous data on luminance–defined gratings is that superimposed luminance–defined gratings produced a clear $(2F_1 + 2F_2)$ Hz nonlinear interaction component that behaved in the opposite way to the $2F_1$ Hz component, being large when the gratings were parallel or orthogonal and small when the gratings were at 45 deg to each other. For cyclopean gratings none of our subjects gave a $(2F_1 + 2F_2)$ Hz component. This suggests that, at least for the subjects in the present and the previous study, the nonlinearity of the orientation–tuned mechanism for cyclopean form is of a

quite different nature to the nonlinearity of the orientation–tuned mechanism for luminance–defined form.

Next we discuss the (F_1 + F_2) Hz response in Fig. 40(A). In Fig.39, even if each bar generated responses at the frequency of local oscillations of disparity (i.e. F_1) it would not be expected that any appreciable response component at F_1 Hz would be observed, because the disparities of adjacent bars were modulated with 180 deg phase difference so that the responses generated by individual bars would sum to near–zero at any given scalp electrode. The situation is different for the (F_1 + F_2) Hz nonlinear interaction component evident in Fig. 40(A). This component can be attributed to a nonlinear interaction between responses to F_1 Hz and F_2 Hz modulations of local disparity. rather than being related to the processing of the spatial structure of the gratings. The (F_1 + F_2) Hz signals produced within any given bar would have a phase difference of 360 deg between adjacent bars (Bennett, 1933) and would, therefore, sum over the entire pattern. The (F_1 + F_2) Hz component would be expected to vanish when the variable grating was tilted through a small angle such that the area of any given bar of the F_1 Hz vertical grating was half covered by one F_2 Hz bar while the other half was covered by a second adjacent F_2 Hz bar that was modulated in antiphase to the first. A similar effect was observed with luminance–defined gratings, but for other terms [(F_1+3F_2), (5F_2–F_1)] as well as the (F_1+F_2) term (Regan & Regan, 1987, 1988).

The 2F_1 component at the pattern–reversal frequency was nonlinearly suppressed, not only when the superimposed grating was parallel to the fixed vertical grating, but also when it was at 45 deg and at right angles. One possible explanation for this finding is that just as in the case of luminance–defined form, there are strong nonlinear interactions. between cyclopean mechanisms that respond best to horizontal and to vertical bars. The complete suppression of the 2F_1 response is not surprising considering that, because of the difference in

modulation frequencies, the variable grating was a stronger stimulus than the fixed grating.

An isolated grating with a bar width the same as in Expt.2 gave a larger pattern–reversal response when orientated obliquely than when it was horizontal or vertical. Therefore, we cannot assume from the finding that the $2F_2$ response was larger in Fig. 40B than Fig. 40A that the sensitivity of the cyclopean mechanism was greatly less at 0 deg (vertical) than at 45 deg. Therefore we conclude that for the subjects reported here the half–sensitivity full orientation bandwidth of the cyclopean form mechanism that prefers bars 1.9 deg wide is greater than 90 deg. This is considerably broader than our previous estimate of the corresponding bandwidth for luminance–defined form (Regan & Regan, 1987). The suppression of the $2F_2$Hz response of the vertical grating by the horizontal grating in Fig.40C indicates that the cyclopean mechanism that responded to the vertical grating was also sensitive to a horizontal grating.

Finally we note that, for luminance–defined gratings of high spatial frequency viewed foveally, contrast sensitivity and grating acuity are less for oblique than for vertical and horizontal gratings (Taylor, 1963; Berkeley et al., 1975). Here, we report that, over a range of bar widths of about 1.2 – 1.9 deg and for the subjects reported here, steady–state evoked potentials to cyclopean gratings show an inverse oblique effect. Wilson et al. (2001) reported that, for the 3 subjects that they tested, psychophysical thresholds for detecting structure in random–dot Glass patterns also showed an inverse oblique effect, and suggested that the relevant common factor in their experiment and our report of an inverse oblique effect for cyclopean gratings (Regan, Hong & Regan, 2000) is that spatial form was carried by a dot pattern.

3. References to Accomplishments /New findings

Abernathey, B. & Burgess-Limerick, R. (1992). Visual information for the timing of skilled movements: a review. In *Approaches to the study of motor control and learning*. (Ed. J.J. Summers). NewYork: Elsevier.

Alderson GJK, Sully DJ, Sully H. (1974). An operational analysis of a one-handed catching task using high-speed photography. *J Motor Behavior*, 6:217-226.

Bennett, W.R. (1933). New results in the calculation of modulation products. *Bell System Technical Journal, 13*, 228–243.

Berkeley, M.A., Kitterle, F. & Watkins, D.W. (1975). Grating visibility as a function of orientation and retinal eccentricity. *Vision Research*, 15, 239-245.

Beverley K. I., Regan D. (1979). Separable aftereffects of changing-size and motion-in-depth: Different neural mechanisms? *Vision Research*, 19:727-732.

Beverley K. I., Regan D. (1979). Visual perception of changing-size: the effect of object size. *Vision Research*, 19:1093-1104.

Beverley, K. I. & Regan, D. (1982). Adaptation to incomplete flow patterns: No evidence for 'filling-in' the perception of flow patterns. *Perception, 11*, 275-278.

Blaquière, A. (1966) *Nonlinear Systems Analysis*. New York: Academic Press.

Bondarko, V.M. & Danilova, M.V. (1999). Spatial interval discrimination in the presence of flanking lines. *Spatial Vision*, 12, 239–253.

Brandt, T., Dichgans, J. & Koenig, E. (1973). Differential effects of central versus peripheral vision on egocentric and exocentric motion perception. *Experimental Brain Research, 23*, 471-489.

Burbeck, C. A. & Hadden, S. (1993). Scaled position integration areas: accounting for Weber's law for separation. *Journal of the Optical Society of America, A*, 10, 5–15.

Burbeck, C.A. & Pizer, S.M. (1995). Object representation by cores: Identifying and representing primitive spatial regions. *Vision Research*, 35, 1917-1930.

Campbell, F.W., Nachmias, J. & Jukes, J. (1970). Spatial frequency discrimination in human vision. *Journal of the Optical Society of America,* 60, 555-559.

Cavanagh, P. (1989). Multiple analysis of orientation in the visual system. In Lam, D (ed.) *Neural mechanisms of visual perception*. Woodlands, Texas: Porfolio Publishing, 25–43.

Chen, S. & Levi, D.M. (1996). Angle judgements: is the whole the sum of the parts? *Vision Research*, 36, 1721-1735.

Cormack, L.K., Stevenson, S.B. & Schor, C.M. (1993) Disparity - tuned channels of the human visual system. *Visual Neuroscience*, 10, 585-596.

Danilova, M.V. & Mollon, J.D. (1999). What do we compare when comparing separate objects? *Journal of Optical Technology,* 66, 857–861.

Denton, G. G. (1976). The influence of adaptation on subjective velocity for an observer in simulated rectilinear motion. *Ergonomics, 19*, 409-430.

Denton, G. G. (1977). Visual motion aftereffect induced by simulated rectilinear motion. *Perception, 6*, 711-718.

Denton, G. G. (1980). The influence of visual pattern on perceived speed. *Perception, 9*, 393-402.

DeValois, R.L., Yund, E.W., & Hepler, N. (1982). The orientation and direction selectivity of sells in macaque visual cortex. *Vision Research*, 22, 531-544.

Ellis, W.D. (1967). *A source book of Gestalt psychology*. New York: Humanities Press.

Eriksen, C. W. & James, J. D. (1986). Visual attention within and around the field of focal attention: a zoom lens model. *Perception & Psychophysics*, 40, 225-240.

Fahle, M. & Harris, J.P. (1992). Visual memory for vernier offsets. *Vision Research*, 32, 1033-1042.

Finney, D.J. (1971). *Probit Analysis*. Cambridge: Cambridge Univ. Press.

Frost BJ, Wylie DR, Wang YC. (1990). The processing of object and self-motion in the tectofugal and accessory optic pathways of birds. *Vision Research*, 30:1677-1688.

Graham, N. (1989). *Visual Pattern Analyzers*. New York: Oxford University Press.

Gray R. (1998). *Estimating time to collision using binocular and monocular visual information*. Ph.D. Dissertation. York University, Toronto, Canada.

Gray, R. & Regan, D. (1996). Estimates of time to collision based on binocular and monocular visual information. *Investigative Ophthalmology and Vision Science,* 37(suppl.), 652.

Gray, R. & Regan, D. (1997). Spatial frequency discrimination and detection characteristics for gratings defined by orientation texture. *Vision Research*, 38, 2601-2617.

Gray R. & Regan D: (1998). Accuracy of estimating time to collision using binocular and monocular information. *Vision Research,* 38:499-512.

Gray, R. & Regan, D. (1999a). Adapting to expansion increases perceived time to collision. *Vision Research, 39*, 3602-3607.

Gray, R. & Regan, D. (1999b). Do monocular time to collision estimates necessarily involve perceived distance? *Perception*, 28, 1257–1264.

Gray, R. & Regan, D. (2000a). Estimating the time to collision with a rotating nonspherical object. *Vision Research*, 40, 49-63.

Greenlee, M.W. (1990). Dimensionality of the neuronal representation of visual images. *Perception*, 20, A40.

Hamstra, S.J. & Regan, D. (1995). Orientation discrimination in cyclopean vision. *Vision Research*, 35, 365-374.

Hatsopoulos N, Gabbiani F, Laurent G. (1995). Elementary computation of object approach by a wide-field visual neuron. *Science*, 270:1000-1003.

Hess, R.F. & Badcock, D.R. (1995). Metric for separation discrimination by the human visual system. *Journal of the Optical Society of America, A*, 12, 3–16.

Howard, I. & Heckman, T. (1989). Circular vection as a function of the relative sizes, distances, and positions of two competing visual displays. *Perception, 18*, 657-665.

Hoyle F. (1957). *In The Black Cloud*. London: Penguin;:26-27.

Julesz, B. & Miller, J. E. (1975). Independent spatial-frequency-tuned channels in binocular fusion and rivalry. *Perception*, *4*, 125, 143.

Koffka, K. (1935). *Principles of Gestalt psychology*. New York: Harcourt, Brace & World.

Kohly, R.P. & Regan, D. (1999). Evidence for a mechanism sensitive to the speed of cyclopean form. *Vision Research* 39, 1011–1024.

Kohly, R.P. & Regan, D. (2000). Coincidence detectors: visual processing of a pair of lines and implications for shape discrimination. *Vision Research*, 40, 2291–2306.

Kohly, R.P. & Regan, D. (2001). Long-distance interactions in cyclopean vision. *Proceedings of the Royal Society of London B*, 268, 213-219

Kohly, R.P. & Regan, D. (2002). Fast long-range interactions in the early processing of luminance–defined form. *Vision Research*, 42, 49-63.

Kowler, E. (1990). The role of visual and cognitive processes in the control of eye movements. In E. Kowler (Ed.) *Eye movements and their role in visual and cognitive processes.* New York: Elsevier, pp.1–70.

Lee DN. (1976). A theory of visual control of braking based on information about time-to-collision. *Perception*, 5:437-459.

Levitt H. (1971). Transformed up-down methods in psychoacoustics. *J Acoustical Soc Amer*, 49:65-69.

Li, W & Westheimer, G (1997). Human discrimination of the implicit orientation of simple symmetrical patterns. *Vision Research, 38, 557-572.*

Lotze, H. (1985). *Microcosmos.* Edinburgh: T&T Clark. Translated by E. Hamilton and E.E. Constance-Jones.

Macmillan, N.A. and Creelman, C.D. (1991). *Detection Theory: A user's Guide.* Cambridge: Cambridge University Press.

Magnussen, S. & Dyrnes, S. (1994). High–fidelity perceptual long–term memory. *Psychological Science*, 5, 99–103.

Magnussen, S., Greenlee, M.W., Asplund, R. & Dyrnes, S. (1990). Perfect visual short–term memory for periodic patterns. *European Journal of Cognitive Psychology,* 2, 345-362.

Marmarelis, P. Z. & Marmarelis, V. Z. (1978). *Analysis of Physiological Systems: the White Noise Approach.* New York: Plenum Press.

Mathews, M. L. (1978). A field study of the effects of drivers' adaptation to automobile velocity. *Human Factors, 20,* 709-716.

Morgan, M. J. & Regan, D. (1987). Opponent model for line interval discrimination: interval and vernier performance compared. *Vision Research,* 27, 107-118.

Morgan, M. J. (1986). Positional acuity without monocular cues. *Perception*, 15, 157-162.

Morgan, M.J. & Ward, R.M. (1985). Spatial and spatial–frequency primitives in spatial–interval discrimination. *Journal of the Optical Society of America*, A, 2, 1205-1210.

Morgan, M.J. (1991). Hyperacuity. In D. Regan (Ed.) *Spatial Vision.* London: MacMillan, pp. 87–113.

Morgan, M.J., Ward, R.M., & Hole, G.J. (1990). Evidence for positional coding in hyperacuity. *Journal of the Optical Society of America*, A, &, 297–304.

Mountcastle, V. B. (1979). An organizing principle for cerebral functions: The unit module and the distributed system. In F. O. Schmitt and F. G. Worden (Eds.)

The Neurosciences: Fourth Study Program (pp. 21-42). Cambridge, Mass.: M. I. T. Press

Mustillo, P., Francis, R., Oross, S., Fox, R., & Orban, G. (1988). Anisotropies in global stereoscopic orientation discrimination. *Vision Research*, 28, 1315-1321.

Obergfell, J., Greenlee, M.W. & Magnussen, S. (1989). Short–term memory for motion: Temporal–frequency discrimination of drifting gratings. *Perception*, 18, A38.

Portfors–Yeomans, C.V. & Regan, D. (1997). Discrimination of the direction and speed of a monocularly–visible target from binocular information alone. *Journal of Experimental Psychology: Human Perception and Performance*, 23, 227–243.

Posner, M. I. , Snyder, C. R. R. , & Davidson, B. J. (1980). Attention and the detection of signals. *Journal of Experimental Psychology: General*, 109, 160-174.

Reeves, A. & Sperling, G. (1986). Attention grating in short–term visual memory. *Psychological Review,* 93, 180-206.

Regan, D. (1966). Some characteristics of average steady-state and transient responses evoked by modulated light. *Electroencephalography and Clinical Neurophysiology*, 20, 238–248.

Regan, D. (1985). Storage of spatial–frequency information and spatial–frequency discrimination. *Journal of the Optical Society of America, A*, 2, 619-621.

Regan, D. (1989). *Human Brain Electrophysiology*. New York: Elsevier.

Regan, D. (1991). Detection and spatial discrimination for objects defined by colour contrast, binocular disparity and motion parallax. In D. Regan (Ed.) *Spatial Vision*. London: Macmillan, pp. 135- 178.

Regan, D. (1995). Spatial orientation in aviation. *J. Vestibular Research*, 5, 455–471.

Regan, D. (2000). *Human Perception of Objects: Early Visual Processing of Spatial Form Defined by Luminance, Color, Texture, Motion, and Binocular Disparity.* Sunderland MA: Sinauer.

Regan, D. & Beverley, K. I. (1978). Looming detectors in the human visual pathway. *Vision Research, 18*, 415-421.

Regan, D. & Beverley, K. I. (1979). Visually guided locomotion: Psychophysical evidence for a neural mechanism sensitive to flow patterns. *Science, 205*, 311-313.

Regan, D. & Beverley, K.I. (1983). Spatial frequency discrimination and detection: comparison of postadaptation thresholds. *Journal of the Optical Society of America*, 73, 1684-1690.

Regan, D. & Beverley, K.I. (1985). Postadaptation orientation discrimination, *Journal of the Optical Society of America, A*, 2, 147-155.

Regan D. & Gray R. (2000). Collision avoidance and collision achievement: visual factors. *Trends Cog Sci*, 4:99-107.

Regan, D. & Hamstra, S.J. (1992). Shape discrimination and the judgements of perfect symmetry: dissociation of shape from size. *Vision Research*, 32, 1655-1666.

Regan, D. & Hamstra, S.J. (1993). Dissociation of discrimination thresholds for time to contact and for rate of angular expansion. *Vision Research*, 33, 447–462.

Regan, D. & Hamstra, S.J. (1994). Shape discrimination for rectangles defined by disparity alone, by disparity plus luminance and by disparity plus motion. *Vision Research*, 34, 2277-2291.

Regan, D. & Regan, M.P. (1986). Monocular and binocular processing of pattern investigated by nonlinear analysis. *Abstracts, Third International Evoked Potentials Congress*, Berlin, p.8.

Regan, D. & Regan, M.P. (1988). Objective evidence for phase–independent spatial frequency analysis in the human visual pathway. *Vision Research*, 28, 187-191.

Regan, D. and Regan, M. P. (1987). Nonlinearity in human visual responses to two-dimensional patterns and a limitation of Fourier methods. *Vision Research*, 27, 2181-2183.

Regan, D. & Vincent A. (1995). Visual processing of looming and time to contact throughout the visual field. *Vision Research*, 35:1845-1857.

Regan, D., Bartol, S., Murray, T.J., & Beverley, K.I. (1982). Spatial frequency discrimination in normal vision and in patients with multiple sclerosis. *Brain*, 105, 735-754.

Regan, D., Gray. R. & Hamstra, S.J. (1996). Evidence for a neural mechanism that encodes angles. *Vision Research*, 36, 323-330.

Regan, M.P. & Regan D. (1989) Objective investigation of visual functions using a nondestructive zoom–FFT technique for evoked potential analysis. *Can J Neurol. Sci. 16*, 168–179.

Regan, M.P. & Regan, D. (1988). A frequency–domain technique for characterizing nonlinearities in biological systems. *Journal of Theoretical Biology*, 133, 293–317.

Regan, M.P., Hong, X.H., & Regan, D. (2000). An inverted oblique effect for cyclopean gratings. *Investigative Ophthalmology and Visual Science*, 41, S948 Abstr. 5042.

Rind EC, Simmons PJ (1999). Seeing what is coming: building collision sensitive neurons. *Trends in Neuroscience*, 22:215-220.

Roelfsema, P. R. , Lamme, V. R. , & Spekreijse, H. (1998). Object–based attention in the primary visual cortex of the macaque monkey. *Nature*, 395, 376-381.

Rushton, S.K., & Wann, J.P. (1999). Weighted combination of size and disparity: a computational model for time a ball catch. *Nature Neuroscience*, 2, 186-190.

Schumer, R. A. & Ganz, L. (1979). Independent stereoscopic channels for different extents of spatial pooling. *Vision Research, 19*, 1303-1314.

Skottun, B.C., Bradley, A., Sclar, G., Ohzawa., I. & Freeman, R.D. (1987). The effect of contrast on visual orientation and spatial frequency discrimination: A comparison of single cells and behaviour. *Journal of Neurophysiology*, 57, 733-786.

Sperling, G. & Weichselgartner, E. (1995). Episodic theory of the dynamics of spatial attention. *Psychological Review*, 102, 503–532.

Sun H, Frost BJ. (1998). Computation of different optical variables of looming objects in pigeon nucleus rotundus neurons. *Nat Neurosci*, 1:296-303.

Taylor, M.M. (1963). Visual discrimination and orientation. *Journal of the Optical Society of America*, 53, 763-765.

Telford, L., Spratley, J. & Frost, B. J. (1992). Linear vection in the central visual field facilitated by kinetic depth cues. *Perception, 21*, 337-349.

Treisman, A. & Gelade, G. (1980). A feature–integration theory of attention. *Cognitive Psychology*, 12, 97–136.

Tyler, C. W. (1974). Depth perception in disparity gratings. *Nature*, 251, 140-142.

Tyler, C.W. (1975). Stereoscopic tilt and size aftereffects. *Perception, 4*, 187-309.

Tyler, C. W. (1983). Sensory processing of binocular disparity. In C.M. Schor, and K.J. Cuiffreda (Eds.), *Vergence Eye Movements* (pp. 199-295). Boston ,MA: Butterworth.

Tyler, C.W. (1991). Cyclopean vision. In D. Regan (Ed.) *Binocular Vision*. London: MacMillan, pp.38-74.

Tyler, C.W. (1995). Cyclopean riches: cooperativity, neurontropy, hysteresis, stereoattention, hyperglobality, and hypercyclopean processes in random–dot stereopsis. In T.V. Papathomas, C. Chubb, A, Gorea, and E, Kowler (Eds.), *Early Vision and Beyond.* Cambridge, Mass.: M.I.T. Press.

VanSanten JPH, Sperling G: Elaborated Reichardt detectors. *J Optical Soc Amer A*, 2:300-321.

Vincent, A. & Regan, D. (1995). Parallel independent encoding of orientation, spatial frequency, and contrast. *Perception*, 24, 491-499.

Vogels, R. & Orban, G.A. (1986). Decision processes in visual discrimination of line orientation. *Journal of Experimental Psychology: Human Perception and Performance*, 12, 115-132.

Wang Y, Frost BJ. (1992). Time to collision is signalled by neurons in the nucleus rotundus of pigeons. *Nature*, 356:236-238.

Warren, W. H. & Kurtz, K. J. (1992). The role of central and peripheral vision in perceiving the direction of self-motion. *Perception & Psychophysics, 51*, 443-454.

Watson, A.B.,. & Robson, J.G. (1981). Discrimination at thresholds labeled detectors in human vision. *Vision Research*, 21, 1115-1122.

Westheimer, G. & McKee, S. P. (1977). Integration regions for visual hyperacuity. *Vision Research*, 17, 89–93.

White, H. J. & Tauber, S. (1969). *Systems Analysis*. Philadelphia: W. B. Saunders Co.

Wilson, H. R. & Gelb, D. J. (1984). Modified line element theory for spatial frequency and width discrimination. *Journal of the Optical Society of America*, A1, 124-131.

Wilson, H., Loffler, G.H., Wilkinson, F & Thistlewaite, W.A. (2001). An inverse oblique effect in human vision. *Vision Research*, 41, 1749–1753.

Wilson, H.R. & Richards, W.A. (1989). Mechanisms of contour curvature discrimination. *Journal of the Optical Society of America, A*, 6, 106-115.

Wilson, H.R. (1991). Psychophysical models of spatial vision and hyperacuity. In D. Regan (Ed.) *Spatial Vision*, London: MacMillan, pp. 64–86.

Yang, Y. & Blake, R. (1991). Spatial frequency tuning of human stereopsis. *Vision Research*, 31, 1177-1189.

Yang, Y. & Blake, R. (1991). Spatial frequency tuning of human stereopsis. *Vision Research*, 31, 1177-1189.

4. PUBLISHED DURING THE GRANT PERIOD

4.1 Papers in peer-reviewed journals (16 papers)

4.1.1 Gray,R. & Regan,D.(1999).Do monocular time to collision estimates necessarily involve perceived distance?*Perception,* 28, 1257-1264.

4.1.2 Gray,R. & Regan,D.(2000).Estimating time to collision with a rotating nonspherical object. *Vision Research*, 40, 49-63, 2000.

4.1.3 Gray, R. & Regan, D. (2000) Simulated self-motion alters perceived time to collision. *Current Biology,* 10,587-590.

4.1.4 Gray,R. & Regan,D.(2000).Risky driving behaviour: A consequence of visual motion adaptation for visually-guided goal-directed motor action.*Journal of Experimental Psychology: Human Perception and Performance,* 26, 1721-1732.

4.1.5. Kohly, R.P. & Regan, D. (2000). Coincidence detectors: visual processing of a pair of lines and implications for shape discrimination. *Vision Research*, 40, 2291-2306.

4.1.6. Steeves, J.K.E., Gray, R., Steinbach, M.J., & Regan, D. (2000). Accuracy of estimating time to collision using only monocular information in unilaterally enucleated observers and monocularly viewing normal controls. *Vision Research*, 40, 3783-3789.

4.1.7. Regan, D & Gray, R. (2000). Visually–Guided collision avoidance and collision achievement. *Trends in Cog. Sci., Vol. 4., No.3.*99-107.

4.1.8. Regan,D. & Gray, R. (2001) Hitting what one wants to hit, and missing what one wants to miss. *Vision Research,* 41, 3321–3339.

4.1.9. Regan, M.P. & Regan, D. (2001). Simulated hair cell transduction of quasi–frequency–modulated and amplitude–modulated tones. *Hearing Research*, 158, 65-70

4.1.10. Kohly, R.P. & Regan, D. (2001). Long–distance interactions in Cyclopean Vision., *Proc. Roc. Soc.*, 268, 213-219.

4.1.11 Kohly, R & Regan, D. (2002). Fast long–range interactions in the early processing of luminance–defined form. *Vision Research*, 42, 49–63.

4.1.12 Regan, D. (2002). The Proctor Lecture: An hypothesis–based approach to clinical psychophysics and to the design of visual tests. *Investigative Ophthalmology and Vision Sciences,* 43(5), 1311–1323.

4.1.13 Regan, M.P. & Regan, D. (2002). Orientation characteristics of a mechanism in the human visual system sensitive to cyclopean form. *Vision Research*, 42,661-668.

4.1.14 Kohly, R. & Regan, D. (2002). Fast long–range interactions in the early processing of motion–defined form and of combinations of motion–defined, luminance–defined, and cyclopean form. *Vision Research*, 42, 969–980.

4.1.15 Grove, P.M. & Regan, D. (2002). Spatial frequency discrimination in cyclopean vision. *Vision Research*, 42, 1837–1846.

4.1.16 Regan, D. (2002). Binocular information about time to collision and time to passage. *Vision Research*, 42, 2479–2484.

4.2. Book Chapters

4.2.1. Regan, D. & Kohly, R.P. (2000). Selective feature-based attention directed to a pair of lines: psychophysical evidence and a psychophysical model. In L. Harris & M. Jenkin (Eds.). *Vision and Attention*, Cambridge University Press, pp.253-280.

4.2.2. Regan, M.P. & Regan, D. (2002)Techniques for investigating and exploiting nonlinearities in brain responses evoked by sensory stimuli. In Z.L. Lu. G. Sperling & L. Kaufman (Eds.) *Magnetic Source Imaging of the Human Brain,* in press.

4.2.3. Regan, D.(2002) Early visual processing of spatial form. In P.Semple (Ed.) *Adler's Physiology.* in press.

4.2.4 Regan, D. Gray, R. (2002). A step-by-step approach to research on time to collision and time to passage. In Savelbergh and Hirsch. *Research on Time to Collision*, in press.

4.2.5 Gray, R. & Regan, D. (2002). Binocular factors in estimating time to collision. In Savelbergh & Hirsch. *Research on Time to Collision*, in press.

4.3. Single–author book

4.3.1 Regan, D. (2000). *Human Perception of Objects: Early Visual Processing of Spatial Form Defined by Luminance, Color, Texture, Motion, and Binocular Disparity*. Sunderland, MA: Sinauer.

5. INTERACTIONS /TRANSACTIONS

5(a) Presentations at meeting, seminars etc.

(1) Kohly, R. & Regan, D:

The Association for Research in Vision and Ophthalmology, Annual Meeting, Fort Lauderdale, FL, May 3, 2000.

-Long–distance interactions in human cyclopean vision.

(2) Regan, M.P., Hong, X.H., & Regan, D.: *An inverted oblique effect for cyclopean gratings.* The Association for Research in Vision and Ophthalmology, Annual Meeting, Fort Lauderdale, FL, May 5, 2000.

(3) Regan, D (2000). *-Hitting what one wants to hit and missing what one wants to miss.* Netherlands Royal Academy

(4) Gray, R. & Regan, D. (2001). *Risky driving behaviour and adaptation to motion.* ECVP, Trieste

(5). Gray, R. & Regan, D. (2001). *Adaptation to motion in depth: a possible cause of highway accidents*? Meeting on Event Perception & Action, Edinburgh.

(6) Regan, D. & Regan, M.P. (2001). *A frequency domain approach to generating and testing nonlinear models of human sensory systems.* University of California, Irvine.

(7) Regan, D. (2001). *Long–distance interactions in the human visual system:* University of California, Irvine.

(8) Regan, D. (2001). *Collision avoidance and collision achievement.* University of California, Berkeley.

(9) Regan, D. (2001). *A critical look at the concept of functional localization.* University of California, Berkeley.

(10) Regan, D. (2001). *Long–distance interactions in the early processing of luminance-defined form, cyclopean form and motion-defined form.* Smith–Kettlewell Institute, San Francisco.

(11) Regan, D. (2001). *Collision avoidance and collision achievement in aviation, on the highway, and in sport.* Festschrift for Bela Julesz.

(12). Regan, D. (2001). *The Proctor Lecture: An hypothesis–based approach to clinical psychophysics and the design of visual tests.* ARVO meeting, Ft. Lauderdale.

(13). Regan, D. (2002). *Visual evoked electrical and magnetic brain responses.* Keynote lecture, annual meeting of Internat. Society for Clinical Electrophysiology.

5(b)2 Editorial Board: *Spatial Vision*
Editorial Board: *Ophthalmic and Physiological Optics*
Editorial Board: *Vision Research.*

5(b)3 Grant Reviewer: National Eye Institute (USA), Wellcome Trust (UK), Medical Research Council (UK).

5(b)4 Journal Reviewer: Vision Research, Nature, Percept. & Psychophysics, Human Factors, J. Sports Science, JOSA, Quarterly J. Exp. Psychol. Perception, Proceedings National Academy of Science USA.

6. HONORS / AWARDS

6.1 Awards during the grant period

In February 2003 the Canadian Psychology Association gave the P.I. the Hebb Award, their highest honour.

In August 2002 the P.I. was awarded the Queen Elizabeth II gold medal.

On July 1 2001 the P.I. was appointed Member of the Order of Canada (for contributions to science, medicine, and highway safety).

In June 2000 the P.I. was awarded the Proctor medal for 2001 by the Association for Research in Vision and Ophthalmology.

In October 2000 the P.I. was selected as one of three scientists, one of whom would receive the Canada Herzberg Gold Medal, Canada's highest award in science and engineering. All three were awarded the NSERC Award of Excellence.

6.2 Lifetime achievement honors prior to grant period

Elected Foreign Fellow of the Netherlands Royal Academy of Science, 1999.
Elected Spinoza Chair for 1999 by the medical faculty of the University of Amsterdam and gave the 5 Spinoza lectures.
Sir John William Dawson Medal, highest award of the Royal Society of Canada, 1997.
Charles F. Prentice Medal, highest award of the American Academy of Optometry, 1990
Fellow of the Royal Society of Canada, 1989
D.Sc. (London University, 1974)
Distinguished Research Professor, York University, 1991
I.W. Killam Fellow, 1991